Geophysics Open File Report No. 27
Geoscience Department
New Mexico Institute of Mining and Technology
Socorro, NM 87801

USE OF LINEAR INVERSE TECHNIQUES TO STUDY POISSON'S RATIOS IN THE UPPER CRUST IN THE SOCORRO, NEW MEXICO, AREA

by

Mark S. Frishman

Submitted in Partial Fulfillment
of the Requirements of Geophysics 590 and the
Degree of Master of Science in Geophysics

New Mexico Institute of Mining and Technology
Socorro, New Mexico
June, 1979

The research described in this paper was sponsored jointly by the National Science Foundation (Grant EAR 77-23166) and the New Mexico Energy Institute - New Mexico State University (Grant EI-77-2312)

TABLE OF CONTENTS

LIST OF FIGURES

LIST OF FIGURES (cont.)

LIST OF TABLES

LIST OF APPENDICES

ACKNOWLEDGEMENTS

The author wishes to thank Dr. Antonius Budding and Chuck Shearer for their help in obtaining general information about Poisson's ratio for the Socorro area. Particular thanks are extended to Dr. Allen Sanford and Roger Ward for their much appreciated assistance in helping the author understand linear inverse methods and their relation to the general characteristics of the Socorro area. The author is particularly thankful to Roger Ward, whose computer and programming expertise made this study possible. Particular appreciation is extended to the author's advisor, Dr. John Schlue, whose quick and thorough editing, advice, and never-ending patience made the completion of this paper possible. A very special thanks is extended to the author's wife for her patient understanding, encouragement, and typing ability.

ABSTRACT

Arrays of high-gain, short-period seismographs were used to record microearthquakes from April, 1975, through January, 1978, in the vicinity of Socorro, New Mexico. The P- and S-wave travel times from 236 microearthquakes were selected from this recording period to model the P- and S-wave velocity distribution, and thus the distribution of Poisson's rato in this area, using linear inverse techniques (Jackson, 1972). Hypocenter locations were obtained employing a damped least squares inversion computer program; the results were used to obtain the observed P- and S-wave travel times of the 600 raypaths from these selected microearthquakes.

Seven different models were studied using this technique. Models 1, 2, 3, 4, and 5 divided the same study area into 1, 4, 9, 16, and 25 blocks, respectively. The other two models studied, Models 4' and 5', were the same as Models 4 and 5 with the exception that the P-wave solutions were chosen in a different manner, such that the P-wave solutions for these two models were more model dependent than the solutions chosen for Models 4 and 5.

The quality factor R, which is a measure of the sum of the squares of the residuals, decreased towards 1.0 as the number of blocks increased from 1 through 16, which indicated that the more complex models provided better solutions. Models 4', 5, and 5' showed increases in R relative to Model

4, which indicated poorer solutions. Model 4 is regarded as the best solution of the seven models studied because it had a value of R closest to 1.0 (1.013). Models 4' and 5' showed generally the same results as Models 4 and 5 but had lower standard deviations on the Poisson's ratios because the solutions were generally more model dependent.

Though Model 4 had the best solution, it was not used for the final interpretation because it was believed that Model 5' would offer more detail for determining small areas with anomalous Poisson's ratios. Though Model 5' was not the best solution, the R value (1.061) was still closer to 1.0 than Models 1, 2, or 3, and it offered the prospect of allowing more detail in the analysis because the block sizes were smaller. This model showed six areas with anomalous Poisson's ratios. Of those six, four are interpreted to be definite anomalies at the 95% confidence level, and two are considered to be only possible anomalies. The locations of the four definite anomalies and their Poisson's ratios (ν) are: 1) the east-central Socorro basin ($\nu = 0.309 \pm 0.006$); 2) the east-central Socorro basin ($\nu = 0.282 \pm 0.001$); 3) the east Socorro basin and west-central Los Pinos Mountains ($\nu = 0.296 \pm 0.003$); and 4) the south-central Los Pinos Mountains ($\nu = 0.281 \pm 0.004$). The locations of the two possible anomalies are: 1) the west-central Los Pinos Mountains north of anomaly 3, above, ($\nu = 0.281 \pm 0.001$); and 2) the west-central Socorro basin ($\nu = 0.315 \pm 0.003$).

The data set used here was not capable of providing more detail than is presented in this study, and could neither confirm nor deny the presence of other areas with anomalous Poisson's ratios postulated in previous studies. Models with smaller (more numerous) blocks would be necessary, and while such models would undoubtedly provide a better fit to the data (smaller F), this decrease in the size of the residuals would not be justified, since the residuals associated with Model 4 are already as small as the uncertainties in the data. Thus, if more resolution (i.e., smaller blocks) is desired using this technique, then either more data, and/or data with smaller errors must be employed.

I. INTRODUCTION

The purpose of this study is twofold: 1) to obtain models of the P- and S-wave velocity distribution around Socorro, New Mexico (and thereby estimates of the areal distribution of Poisson's ratio); and 2) to evaluate the usefulness of linear inverse techniques in obtaining these distributions.

I have chosen to use linear inverse techniques (Jackson, 1972) to model the P- and S-wave velocity distribution using the travel times of 600 raypaths from 236 microearthquakes that occurred in the vicinity of Socorro, New Mexico. The linear inverse techniques, described in detail within this report, were chosen to be used because: 1) obtaining a distribution of Poisson's ratio for this area had not been previously attempted using these techniques and 2) this method had advantages in that large amounts of data and various models could be used along with more formal analyses of the models. One disadvantage was the limitation on the size of the anomalous areas that could be defined from the data set used.

From these modelled velocity distributions, a map of Poisson's ratio can be found for the study area. Poisson's ratio is a dimensionless quantity representing a measure of the general characteristics of a material. Poisson's ratio has a range of values from 0.0 to 0.5, which corresponds to a perfectly rigid solid and a perfect liquid, respectively.

Previous studies, using less formal techniques, have found numerous small areas of anomalously high Poisson's ratios in the vicinity of Socorro, New Mexico. It is believed that these areas with anomalously high Poisson's ratios may be associated with shallow ($<$ 10 km) magma bodies. This study evaluates the usefulness of linear inverse techniques in resolving these small areas of anomalous Poisson's ratios as well as in resolving new anomalous areas.

II. GEOLOGIC SETTING

The area of study, delineated by the heavy lines in Figure 1, is located in central New Mexico approximately 120 kilometers (km) south-southwest of Albuquerque, New Mexico. A major extensional structure known as the Rio Grande rift, is the dominating structural feature of the study area. The rift was formed by east-west tension which began approximately 25 to 29 million years (m.y.) ago and continuing to the present (Chapin and Seager, 1975). The rift extends from southern New Mexico in a northward trend into southern Colorado. Intragraben horsts, believed to be 9 to 10 m.y. old (Chapin and Seager, 1975), appear as mountain ranges, such as the Socorro-Lemitar and Chupadera Mountains (see Figure 1); these separate deep, sediment-filled grabens, such as the La Jencia and Socorro basins. For further information, the reader is referred to Chapin and Seager (1975), Sanford (1968), and Chapin, et al. (1978).

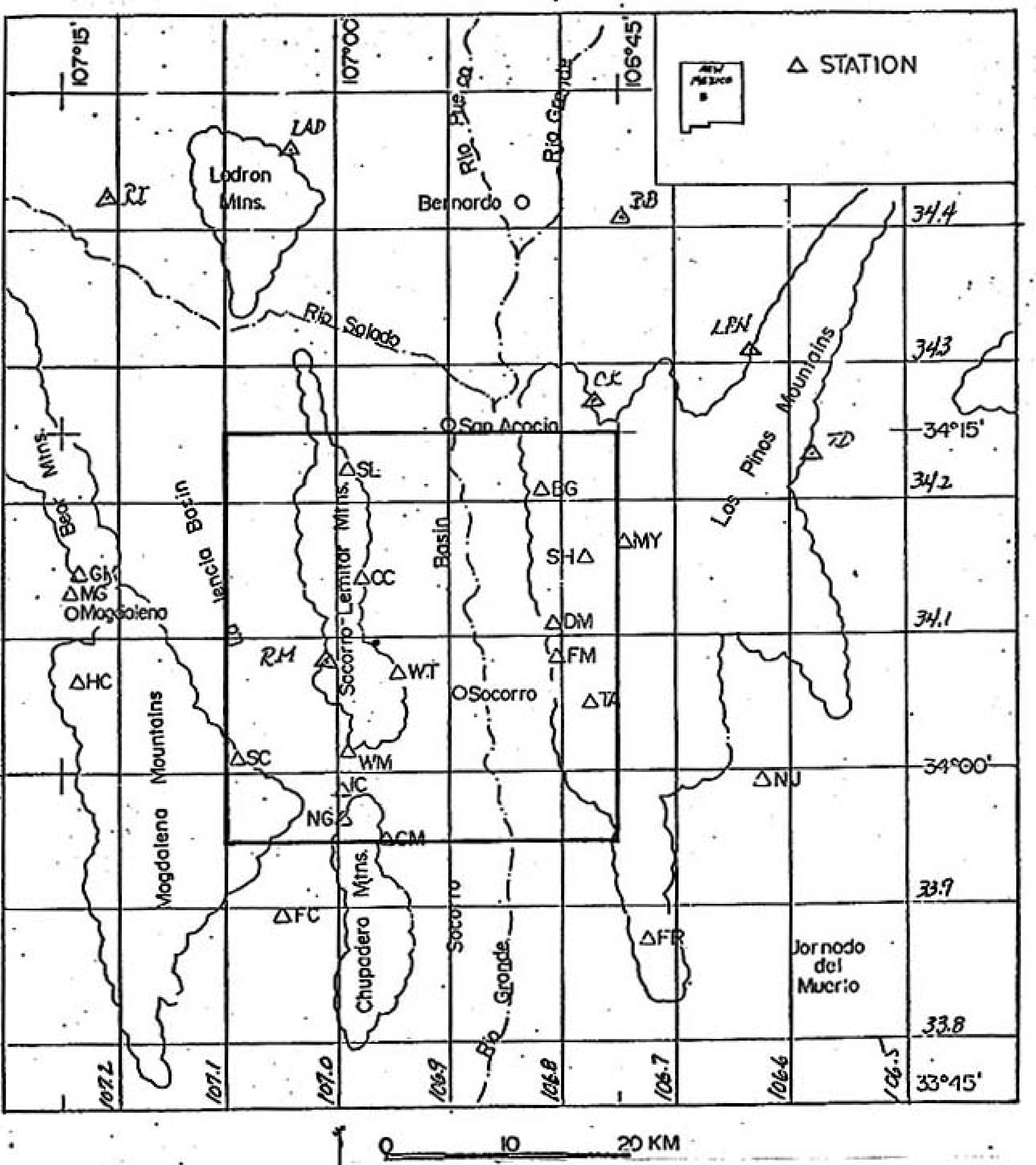

Figure 1. Location of study area and seismic stations; study area delineated by heavy line.

III. PREVIOUS STUDIES

A study of Poisson's ratio and the P-wave velocity - S-wave velocity ratio between Socorro and Albuquerque, New Mexico was conducted by Sakdejayont (1974). His study used 32 well-recorded microearthquakes in the Rio Grande rift within 45 km of the Socorro seismic station (SNM). Sakdejayont found a P-wave:S-wave velocity ratio of 1.664 and a Poisson's ratio of 0.217 for his study area, with associated standard deviations of ±0.022 and ±0.0121, respectively. Sakdejayont concluded that the values obtained, though somewhat low, were, nevertheless, normal.

A second study of Poisson's ratio around Socorro was undertaken by Caravella (1976). Caravella used a composite Wadati diagram, or raypath technique, obtained from 50 microearthquakes located in and around the southern margins of the Socorro and La Jencia basins, to obtain a spatial distribution of Poisson's ratio for the Socorro region. Caravella found an average Poisson's ratio of 0.262 with a standard deviation of ±0.034. He noted that his value is nearly 21 percent greater than that obtained by Sakdejayont for his study area further north. Caravella concluded that the differences in the Poisson's ratios obtained from the two studies can be attributed to the difference in the S-wave velocities obtained, 3.30 km/sec versus 3.49 km/sec. Caravella further attempted to determine a spatial variation of Poisson's ratio. However, he could not reach any definite conclusions because his data were insufficient. The data were sufficient, however, to define three anomalous areas. The areas, and their associated Poisson's ratios are: 1) southern La Jencia basin with a Poisson's ratio of 0.292; 2) Socorro Mountain with a Poisson's ratio of 0.289; and 3) central La Jencia Basin with a Poisson's ratio of 0.284 (see Figure 2).

A more recent study of Poisson's ratio near Socorro, New Mexico was conducted by Fender (1978), who utilized methods similar to those used by Caravella. Fender used a weighted least-squares linear regression on 277 Wadati diagrams obtained from 294 microearthquakes to obtain an average, as well as a spatial distribution, of Poisson's ratio. Fender obtained an average Poisson's ratio of 0.251 with a standard deviation of ±0.052. His results, as well as Caravella's and Sakdejayont's, all fall within range of each other when their respective standard deviations are applied. Fender was able to describe four areas of anomalously high Poisson's ratios. These areas are: 1) the southern La Jencia basin with a Poisson's ratio of 0.280; 2) east-central La Jencia basin with a Poisson's ratio of 0.275; 3) the northern tip of the Chupadera Mountains with a Poisson's ratio of 0.279; and 4) east-central Socorro basin with a Poisson's ratio of 0.275 (see Figure 2). The first three anomalous areas lie near the same anomalous areas found by Caravella. However, Fender's values for Poisson's ratios are about three percent lower than those values obtained by Caravella. The exact locations differ to

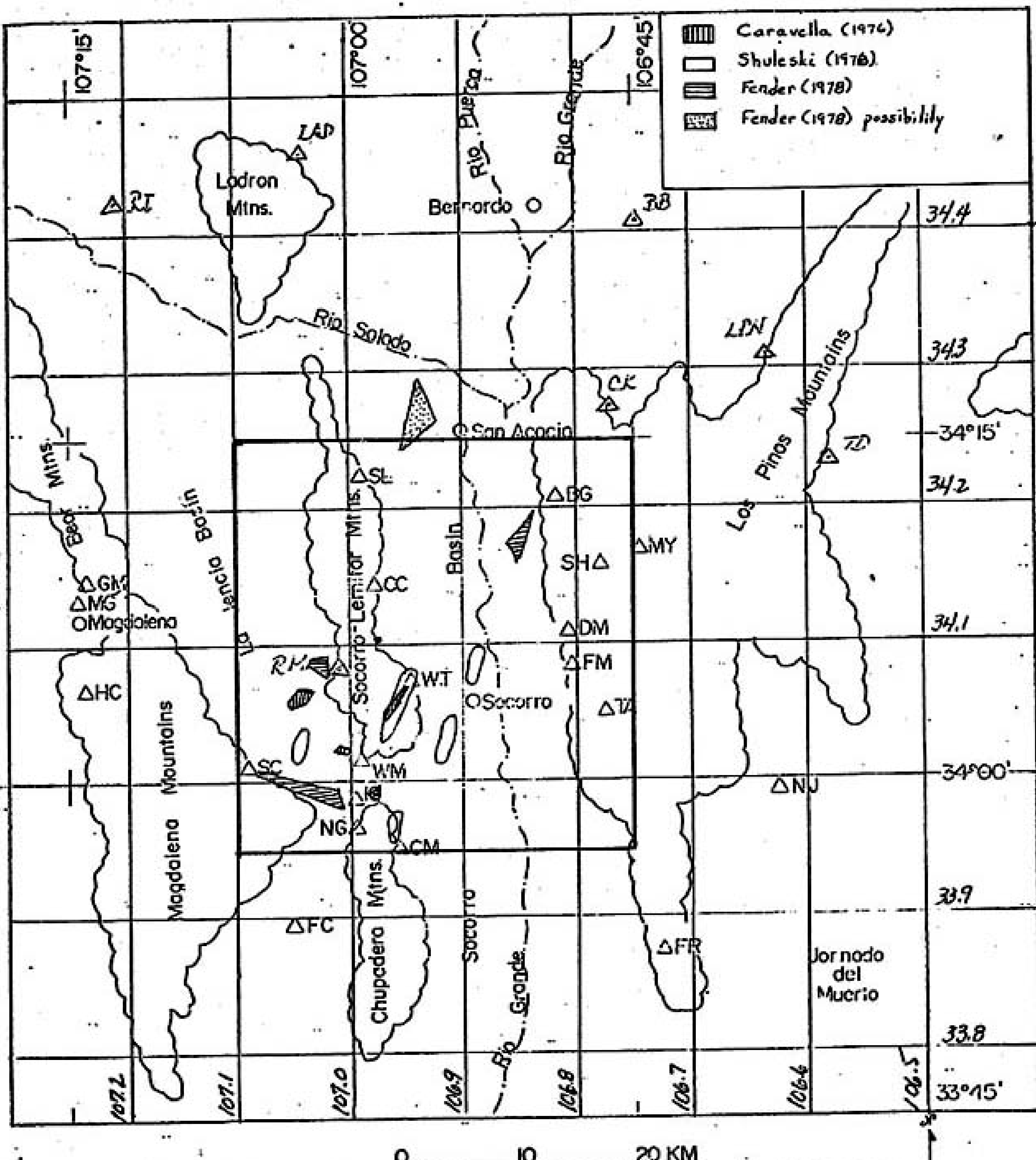

Figure 2. Locations of anomalously high Poisson's ratios determined from past studies.

the extent that none of the anomalies found by Fender overlaps those of Caravella (see Figure 2).

A study using linear inversion techniques similar to that of Aki et al. (1977) was conducted by Tang (1978) to obtain a three dimensional crustal model using relative travel-time residuals of P-waves. Tang concluded from his model that minor low velocity zones appear to exist at shallow depths (within nine km below the surface) roughly in the area where shallow magma bodies were proposed by Shuleski (1976) (see Figure 2). Tang's study is the only completed study to date (June, 1979) in which linear inverse techniques were used to obtain information about the upper crust in the neighborhood of Socorro, New Mexico.

IV. APPLICATION OF INVERSION TECHNIQUES TO SEISMIC DATA

The linear inverse method (Jackson, 1972) is used in this study to determine seismic P- and S-wave velocities in a crustal model of the Earth. The data consist of 236 microearthquakes for which hypocenters and the P- and S-wave arrival times are known. These 236 microearthquakes produce 600 raypaths.

Suppose that n observations are obtained. Let these observations, or data, which are the P- and S-wave travel times, be denoted by y_i, where $i = 1,\ldots,n$. Construct an Earth model that reasonably fit these data. This model will have characteristic parameters or unknowns. Let these unknowns, which are the P- and S-wave velocities, to be determined in this study, be denoted as x_j^o for $j = 1,\ldots,m$, where m is the number of model parameters.

Using the model, theoretical data are generated, i.e., y_i^{th} for $i = 1,\ldots,n$. These are obtained from solving the forward problem. The theoretical data, generally, will not have the same values as the corresponding observed data for a variety of reasons. By adjusting the model parameters, new theoretical data values are generated. This adjustment is repeated until the theoretical data are as close to the observed data as is possible or necessary. The final model represents one possible earth model that would produce theoretical values that are similar to those observed in the field.

Arbitrary adjustment of model parameters to fit the observed data may not be simple. The model may be very complex and large amounts of numeric manipulation may be required. For this reason, some means of relating the data to the model parameters is needed, i.e.

$$y_i^\circ = f_i(x_1, x_2, \ldots x_m) \tag{1}$$

for i = 1,...,n.

Assume that the y_i^{th}'s may be expanded in a Taylor series expansion about the x_j°'s as follows:

$$y_i^{th} = \sum_{j=1}^{m} f_i(x_j^\circ) + \sum_{j=1}^{m} \frac{\partial f_i(x_j^\circ)}{\partial x_j} (x_j - x_j^\circ) + \text{higher order terms} \tag{2}$$

where the x_j's are the new model parameters. By ignoring the higher order terms, linearity is assumed and equation (2) can be modified as follows:

$$y_i^{th} - f_i(x_j^\circ) = \frac{\partial f_i(x_j^\circ)}{\partial x_j} (x_j - x_j^\circ) \tag{3}$$

Applying equation (1) to equation (3) yields:

$$y_i^{th} - y_i^\circ = \frac{\partial f_i}{\partial x_j} \Delta x_j$$

or

$$\Delta y_i = A_{ij} \Delta x_j \tag{4}$$

where $\Delta y_i = y_i^{th} - y_i^{\circ}$ is always known because the y_i^{th}'s are the calculated theoretical data and the y_i°'s are the measured observed data; the A_{ij}'s are the elements of the matrix obtained from the $\partial f_i / \partial x_j$'s; and $\Delta x_j = x_j - x_j^{\circ}$. The only unknowns in equation (4) are the x_j's, the new model parameters. Because linearity is assumed, this procedure is known as the linear inverse method.

Every inverse problem can be classified into one of three categories: 1) Those problems in which the number of data equal the number of unknowns, i.e., $n=m$; 2) Those problems in which the number of data are less than the number of unknowns, i.e., $n < m$, known as the underdetermined inverse problems; 3) Those problems in which the number of data are greater than the number of unknowns, i.e., $n > m$, known as the overdetermined inverse problems. The overdetermined case for computing seismic wave velocities in the upper crust will be used in this study.

IV.1 FORWARD PROBLEM

The travel time of a P-wave, the first arrival of a seismic event, may be represented by the equation

$$t_p = \frac{D}{\alpha} \tag{5}$$

where D is the distance from the event to the recording station and α is the velocity of the P-wave (see Figure 3). Similarly, the travel time of the S-wave may be represented by the equation

$$t_s = \frac{D}{\beta} \tag{6}$$

where β is the velocity of the S-wave for the homogeneous space in Figure 3.

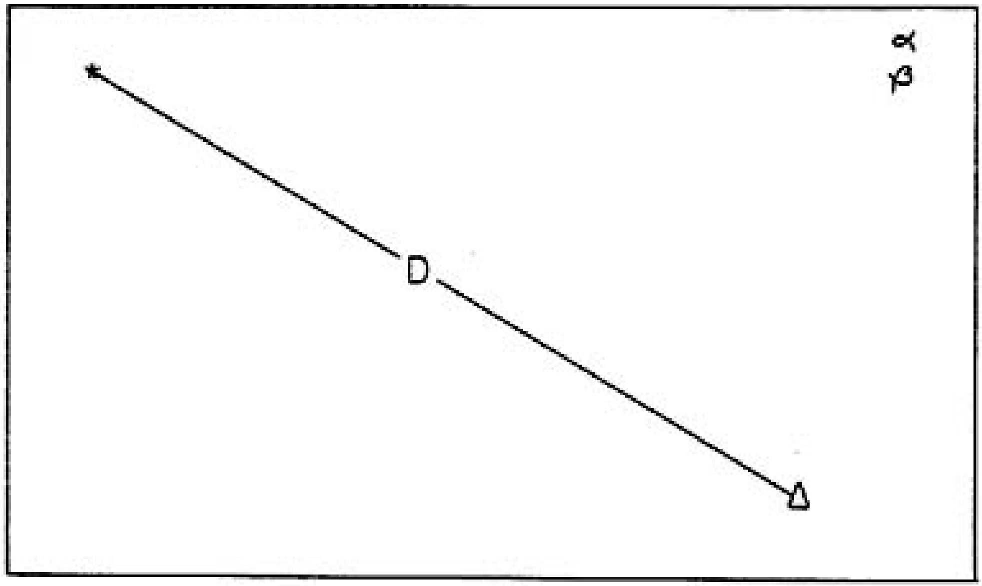

Figure 3

Example: Single Homogeneous Space

* event

Δ station

For a space composed of two dissimilar blocks (see Figure 4), equations (5) and (6) become

$$t_p = \frac{D_1}{\alpha_1} + \frac{D_2}{\alpha_2}$$

and

$$t_s = \frac{D_1}{\beta_1} + \frac{D_2}{\beta_2}$$

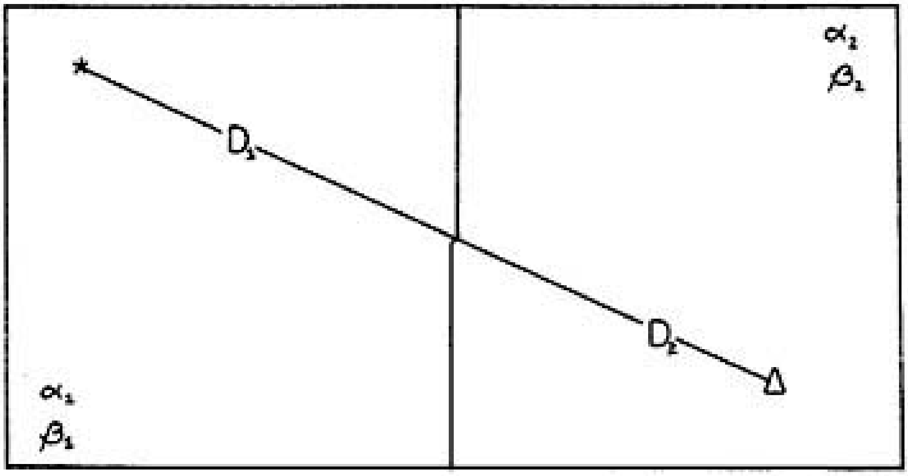

Figure 4 * event

Two Block Example Δ station

Any refraction of the raypath crossing the boundary is neglected by assuming that the raypath crosses the boundary at a point perpendicular to the boundary. An infinitesimal section of the boundary is distorted in such a way as to cause the raypath to intersect the boundary at right angles (see Figure 4).

This procedure is expandable to any number of blocks. By solving for the α's and β's, given the travel times and the distances travelled, Poission's ratio, ν, for each block is calculated from the equation

$$\nu_i = \frac{\left(\frac{\alpha_i}{\beta_i}\right)^2 - 2}{2\left[\left(\frac{\alpha_i}{\beta_i}\right)^2 - 1\right]} \tag{7}$$

Bullen (1963, page 213). Poisson's ratio is a dimensionless value which may vary between 0.0 and 0.5 for different materials. Usually, Poisson's ratio is in the neighborhood of 0.25 (Nettleton, 1940). The case where Poisson's ratio is 0.0 corresponds to a perfectly rigid solid, while the case where Poisson's ratio is 0.5 corresponds to a perfect liquid, which has no rigidity ($\mu = 0$). The Poisson's ratios to be calculated for the blocks will provide a measure of the general characteristics of the material that compose the blocks.

The forward problem is solved by assuming initial estimates for α_i and β_i and computing the theoretical travel times. For the simple homogeneous case above, the Δy term in equation (4) in matrix form is

$$\Delta y = \begin{bmatrix} \Delta t_p \\ \Delta t_s \end{bmatrix}$$

where Δt_p and Δt_s are the theoretical travel times, t^{th}, obtained from the forward problem minus the observed travel times of the P- and S-waves, respectively. The Δx term in equation (4) in matrix form for the simple homogeneous case above is

$$\Delta x = \begin{bmatrix} \Delta \alpha \\ \Delta \beta \end{bmatrix}$$

where $\Delta\alpha = \alpha - \alpha^{\circ}$ and $\Delta\beta = \beta - \beta^{\circ}$. α and β are the new model parameters to be determined. α° and β° are the initial P-and S-wave model parameters, respectively. It has been found from previous studies (Caravella, 1976; Fender, 1978) that the average crustal P-wave velocity in and near the study area is 5.8 kilometers per second (km/sec). Fender (1978) has found that the average Poisson's ratio in the study area is 0.25. Using this value yields a P- to S-wave ratio of $\sqrt{3}$: 1, and the S-wave velocity is thus

$$\beta^{\circ} = \alpha^{\circ}/\sqrt{3} = \frac{5.8 \text{ km/sec}}{\sqrt{3}} = 3.35 \text{ km/sec.}$$

These values, 5.8 km/sec and 3.35 km/sec for α° and β°, respectively, are assumed for each block of the initial model.

The A matrix in equation (4) for the simple homogeneous case becomes

$$A = \begin{bmatrix} \frac{\partial t_p}{\partial \alpha} \\ \\ \frac{\partial t_s}{\partial \beta} \end{bmatrix} = \begin{bmatrix} \frac{\partial (D/\alpha)}{\partial \alpha} \\ \\ \frac{\partial (D/\beta)}{\partial \beta} \end{bmatrix} = \begin{bmatrix} -\frac{D}{\alpha^2} \\ \\ -\frac{D}{\beta^2} \end{bmatrix}$$

The inverse problem (equation 4) expressed in matrix form for the simple homogeneous case thus is

$$\begin{bmatrix} \Delta t_p \\ \Delta t_s \end{bmatrix} = \begin{bmatrix} -\frac{D}{\alpha^2} & 0 \\ 0 & -\frac{D}{\beta^2} \end{bmatrix} \begin{bmatrix} \Delta \alpha \\ \Delta \beta \end{bmatrix} .$$

Now consider a more complex theoretical study area partitioned as shown in Figure 5. Suppose that within this study area there are two events and two stations. The origin times, travel times, and event locations are known. The raypaths are numbered as shown in Figure 5. The raypaths are shown in map view, but depth of focus and station elevations must be considered when the distances travelled in each block are calculated.

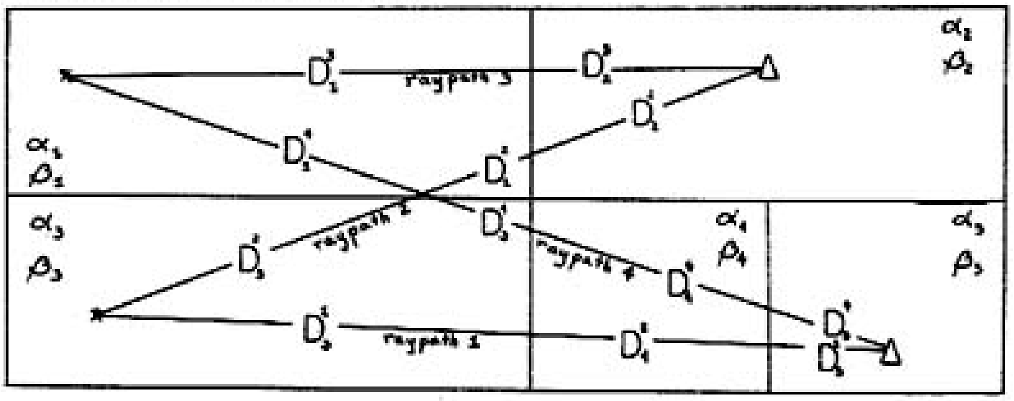

Figure 5. * Event

Example: Theoretical Study Area Δ Station

In matrix form for these two events, the problem is now written

$$\begin{bmatrix} \Delta t_p^1 \\ \Delta t_s^1 \\ \Delta t_p^2 \\ \Delta t_s^2 \\ \Delta t_p^3 \\ \Delta t_s^3 \\ \Delta t_p^4 \\ \Delta t_s^4 \\ \Delta t_p^5 \\ \Delta t_s^5 \end{bmatrix} = \begin{bmatrix} 0 & 0 & \frac{-D}{(\alpha_3)^2} & \frac{-D}{(\alpha_4)^2} & \frac{-D}{(\alpha_5)^2} & 0 & 0 & 0 & 0 & 0 \\ 0 & 0 & 0 & 0 & 0 & 0 & 0 & \frac{-D}{(\beta_3)^2} & \frac{-D}{(\beta_4)^2} & \frac{-D}{(\beta_5)^2} \\ & & & & & & & & & \\ & & & & & & & & & \\ & & & & \text{etc.} & & & & & \\ & & & & & & & & & \\ & & & & & & & & & \\ & & & & & & & & & \\ & & & & & & & & & \\ & & & & & & & & & \end{bmatrix} \begin{bmatrix} \Delta \alpha_1 \\ \Delta \beta_1 \\ \Delta \alpha_2 \\ \Delta \beta_2 \\ \Delta \alpha_3 \\ \Delta \beta_3 \\ \Delta \alpha_4 \\ \Delta \beta_4 \\ \Delta \alpha_5 \\ \Delta \beta_5 \end{bmatrix}$$

The blocks which are not sampled by a given raypath will have zero for their corresponding A matrix elements, since their distances equal zero. It is not necessary for the event or station to lie within the study area so long as a portion of the raypath is within the study area. The total length of the raypath is required to calculate the theoretical travel time but only the distance in the study area is required for the matrix A.

The procedure behind the linear inverse method is to produce a matrix by inverting the matrix A such that equation (4) can be solved, i.e.

$$\Delta x = H\,\Delta y \qquad (8)$$

where H can be considered as the "generalized inverse" of A. If the matrix A is square (n=m) and nonsingular, then H = A^{-1}, which can be easily calculated.

For the overdetermined and underdetermined cases in which the number of data points does not equal the number of model parameters, the matrix A is not square. This means that A^{-1} is not defined by matrix theory. The generalized inverse of matrix A (=H) must be obtained in order to transform equation (4) to a solvable form similar to equation (8).

IV.2 LEAST SQUARES METHOD

Residuals will occur due to noisy data and/or poor model parameters. These residuals, denoted as ϵ_i for i = 1,...,n, are defined as

$$\epsilon_i = \Delta y_i - A\,\Delta x_j$$

for j = 1,...,m. These residuals can be minimized in the least squares sense. In the least squares measure, these residuals are assumed to be random and normally distributed and primarily due to noise. The residuals are minimized with respect to the Δx_j's. Let

$$\begin{aligned}\epsilon^t\epsilon = R^2 &= (y-Ax)^t(y-Ax) \\ &= (y^t - x^tA^t)(y-Ax) \\ &= y^ty-y^tAx-x^tA^ty+x^tA^tAx \qquad (9)\end{aligned}$$

where the subscripts and the deltas, Δ, have been omitted; and the superscript "t" implies the matrix transpose. Let $y^ty = S$, which is a scalar; $A^ty = V$, which is a vector; and $A^tA = M$, which is a matrix. Equation (9) becomes

$$R^2 = S-2\sum v_jx_j+\sum m_{jk}x_jx_k \qquad (10)$$

Taking the partial derivative of equation (10) with respect to x_l and setting it equal to zero yields

$$\frac{\partial R^2}{\partial x_l} = -\sum_{j=1}^{m} v_j \delta_j + \sum_j \sum_k M_{jk}\left[x_k \delta_{il} + x_j \delta_{kl}\right] = 0 \qquad (11)$$

The S term drops out because it is a scalar. The Kronecker delta, δ, has the value of 1 when j = l = k and a value of 0 when j ≠ l ≠ k. Equation (11) can be rewritten as

$$\frac{\partial R^2}{\partial x_l} = -2V_l + \sum_k M_{lk}X_k + \sum_j M_{jl}X_j = 0 \qquad (12)$$

M is a symmetric matrix because A^tA is a symmetric square matrix. Equation (12) becomes

$$\frac{\partial R^2}{\partial x_1} = -2V_1 + 2\sum_j M_{1j}x_j = 0$$

which implies that

$$M\ X = V$$

or

$$A^tAx = A^ty$$

If A^tA is nonsingular, then its inverse $(A^tA)^{-1}$ exists and

$$\hat{x} = (A^tA)^{-1}A^ty + x^{\circ} \qquad (13)$$

where $\hat{x}$ is the vector containing the new model parameters, and x° are the initial model parameters. Equation (13) is the least squares solution similar to equation (8) for the overdetermined problem. The matrix $(A^tA)^{-1}A^t$ is the matrix required to solve the overdetermined problem in the least squares sense.

IV.3 EIGENVALUE/EIGENVECTOR DECOMPOSITION METHOD

Another method of solving equation (4) is by the eigenvalue/eigenvector decomposition method. The least squares method, described above, for the overdetermined case, i.e., $n > m$ is valid provided that the matrix A^tA is non-zero and the inverse $(A^tA)^{-1}$ exists. The eigenvalue/eigenvector decomposition method offers an alternative method for obtaining a generalized inverse of the matrix A. For the overdetermined problem, the matrix A is not square. The matrix A^tA, however, is square. If the matrix A^tA is singular, or nearly so, then the eigenvalue/eigenvector decomposition is applied.

The eigenvalue equation associated with an arbitrary n x n square matrix A is

$$A_{ii}U_i = \lambda_i U_i \tag{14}$$

where the scalars λ_i for i = 1,...,n are the eigenvalues and U_i for i = 1,...,n are the eigenvectors or principal axes. The eigenvalues λ_i satisfy the equation

$$\det \left| A - \lambda \right| = \begin{vmatrix} a_{11} - \lambda_1 & a_{12} & \cdots & a_{1n} \\ a_{21} & a_{22} - \lambda_2 & \cdots & a_{2n} \\ a_{n1} & a_{n2} & \cdots & a_{nn} - \lambda_n \end{vmatrix} = 0$$

If the eigenvalues are distinct, then

$$Ax = \lambda x$$

yields n distinct eigenvectors. These eigenvectors can be normalized to the value one by

$$x^t x = 1$$

If λ is a solution to equation (14), then so is $(-\lambda)$. Now consider an arbitrary n x m matrix A and the n x m system

$$Ab = c$$

where b and c are representative of the x and y forms in equation (4). Taking the adjoint of this n x m system yields the m x n system

$$A^T d = c.$$

This m x n system can be written as one matrix equation

$$Fg = h$$

where

$$F = \begin{bmatrix} O & A \\ A^T & O \end{bmatrix}$$

$$g = \left[\frac{b}{d}\right]$$

and

$$h = \left[\frac{c}{e}\right]$$

The matrix F is an (n + m) x (n + m) system. The matrix F, which is symmetric, will yield m + n eigenvalues in the manner described below.

The eigenvalue/eigenvector decomposition proceeds in the following manner:

$$\lambda \begin{bmatrix} U \\ V \end{bmatrix} = \begin{bmatrix} O & A \\ A^t & O \end{bmatrix} \begin{bmatrix} U \\ V \end{bmatrix}$$

This yields

$$Av = \lambda u \tag{15}$$

and

$$A^t u = \lambda v \tag{16}$$

Equations (15) and (16) yield the "shifted eigenvalues" (Lanczos, 1961, p. 117). Equations (15) and (16) in matrix form are

$$AV = \Lambda U \tag{17}$$

and

$$A^t U = \Lambda V \tag{18}$$

Postmultiplying equation (17) by V^t yields

$$AVV^t = U \Lambda V^t.$$

Since $VV^t = I$, the identity matrix, then

$$A = U \Lambda V^t \tag{19}$$

From equation (13)

$$\hat{x} = \left[(U \Lambda V^t)^t \, U \Lambda V^t \right]^{-1} (U \Lambda V^t)^t y \tag{20}$$

where the expression for the matrix A, given by equation (19), is substituted into equation (13) to yield equation (20). Taking the transpose of $U \Lambda V^t$ in equation (20) results in

$$\hat{x} = \left[V \Lambda \, U^t \, U \Lambda V^t \right]^{-1} (V \Lambda U^t) y. \tag{21}$$

$U^t U = I$, the identity matrix, and Λ are symmetric which implies that $\Lambda = \Lambda^t$. Applying these relationships, equation (21) becomes

$$\hat{x} = \left[V \Lambda^2 V^t \right]^{-1} (V \Lambda U^t) y \tag{22}$$

Performing the multiplication in equation (22) gives

$$\hat{x} = (V \Lambda^{-1} U^t) y$$

The matrix $(V \Lambda^{-1} U^t)$, designated as the matrix H, is the generalized inverse matrix required to solve the overdetermined problem, and is equivalent to the least squares solution given by equation (13).

There are at most m non-zero eigenvalues obtained for this example. If p of the m eigenvalues are non-zero, then this same formulation may be used by discarding the row or rows of the eigenvalue matrix for which the zero eigenvalues occur. The matrix Λ then becomes a p x m matrix. The corresponding eigenvector or vectors of the eigenvector matrix V must also be discarded by omitting the corresponding columns in matrix V. Matrix V then becomes an m x p matrix. The same procedure must also apply to the matrix U.

The number of eigenvalues retained, p, corresponds to the customary definition of the rank of the matrix. In this method, p also corresponds to the number of degrees of freedom in the problem. Eigenvalues and eigenvectors of non-zero value may also be discarded. However, discarding eigenvalues reduces the number of degrees of freedom in the problem, and the resulting solution no longer corresponds to that of the classical least squares solution (equation 13).

IV.4 UNCERTAINTIES - σ

In any data acquisition procedure, there are always some errors which occur in the actual readings or measurements. The inaccuracies arise from a number of reasons, such as noise, human reading errors, calculations and instrument inaccuracies. In many cases, the size of these errors may be known. In linear inversion, these errors are applied to the matrix A. For each datum, y_i^o, there is an associated uncertainty called σ_i. These uncertainties are applied to the rows of the A matrix in such a manner that each element of row i of the matrix A, a_{ij}, is divided by the corresponding σ_i. These same σ_i's are also applied to the data matrix Δy in the same manner. The σ_i's are applied prior to any manipulation of the matrix A. Any uncertainties in the data, then, are applied, carried through the calculations, and are reflected in the final solution and variances. In this paper, the uncertainties represented by the σ_i's are assumed to correspond to one standard deviation.

IV.5 A PRIORI ESTIMATES - τ

A similar procedure can be applied to the model. If some information about the model parameters is known, then an a priori estimate, τ_j, can be applied to the model. For instance, if a certain model parameter is suspected to fall within a certain limit determined from additional data or previous studies, then that limit can be applied to the initial model. These estimates are applied to the matrix A in such a manner that each element of the column j of the matrix A is multiplied by the corresponding τ_j.

A small τ_j implies that 1) the corresponding model parameter, x_j^o, is well known and 2) the τ_j will diminish the corresponding column in matrix A and thus the final model parameter will be more dependent on the initial model parameter than on the data. A large τ implies that 1) the corresponding initial model parameter is not well known and 2) the corresponding parameter will be determined more by the data than the model.

The *a priori* estimates, like the uncertainties, are applied prior to any manipulation of the matrix A. In this way, the *a priori* estimates are carried through the calculations and are reflected in the final solution.

IV.6 VARIANCE AND STANDARD DEVIATION

To speak of a final solution without including a statement about the uncertainties in the final solution is useless. The variances are easily obtained through the matrix H. The diagonals of the matrix HH^t are the variances on the final model parameters, x_j, i.e., the variance on the parameter x_j is the element $(HH^t)_{jj}$. When the *a priori* estimates, τ_j, are applied to the matrix A, these same estimates must be applied to the variances. The variances, var $(\hat{x}_j)$, are thus determined by the equation

$$\mathrm{Var}\ (\hat{x}_j) = (HH^t)_{jj}\, \tau_j^2$$

The standard deviation is defined as the square root of the variance.

IV.7 STANDARD DEVIATION ON POISSON'S RATIO

The linear inverse method produces P- and S-wave velocities and associated standard deviations. When these velocities are substituted into equation 7, a Poisson's ratio is obtained. To obtain a standard deviation on the Poisson's ratio, the derivative of equation 7 is taken with respect to α and β, i.e.,

$$d\nu = \frac{\partial \nu}{\partial \alpha}\, d\alpha + \frac{\partial \nu}{\partial \beta}\, d\beta\ .$$

Thus, an equation relating the change in Poisson's ratio with respect to the change in the given α and β is obtained, e.g.

$$\left|d\nu\right| = \frac{\alpha\beta}{(\alpha^2-\beta^2)^2}\left[\beta\left|d\alpha\right| - \alpha\left|d\beta\right|\right]$$

where $d\alpha$ is the standard deviation on the P-wave velocity (α), $d\beta$ is the standard deviation on the S-wave velocity (β), and $d\nu$ is the resulting change in the Poisson's ratio for the given α and β.

IV.8 PERFORMANCE INDEX "R"

The scalar R is an indication of the 'performance' of the calculations in relation to the real data (collected in the field), the data created from the model, and the initial uncertainties σ_i of the real data. R is defined as

$$R = \left[\frac{1}{n}\sum_{i=1}^{n}\left(\frac{\Delta y_i}{\sigma_i}\right)^2\right]^{\frac{1}{2}}$$

where n is the number of data points,

$$\Delta y = y_i^{\circ} - y_i^{th} - \Delta\hat{y}_i$$

where y_i° is the i^{th} observed data and y_i^{th} is the i^{th} theoretical data. $\Delta\hat{y}_i$ is created by convolving the difference, $y_i^{\circ} - y_i^{th}$, with the matrix S, where S = AH. σ_i is the uncertainty of the observed data y_i°.

A value of R that is much less than the value 1.0 indicates 1) that the uncertainties σ_i are too large and/or 2) there are too many model parameters to be justified by the data given. The reverse is true for an R value that is much greater than 1.0. A value of R that is approximately equal to 1.0 implies that 1) the uncertainties on the data are justifiable and/or 2) the model is of sufficient size and number of parameters that an acceptable solution can be resolved.

V. DATA ACQUISITION AND REDUCTION

V.1 DATA ACQUISITION

The linear inverse techniques, described above, are applied to microearthquake data to determine Poisson's ratio by solving for the velocities of the P- and S- waves in a crustal model. Microearthquake data used in this study were collected from the Socorro, New Mexico area between April, 1975 and February, 1978. The data were collected by the New Mexico Institute of Mining and Technology (NMIMT) geophysics group using various arrays of four to six Spengnether Instrument Company MEQ-800 analog recording units. Each station consists of an MEQ-800 unit, either a Mark Products L4C or Willmore vertical seismometer having natural frequencies of 1.0 and 1.5 Hertz (Hz) respectively, a gain-stable amplifier, a quartz-crystal-controlled timing unit, and a smoked-paper helical recorder which operates at a recording speed of 120 millimeters per minute (mm/min). For further information on these instruments, their specifications and additional data acquisition procedures used in acquiring the microearthquake data for this study, the reader is referred to the descriptions offered by Caravella (1976), Rinehart (1976), and/or Fender (1978).

The area of study is located in the vicinity of Socorro, New Mexico, and includes portions of the Rio Grande Valley and rift system covering about 1075 km^2. The area, located between north latitudes 34.25° and 33.95° and west longitudes

107.1° and 106.75°, was selected on the basis of previous studies of this area and raypath coverage. Originally, raypaths from events to stations which had more than 75 percent of their total length lying inside the study area were used. However, this produced more than 1800 raypaths which proved to require too much computer storage. The data set was reduced to only those events and stations which lie entirely within the study area. This reduced the number of raypaths to 1108. This still produced an overload on the computer when a model consisting of 16 or more blocks was used. So the number of raypaths was reduced to 620 by retaining only those raypaths whose P- and S-wave travel time residuals were less than 0.2 sec. and 0.5 sec., respectively. The values of 0.2 sec. and 0.5 sec. were suggested by Sanford (personal communication, 1979) who felt that after any reading error and station correction have been applied to a travel time, any delay or advance in the observed travel time due to crustal variations would affect the P- and S-wave by not much more than 0.2 and 0.5 seconds, respectively. Of the 245 events comprising the 620 raypaths, 236 of these events had standard deviations on their origin times of less than 1 second. Three events had standard deviations on their origin times of greater than 6 seconds. The nine events with standard deviations greater than one second were eliminated. This reduced the number of raypaths to 600 for 236 events. These events appear in Appendix A, and a complete listing of the data set, including the P- and

S-wave arrival times, appears in Appendix J. Eleven of these 236 events showed calculated depths that were negative. These events were not eliminated because it was assumed that any discrepancies in the microearthquake location would be reflected in the origin time standard deviations. Any negative depths were corrected for within the subroutine program TTYM (discussed below). The difference between the depth of the microearthquake and the station elevation was calculated in this subroutine and this value is squared in the calculations which eliminated the negative numbers (Ward, personal communication, 1979).

The reduction of the number of raypaths to 600 had its advantage in the fact that the problem could be handled by the computer. The disadvantage lies in the fact that the reduced data set greatly reduced the desired level of raypath coverage of parts of the study area.

The seismic stations within the study area and which recorded data used in the study are listed in Table 1 along with their respective locations, elevations and station corrections (see also Figure 1).

The event locations were calculated using a computer program (CRUNCH, written by Roger Ward of N.M. Tech) which utilized a damped least squares method to determine the longitude, latitude, depth, origin time, and the respective standard deviations for a given event. The station locations and an assumed P-wave half-space velocity of 5.8 km/sec, and P-wave arrival times were used as input for CRUNCH. Only

TABLE 1
Station Designations, Locations, Elevations and Station Corrections Used in this Study

Station Name	Station Designation	Latitude (degrees)	Longitude (degrees)	Elevation (km)	Station Correction (secs)
Puerticito de Bowling Green	BG	34.2068	106.8205	1.516	0.00*
Corkscrew Canyon	CC	34.1442	106.9812	1.649	-0.12
Chupadera Mine	CM	33.9501	106.9576	1.640	0.18
Duchess Mine	DM	34.1075	106.8079	1.536	-0.06
Fluorite Mine	FM	34.0829	106.8047	1.537	0.00*
Indian Cave	IC	33.9870	106.9967	1.730	0.14
Nogal Canyon	NG	33.9648	106.9933	1.730	0.13
South Canyon	SC	34.0100	107.0894	2.073	0.25
Stone House	SH	34.1570	106.7802	1.577	0.00[t]
San Lorenzo Canyon	SL	34.2234	106.9910	1.615	-0.08
Tajo Arroyo	TA	34.0498	106.7751	1.558	-0.05
Windmill	WM	34.0120	106.9929	1.673	0.12
Wood's Tunnel	WT	34.0722	106.9459	1.555	-0.15

* calculated correction equals 0.00 with respect to Station WT.

[t] not enough information available to determine a correction, therefore correction set at 0.00.

events recorded by four or more stations are used in this study.

The P- and S-wave arrival times were obtained by reading the seismograms with a Gaertner travelling microscope. This microscope has a reading accuracy equivalent to ±0.003 seconds. Tests have shown that the human eye can read the same record with an accuracy of about 0.02 seconds (Fender, 1978).

The uncertainties σ_i applied to the P-wave travel times were obtained directly from the standard deviations obtained from the computer-calculated origin times. Any inaccuracies in the P-wave arrival times were assumed to have been reflected in the origin time standard deviation given by CRUNCH. Thus, if CRUNCH gives a standard deviation on the origin time of 0.26 seconds, then the uncertainty used for the P-wave travel times for that event is 0.26 seconds. The uncertainties σ_i applied to the S-wave arrival times are relatively harder to determine because the S-wave phase, arriving after the P-wave, may not be clearly evident. From experience, Sanford (personal communication, 1979) indicates that the true S-wave arrival usually lies within 0.2 seconds of the arrival that is normally chosen as the S-wave. Thus, the uncertainties σ_i for the S-wave travel times are obtained by adding 0.2 seconds to the respective origin time standard deviations.

The _a priori_ estimates, τ_j, were obtained in the following manner: The depths of the events used in this study range primarily from near surface to depths of 12 km. It is likely that the microearthquakes originated in the deeper, more brittle Precambrian rocks rather than the overlying softer sediments which tend to transfer stress by plastic deformation more than by brittle fracturing. Thus, the microearthquake depths and the high angles of emergence of the raypaths at the stations indicate that the raypaths travel primarily through the Precambrian. If the station corrections account for the sediments that overlie the Precambrian rocks, then any variations of the velocity of the seismic waves would be due to the variations in the properties of the Precambrian rocks. Hughes and Maurette (1957) have shown that the Poisson's ratio of a rock is dependent on mineral composition of the rock. Thus, the Poisson's ratio of a particular rock can be determined by the percentage of its mineral constituents and the velocities of these mineral constituents. By determining the mineral percentages in the Precambrian rocks in and around the study area, and multiplying these percentages by their respective mineral velocities, and then summing the results, the probable range in the P- and S-wave velocities can be determined. Listed in Table 2a are the laboratory-derived P- and S-wave velocities for the individual mineral constituents (Christiansen and Fountain, 1975). The mineral percentages for the Precambrian rocks near the study area are listed in Table 2b. Assuming that these rocks are a fair representation of the Precambrian material through which the raypaths

Table 2a[1]

Mineral Velocities and Mineral Percentages of Precambrian Basement Rocks Near Socorro, New Mexico

Mineral	P-wave Velocity (km/sec)	S-wave Velocity (km/sec)
Quartz	6.05	4.09
Microcline	6.01	3.34
Plagioclase with 25% Anorthite	6.25	3.41
Biotite-Muscovite	5.16	2.87
Magnetite	7.40	4.20
Hornblende	7.04	3.81

1 Christiansen and Fountain (1975)

Table 2b
Mineral Assemblages and Associate
Mineral Percentages for Precambrian Basement
Rocks Near Socorro, New Mexico and the Associate Velocities

Basement Rock	Percentage of Mineral in Basement Rock Assemblage[2] Qtz	Microcline	Plag An_{25}	Biot-Musc.	Magn	Horn	P-wave Velocity (km/sec)	S-wave Velocity (km/sec)	Poisson's ratio
Qtz-Monz. East of Rio Grande, Socorro, NM	32	34	25	8	1	0	6.029	3.569	0.230
Qtz.-Monz. Oscura Mtns, NM	31	31	30	7	1	0	6.049	3.569	0.233
Qtz.-Monz., Ladron Mtns, NM	31	29	33	6	0.3	0	6.013	3.547	0.233
Qtz.-Monz.-Granite, Los Pinas Hills, NM	38½	40	15½	3½	1	1	6.027	3.620	0.218
Granite-Gneiss, La Joyita Hills, NM	30	45	17	6	1	0	5.966	3.524	0.232
Granite-Gneiss, Polvadera Mtns, NM	35	45	10	8	1	0	5.934	3.547	0.222

Average P-wave velocity - 6.00 ± 0.04
Aveage S-wave velocity - 3.56 ± 0.03
Resultant Poisson's ratio - 0.23 ± 0.01
calculated from average velocities

2 Budding (personal communication, 1979)

travel, the average P- and S-wave velocities and standard deviations are 6.00 ± 0.04 km/sec and 3.56 ± 0.03 km/sec, respectively. The resulting Poisson's ratio for these velocities is 0.23. These velocity standard deviations are used as the values for the a priori estimates, τ_j.

V.2 DATA INVERSION

A computer program was written to perform the calculations outlined in the section entitled Application of Inverse Techniques. The master program (see Appendix B), designed for use on the DEC-20 computer, is a FORTRAN language program that computes the matrices, eigenvalues, eigenvectors, and does matrix inversions and matrix multiplications using IMSL (International Mathematics and Statistics Library) subroutines. A program for calculating the raypath distances in each block was obtained from R. Ward of New Mexico Tech. This program creates a grid pattern of specified dimensions which then uses the station and event locations to calculate the lengths of the raypaths in each block. This program was incorporated into the master program as subroutine TTYM (see Appendix B).

Five different models of the study area were constructed for use in the inversion program. The first model consisted of a single block (Figure 6a). The second model divided the study area into four equal blocks (see Figure 6b). This created four unknowns or model parameters to be obtained from the inversion program. The third model divided the

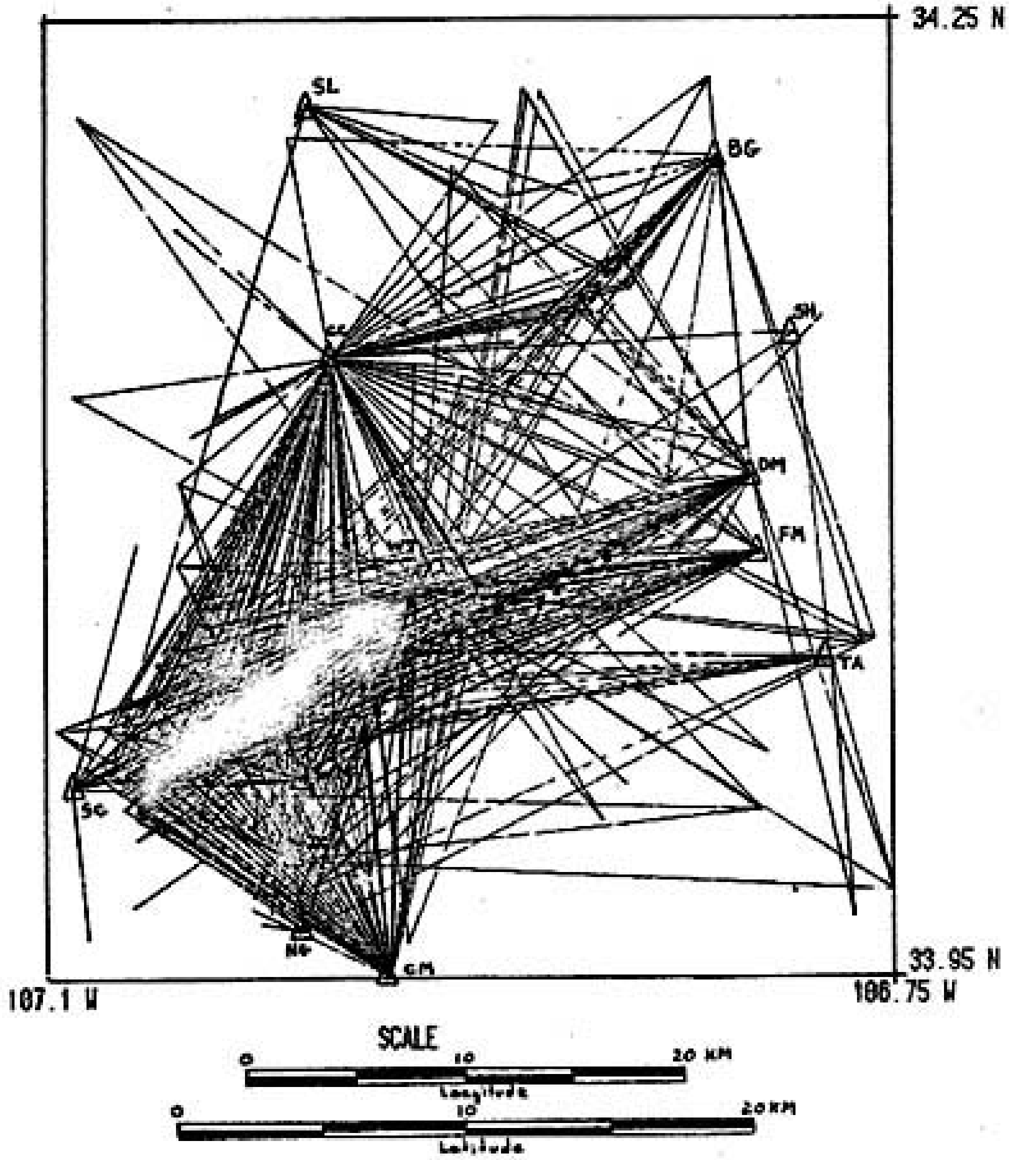

Figure 6a. Model 1 - Single block and distribution of raypaths in study area.

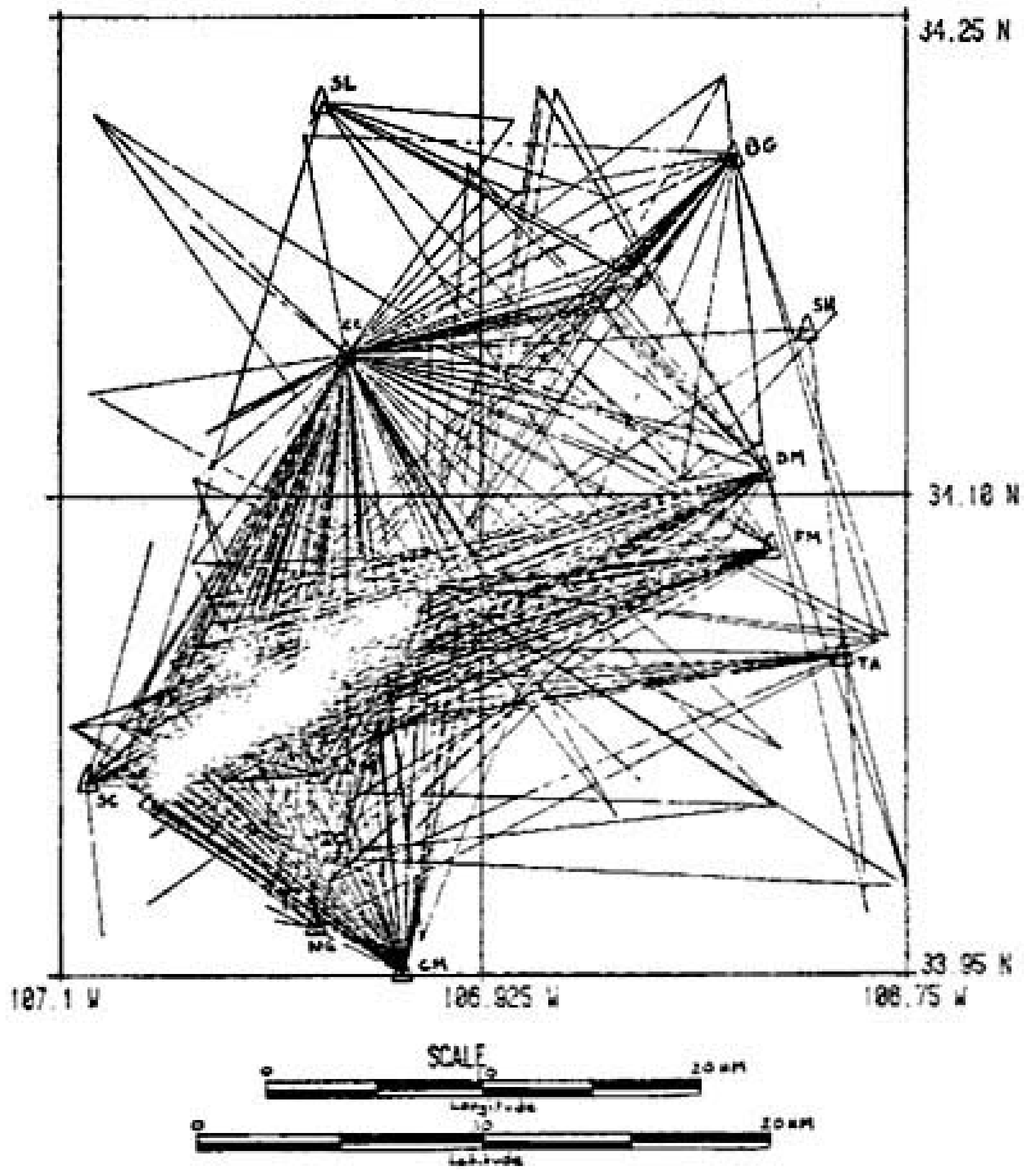

Figure 6b. Model 2 - Study area divided into 4 equal area blocks. Distribution of raypaths in blocks.

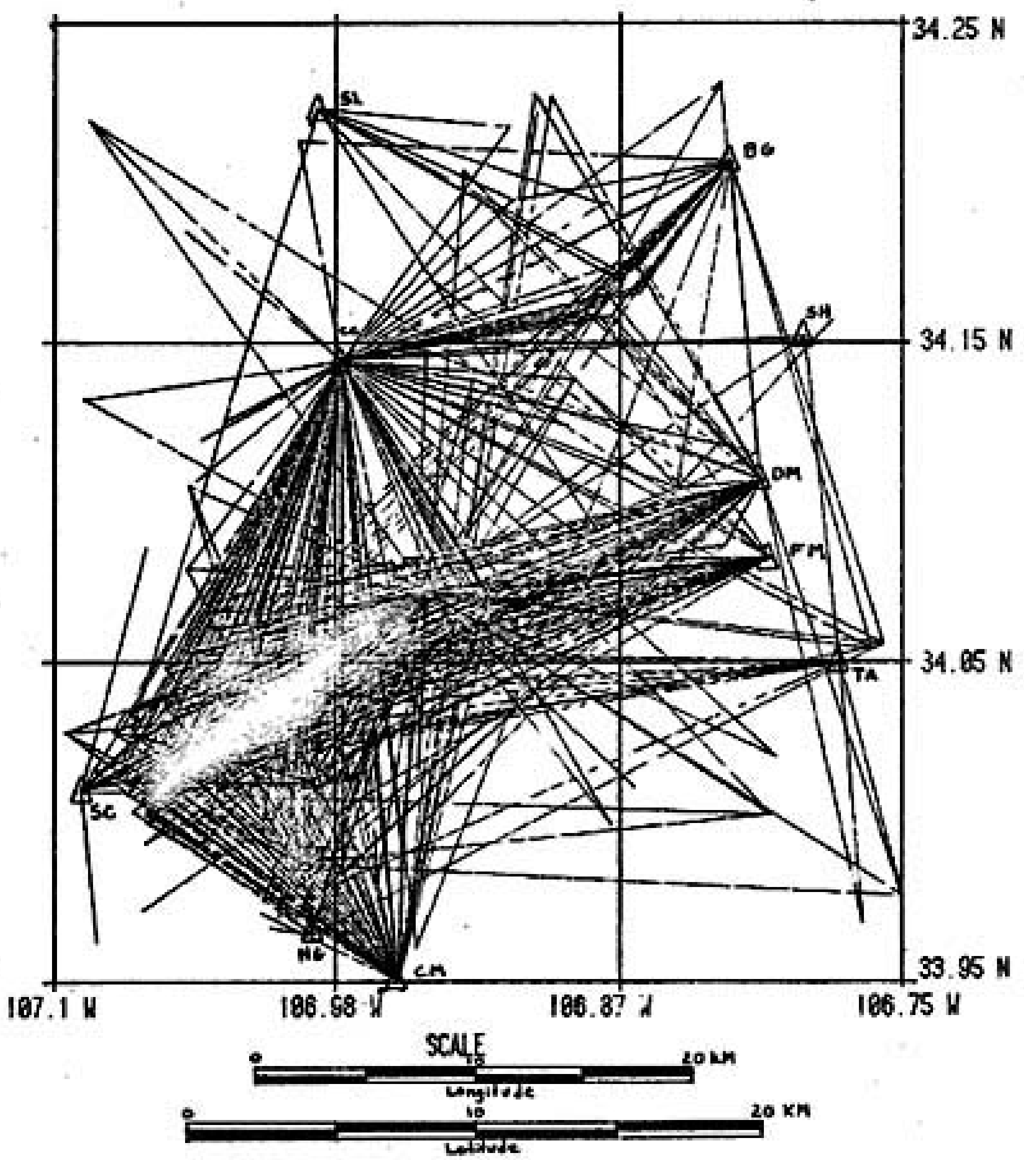

Figure 6c. Model 3 - Study area divided into 9 equi-area blocks. Distribution of raypaths in blocks.

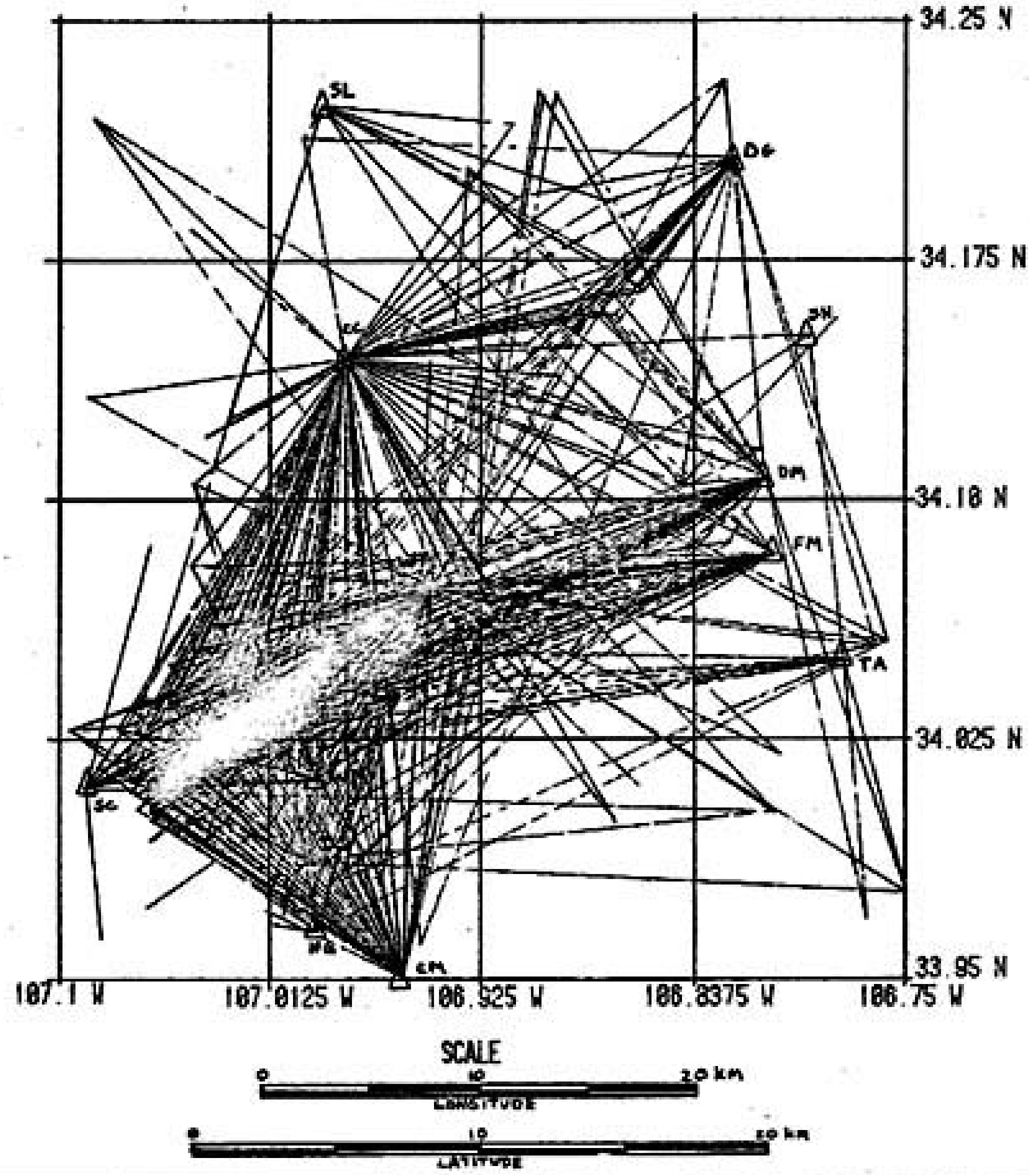

Figure 6d. Model 4 - Study area divided into 16 equi-area blocks. Distribution of raypaths in blocks.

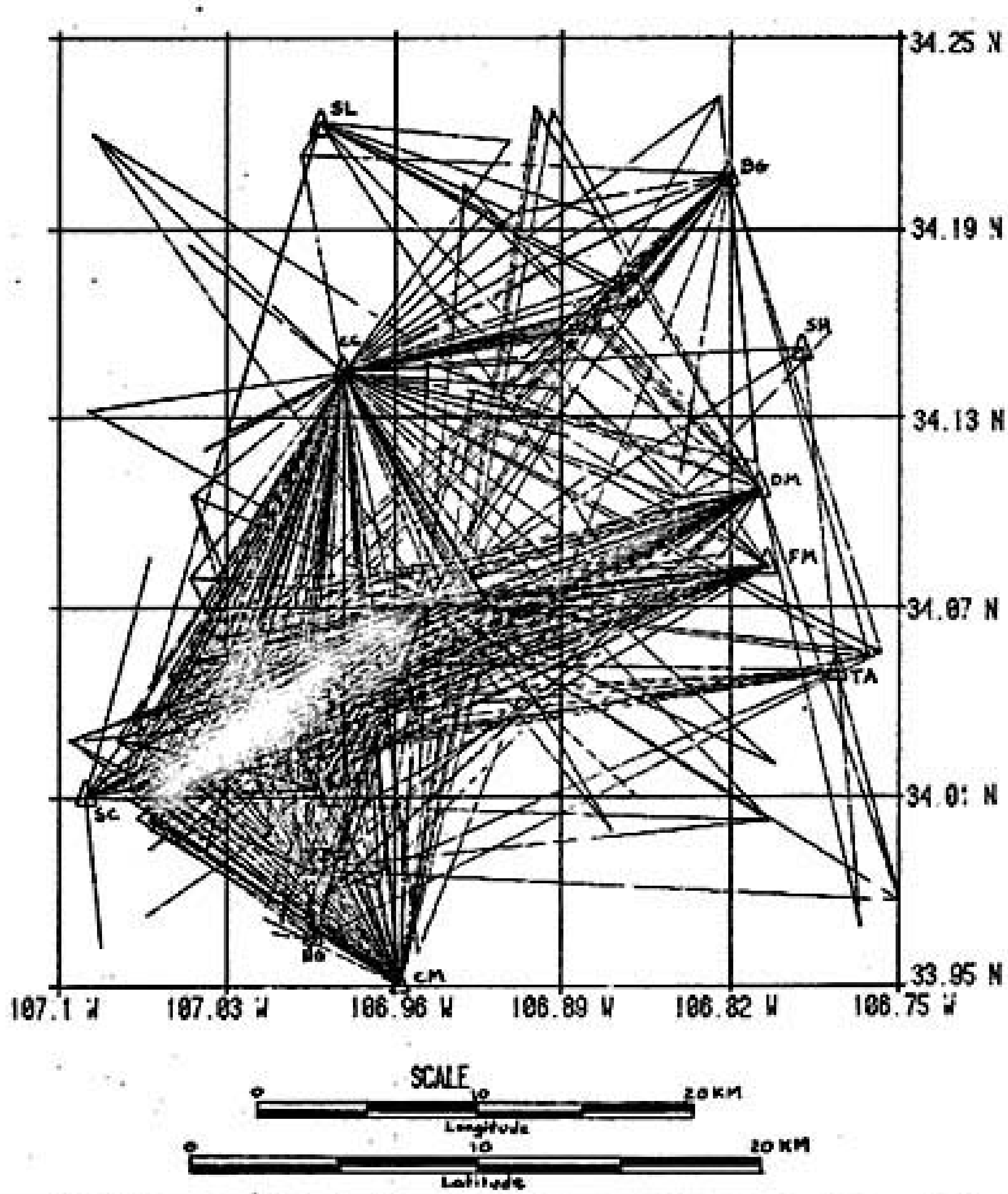

Figure 6e. Model 5 - Study area divided into 25 equi-area blocks. Distribution of raypaths in each block.

study area into nine equal blocks (see Figure 6c) creating nine model parameters. Sixteen model parameters were created in the fourth model, which divided the study area into 16 equal blocks (see Figure 6d). Finally, the fifth model divided the area into 25 equal blocks (see Figure 6e). This created 25 model parameters to be solved for by the inversion process.

Each of the models had initial P- and S-wave velocities of 5.8 km/sec and 3.35 km/sec, respectively, for all of the blocks. The same data set of 600 raypaths was used for each model computation as well as the same σ_i's (listed in Appendix A) and τ_j's.

The model parameters, which are the velocities of the P- and S-waves for each block, were designated as α_j and β_j, respectively.

For computer efficiency, the program was designed to set up the matrix A and calculate the α_j's and β_j's separately. The program calculated the respective eigenvalues and eigenvectors for the α and β calculations and proceeded with the decomposition; that is, the lowest eigenvalue and eigenvector was systematically eliminated and the velocities, standard deviations, and R value was calculated each time an eigenvalue was eliminated. Thus, if m eigenvalues and eigenvectors were calculated for the α calculations, for example, then m different sets of P-wave velocities and standard deviations and m R values were obtained.

The choice of the set of velocities to be used as a new model was based on the following criterion:

1) If the R value was greater than 1.0, then the alpha and/or beta decomposition closest to 1.0 was used.

2) If the R value was less than 1.0, the velocity distribution chosen was that which had the average of its standard deviations closest to, but less than, the _a priori_ estimate, τ. For example, if keeping p of the m eigenvalues generated for the P-wave solution produced an average standard deviation that was less than 0.04, which is the P-wave _a priori_ estimate, then these P-wave velocities obtained by keeping p eigenvalues were used as new model velocities, if R was less than 1.0. The upper limit of the average of the standard deviations for the S-wave model was set a 0.03 seconds.

The two chosen sets of velocity distributions were applied to equation (7) to calculate a Poisson's ratio distribution for this new model, which was created by the chosen velocity distributions. This new model was again applied to the program and the procedure repeated. Each time that this procedure was repeated constituted one iteration. The program was allowed to iterate in the manner described above until no significant changes occurred in the results. This was usually attained after two iterations.

VI. DISCUSSION AND DATA ANALYSIS

Each of the five models described above were subjected to the linear inverse procedure. Though the preferred solutions for the five models differ, they exhibit similar general characteristics.

Retaining all eigenvalues gives the classical least squares solution. This solution yields the largest changes in the velocities from those of the initial model as well as the largest standard deviations. This occurs because the solution is most data dependent when all of the eigenvalues are retained.

Systematically eliminating the lowest eigenvalues, that is, proceeding with the decomposition, effectively eliminates the data dependency of the model parameter or block that has the least amount of data. The greatest effect of eliminating an eigenvalue is evident in the block associated with the eigenvalue that was eliminated. The standard deviation of that block decreases and its associated velocity approaches that of the initial model.

As eigenvalues are eliminated, the standard deviations decrease and the velocities approach those of the initial model. This occurs because eliminating eigenvalues decreases the number of degrees of freedom. Nearly complete model dependency is achieved when only the largest eigenvalue is retained.

R for all five models was initially 1.88 and 0.90 for the α and β calculations, respectively. The initial R values were the same for all five models because the same initial P- and S-wave velocities of 5.8 km/sec and 3.35 km/sec, respectively, were assumed. Prior to each decomposition sequence (iteration), an R value was calculated for the model. The R value obtained when all eigenvalues were retained was initially much smaller than the R for the initial model. As the decomposition proceeds, i.e., as eigenvalues are eliminated, the R value increases until it approaches the value of the initial model. This is because model dependency is being approached. As expected, the R values for the new initial models tend to decrease slightly from iteration to iteration indicating better agreement between model parameters and data is being attained.

The final R values for the preferred alpha solutions for the five models are all greater than 1.0. Though the values are not much larger than 1.0 (around 1.4), this does imply that 1) the models used for the P-wave calculations are somewhat crude, i.e., the area could have profitably been divided into more blocks, and/or 2) the uncertainties, σ_i, used are too small. Because R is greater than 1.0, the P-wave velocities chosen to be carried to the next iteration are based on the corresponding R that is closest to 1.0. Since the R value is smallest when all eigenvalues are retained, the P-wave velocities chosen are always those of the least squares solution, i.e., all eigenvalues retained.

This solution also has the largest standard deviations of any of the solutions.

The R values for the S-wave calculations are consistently less than 1.0. Again, the values are not much less than 1.0 (around 0.8). However, this does imply that 1) the model given for the S-wave is somewhat too detailed, i.e., too many blocks are used, and/or 2) the uncertainties, σ_i, used are too large. Because R is less than 1.0 the preferred S-wave solution is based on the average of the standard deviations that is less than, but closest to, 0.03 sec.

The same model, in terms of the number of blocks, is applied to both the α and β calculations. The R values indicate that a more detailed model could be used for the α calculations and a model with less blocks could be used for the β calculations in order to obtain R values closer to 1.0. However, this would present problems when the two models are combined to calculate Poisson's ratios because of the difference in the number of blocks and block dimensions of the two models. Thus, a smaller difference between the R values of the α and β calculations may be achieved by changing the uncertainties on the model. The β uncertainties are 0.2 seconds greater than the α uncertainties. By lowering the uncertainties on the β calculations, the R value would be increased. If the additional 0.2 seconds is somewhat too large, then this would imply that the S-wave arrival could be identified to better than ±0.2 seconds.

The Poisson's ratios produced for each model are reasonable values. In other words, there are no extreme values such as 0.1 or 0.4. The standard deviations on the Poisson's ratios are dominated by the large standard deviations on the P-wave velocity solutions.

The preferred results for each of the five models are examined in detail below, and summarized in Table 3.

Model 1 uses a single block of dimensions 0.35° x 0.3° (longitude x latitude = 31.93 km x 33.68 km) to describe the entire study area. This produces only one eigenvalue when the linear inverse techniques are applied to the model. The results of the iterative procedure appear in Appendix C.

After one iteration, the results are unchanged, which indicates that the best solution has been attained. The results show that Poisson's ratio for the entire study area is 0.265 ± 0.001 (see Figure 7). The R value of 1.390 suggests that the model is somewhat crude. This is understandable because this is the simplest model possible. However, this R value is not unreasonable.

Model 2 divides the study area into four equi-area blocks (see Figure 8). Appendix D gives the computed results for model 2. Table 3 summarizes the results obtained for this model. The R value calculated for the final model stabilizes after one iteration (see Table 3).

The basic difference between this model and Model 1 is that more model parameters are used in this model. This results in lower R values for the 4-block model, indicating that the process has found a better solution.

Table 3
Summary of Model Results

Model	Number of blocks	Block Dimensions (longitude x latitude) degrees	Block Dimensions (longitude x latitude) kilometers	Typical Block Area (km^2)	Number of Eigenvalues Retained for Final Model α	Number of Eigenvalues Retained for Final Model β	Number of iterations for final model	R Values α	R Values β	R Values final model
1	1	0.350 x 0.300	31.93 x 33.68	1075	1	1	1	1.751	0.893	1.390
2	4	0.175 x 0.150	15.96 x 16.84	269	4	4	1	1.620	0.867	1.299
3	9	0.117 x 0.100	10.64 x 11.23	119	9	6	1	1.429	0.830	1.169
4	16	0.088 x 0.075	7.98 x 8.42	67	16	8	2	1.216	0.759	1.013
4'	16	0.088 x 0.075	7.98 x 8.42	67	11	8	2	1.225	0.759	1.019
5	25	0.070 x 0.060	6.39 x 6.74	43	22	10	2	1.234	0.771	1.029
5'	25	0.070 x 0.060	6.39 x 6.74	43	14	10	3	1.287	0.771	1.061

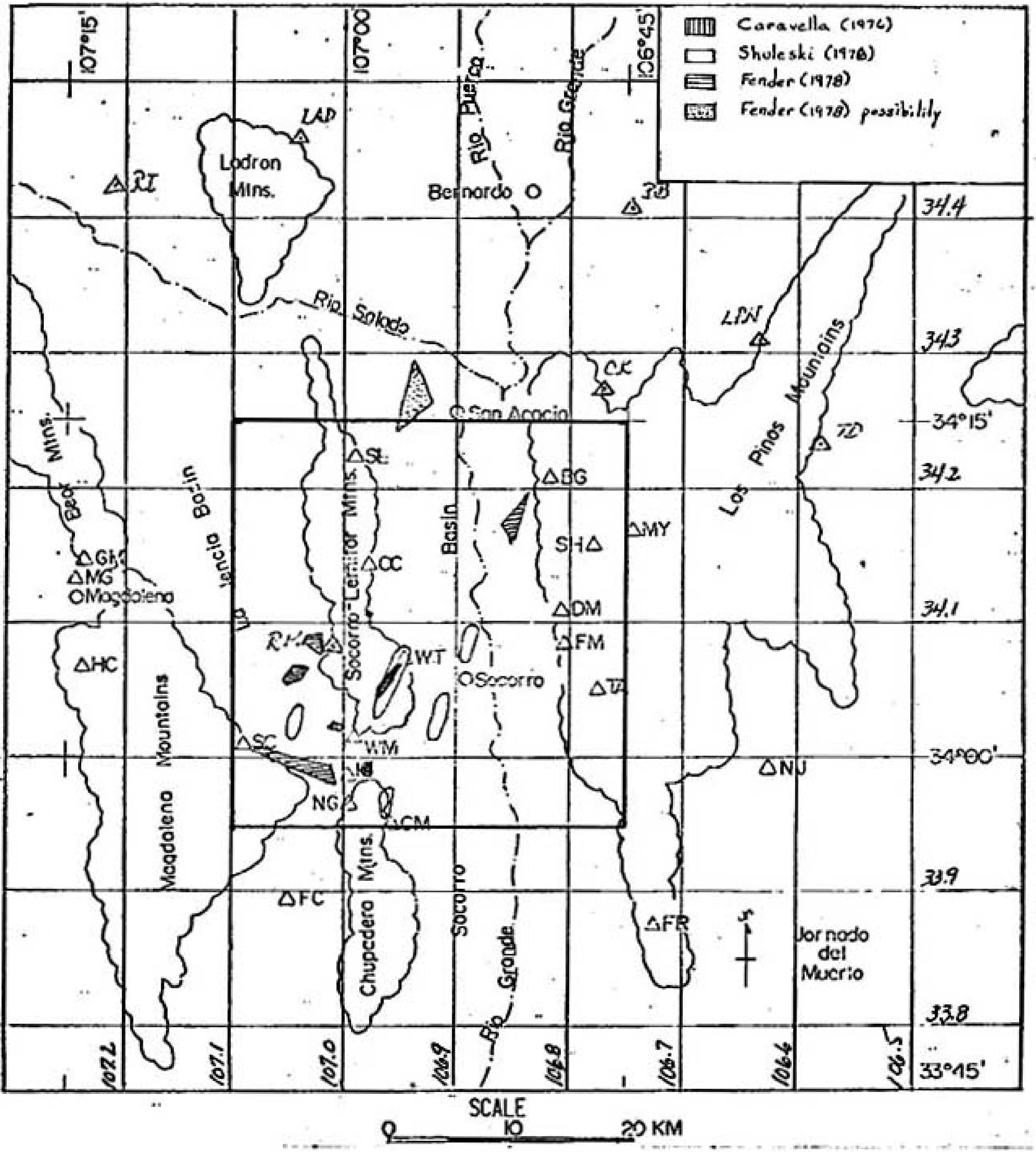

Figure 7. Locations of previously determined areas with high Poisson's ratios in relation to the Poisson's ratio distribution of Model 1 (overlay).

The distribution of the resulting Poisson's ratios are shown in the overlay of Figure 8. It is evident that the linear inverse method defines higher than average Poisson's ratios (0.278 and 0.291) for the northern half of the study area. These values are not significantly different even at their 95% confidence limits.

Model 2 will serve as example of the effects that data quantity has on the eigenvalues. The P- and S-wave solutions for Model 2 are obtained while keeping all eigenvalues and eigenvectors (see Table 3). The eigenvalues produced from the initial model are 5.06, 2.48, 2.26, and 1.67 (see Appendix D). Eliminating the lowest eigenvalue causes the greatest velocity and standard deviation changes to occur in block 1. This implies that block one has the least amount of data. Figure 6b supports this implication. When the next lowest eigenvalue is eliminated, block number 4 exhibits the next greatest change indicating that block 4 has the next least amount of raypath travel distance. Eliminating the three lowest eigenvalues causes block 2 to take the next plunge toward model dependency. Block 3 shows the least drastic velocity and standard deviation changes which indicates that block 3 has the most data. Figure 6b confirms this indication that block 3 does indeed contain the maximum amount of data in terms of raypath travel distances.

Model 3 divides the study area into nine equi-area blocks (see Figure 9). This creates nine model parameters

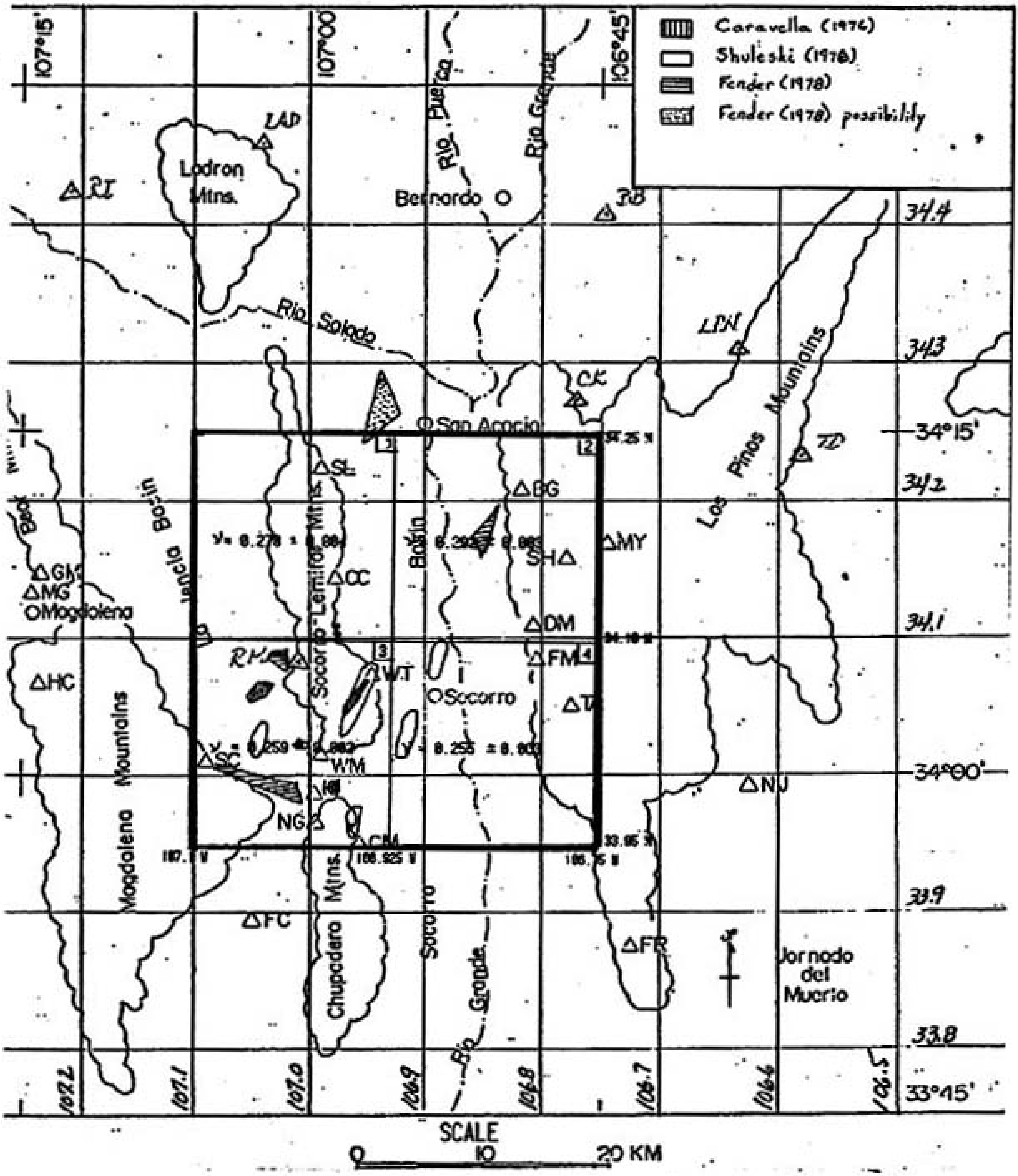

Figure 8. Locations of previously determined areas with high Poisson's ratios in relation to the Poisson's ratio distribution of Model 2 (overlay).

to solve and nine eigenvalues and eigenvectors to decompose. Appendix E gives the results for this model. The iterative process obtains an R value of 1.17, which indicates that a more complex model such as this one produces a better solution than Model 2. Table 3 summarizes the results from Model 3.

The final model chosen is that which is produced after one iteration. Further iterations reveal minor changes in the velocities and standard deviations, but the final model R value remains stable.

The overlay of Figure 9 shows the Poisson's ratio distribution obtained from the final model of iteration 1. The Poisson's ratios remain above the previously assumed value of 0.25, especially in the northwest and northcentral portions of the study area, with one particularly large value for block 2.

The blocks in Model 3 are still too large to delineate small areas of anomalous Poisson's ratios, so Model 4 is created in an attempt to better delineate small anomalous areas. Model 4 divides the study area into 16 equi-area blocks (see Figure 10). This creates 16 eigenvalues and eigenvectors to decompose and 16 model parameters to solve when the linear inverse techniques are applied. Appendix F gives, in more detail, the results of this model while Table 3 summarizes these results. The R value calculated for the final model is 1.013. This R value indicates that the final model has a better relation between the size and number of parameters and/or the uncertainties on the data are more compatible with this model than with Model 3.

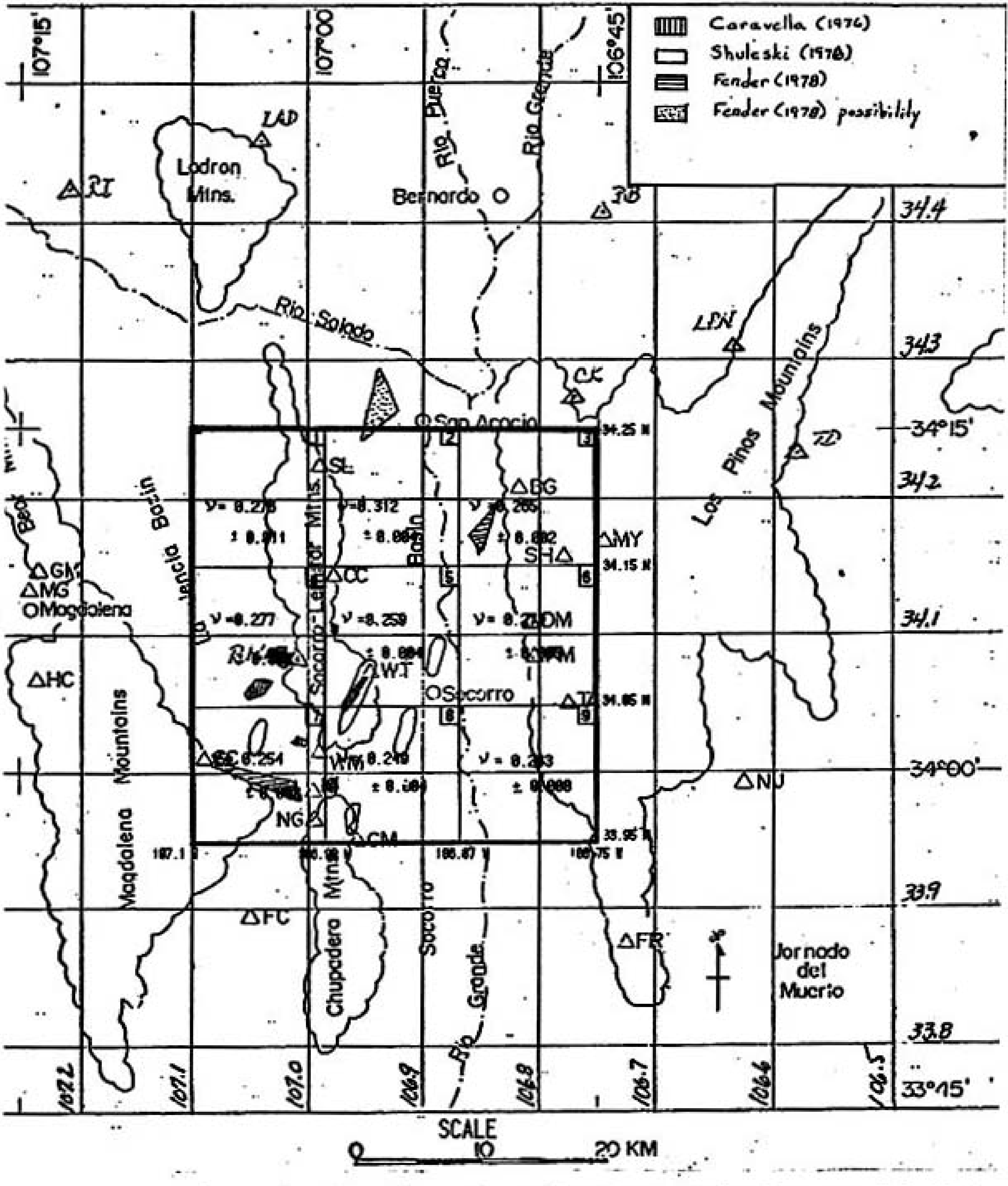

Figure 9. Locations of previously determined areas with high Poisson's ratios in relation to the Poisson's ratio distribution of Model 3 (overlay).

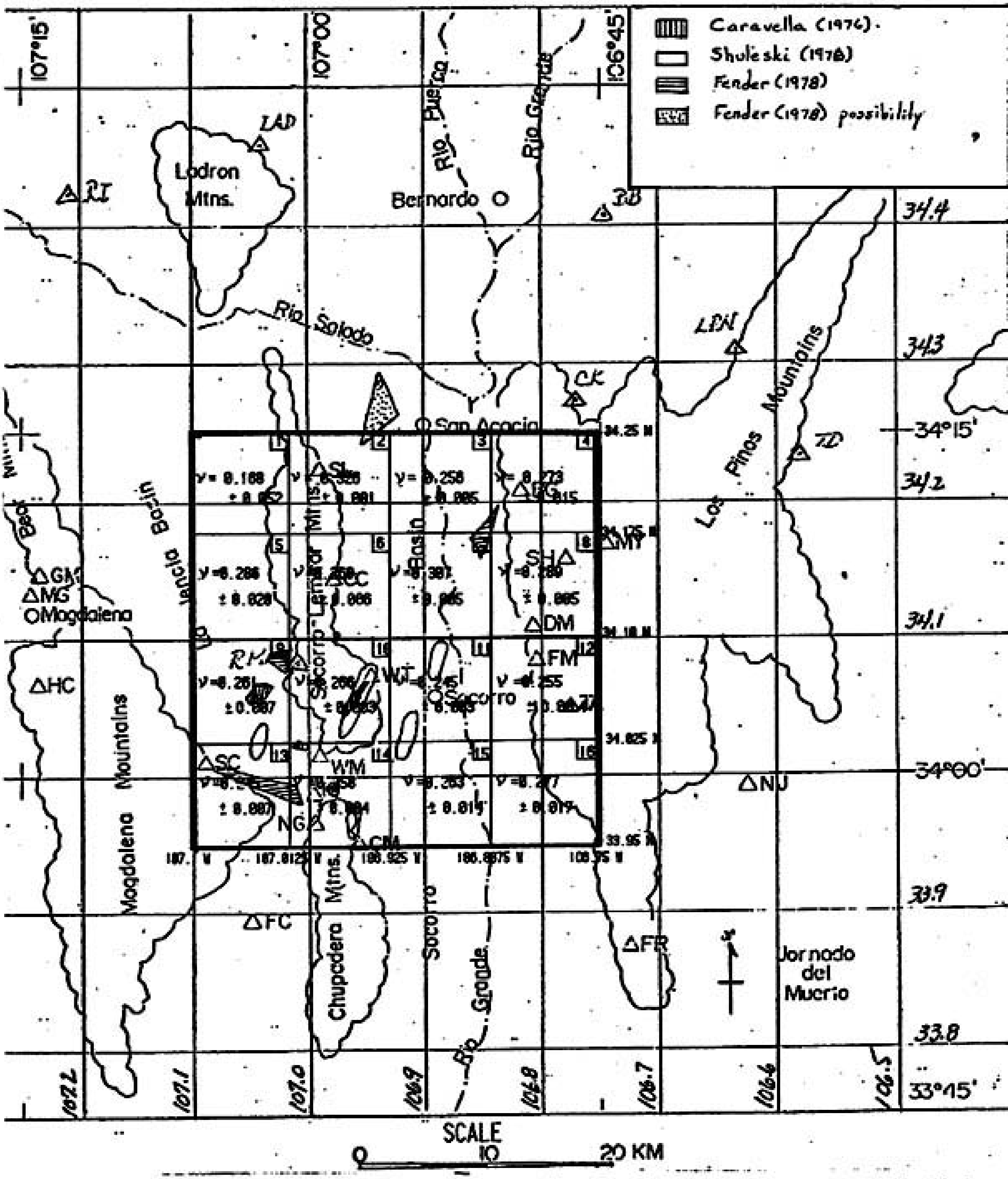

Figure 10. Locations of previously determined areas with high Poisson's ratios in relation to the Poisson's ratio distribution of Model 4 (overlay).

The only changes that occur after two iterations are minor changes in the block velocities and standard deviations (see Appendix F). Thus, the final velocities for Model 4 are chosen from the solutions of iteration 2. This solution produces an R value on the final model of 1.013 (see Table 3).

The overlay of Figure 10 shows the Poisson's ratio distribution obtained for this model. The standard deviations on the velocities are larger than for the previous model, especially on those blocks that have few raypaths. Still evident is the large Poisson's ratio obtained for block 2. At the 95% confidence level the minimum Poisson's ratio that this block could attain is 0.324, which is still anomalously high. It should be noted that the standard deviation on the Poisson's ratio of block 10 is about 2.5 times larger than that of block 2, yet block 10 has the most data while block 2 is one of the five blocks with the least data (see Figures 6d and 10). It would be expected that the block with the most data would have a lower standard deviation than a block with less data. However, an inspection of the number of eigenvalues retained for the chosen solution reveals that, though all 16 eigenvalues are retained for the α calculations, the solution for the β calculations retains only eight eigenvalues. Thus, the solution for block 2 would be more model dependent than data dependent, since its eigenvalue has been eliminated, and thus, the standard deviation on Poisson's ratio for block 2 could conceivably be lower than that for a block with more data. Other blocks with large Poisson's ratios are blocks 7 and 8 (see Figure 10). A low Poisson's ratio is associated with block 1. However, its standard deviation range brings the value to a maximum Poisson's ratio of 0.27 with 95% confidence.

Model 5 is created to study the effects of additional blocks on the inversion method, as well as to attempt to further delineate smaller areas of anomalous Poisson's ratios. Appendix G gives the results of this model. The linear inverse technique creates 25 eigenvalues and eigenvectors for this model. Because of the large differences between the largest and the three smallest eigenvalues obtained for this model, and to save computer computational time, the three lowest eigenvalues are immediately eliminated.

Table 3 summarizes the results obtained for this model. This R value is slightly larger than that obtained for Model 4 (see Table 3), which indicates that no further improvement in the model is gained by increasing the number of model parameters. Furthermore, additional model parameters are not justifiable unless a better distribution of data is obtained because otherwise some of the blocks would not have any data associated with them.

The final model solutions stabilize after two iterations with only minor changes occurring thereafter; therefore, the final Model 5 is selected from the solutions of iteration 2 (see Table 3). Any iterations thereafter produces only minor changes in the Poisson's ratios and their associated standard deviations, with the R value remaining stable. The overlay of Figure 11 shows the Poisson's ratio distribution for Model 5. Model 5 delineates three lower-than-average Poisson's ratios in blocks 1, 6, and 23. At the upper end of the 95% confidence interval, these values are 0.246, 0.244, and 0.118 for blocks 1, 6, and 23, respectively, and thus only block 23 can be considered to have an anomalously low Poisson's ratio. Blocks 2, 7, 9 and 11 show higher-than-average Poisson's ratios at the 95% confidence level.

All five models have the α solutions for the next iteration chosen on the basis of R. Table 3 shows that the α solutions that are chosen for the final Models 1 through 4 have all eigenvalues retained. This causes the α solutions to be totally data dependent, and produces large standard deviations on the P-wave velocities which increase the standard deviations on the Poisson's ratios as well. The β solutions for all five models are selected on the basis of the decomposition that is closest to, but less than, 0.03 seconds, the calculated α _a priori_ estimate (see Table 3). To determine what effects the standard deviation-based solutions have on the final model, the five initial models are again introduced to the linear inversion program with the modification that the α solutions are to be selected using as a basis the average of the standard deviations of the calculated P-wave velocities. The decomposition solutions that have an average of the standard deviations closest to, but less than, 0.04 seconds, the α _a priori_ estimates, are

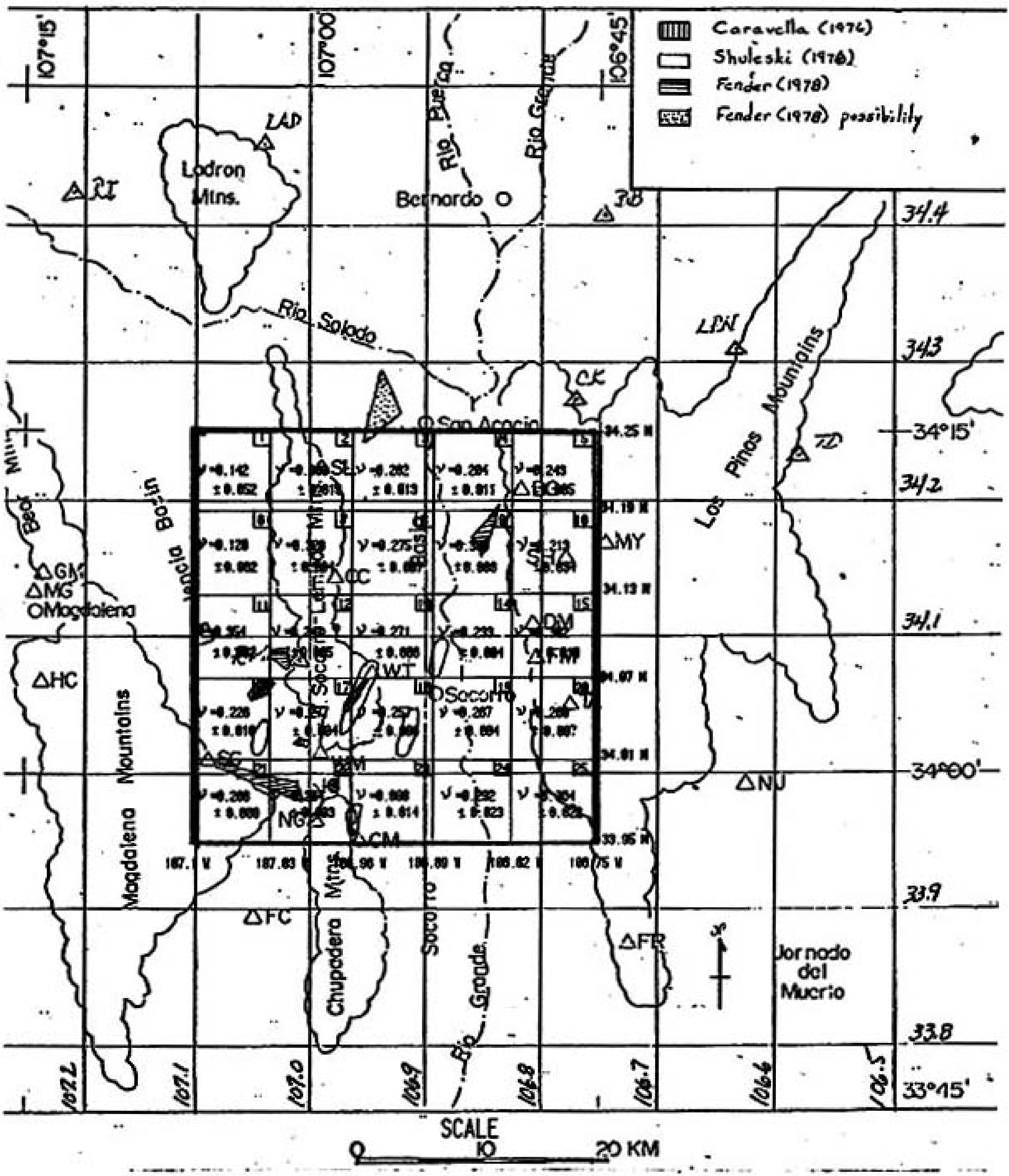

Figure 11. Locations of previously determined areas with high Poisson's ratios in relation to the Poisson's ratio distribution of Model 5 (overlay).

selected as the initial model for the next iteration. The solutions are based on an average of the standard deviations of the calculated S-wave velocities of 0.03 seconds as described for the previous models. The only α models that this new modification affects are Models 4 and 5. Models 1, 2, and 3 all have an average α standard deviation less than 0.04 seconds when all eigenvalues are retained, and to rerun these models would only produce the same results.

When these new modifications are applied to Model 4, the solutions selected for the α calculations are those obtained when 11 eigenvalues are retained. This put more model dependency on blocks 1, 4, 5, 15, and 16 than on the other blocks. The β solutions, as before, are obtained when eight eigenvalues are retained. This put more model dependency on blocks 1, 4, 5, 15, and 16 as well as blocks 2, 8, and 12 than on the other blocks. With nearly complete model dependency, blocks 1, 4, 5, 15, and 16 would be expected to exhibit values similar to those of the initial model with small standard deviations. Blocks 2, 8, and 12 would be expected to be close to the initial model, but with somewhat larger standard deviations. The result for this modified Model 4, herein designated as Model 4', are selected from iteration 2. Listed in Table 3 are the results obtained for Model 4'. Appendix H shows the computer output for this model. The Poisson's ratios calculated for this final model are shown in Figure 12. As expected, blocks 1, 4, 5, 15, and 16 have Poisson's ratios of about 0.25, the assumed initial model Poisson's ratio. These blocks also exhibit the lowest standard deviations. However, blocks 2, 8, and 12 do not show model dependence to the degree that was first expected.

Model 4' has an R value slightly larger than that of Model 4 (see Table 3) because some of the α solutions chosen for Model 4' are more model dependent than those of Model 4, which are all data dependent. This causes the final Model 4' to be more model dependent than final Model 4. Being more model dependent implies that the final R value on the Model 4' would be closer to the initial R value for Model 4' than the final R value for Model 4 would be to its initial R value.

Comparing Figures 10 and 12, it is evident that the lower than average Poisson's ratio associated with block 1 is eliminated. Similarly, the relatively large Poisson's ratios associated with blocks 4 and 5 are reduced. The high Poisson's ratio associated with block 2 is reduced, as well. However, at the 95% confidence level, block 2 could still be a higher than normal 0.313. The remaining blocks show little or no changes in their Poisson's ratios or standard deviations.

Considering the Poisson's ratios for both Models 4 and 4' at the 95% confidence level, the only blocks that show anomalous Poisson's ratios are blocks 2 and 8. Even at the 95% confidence level, these Poisson's ratios are higher than normal.

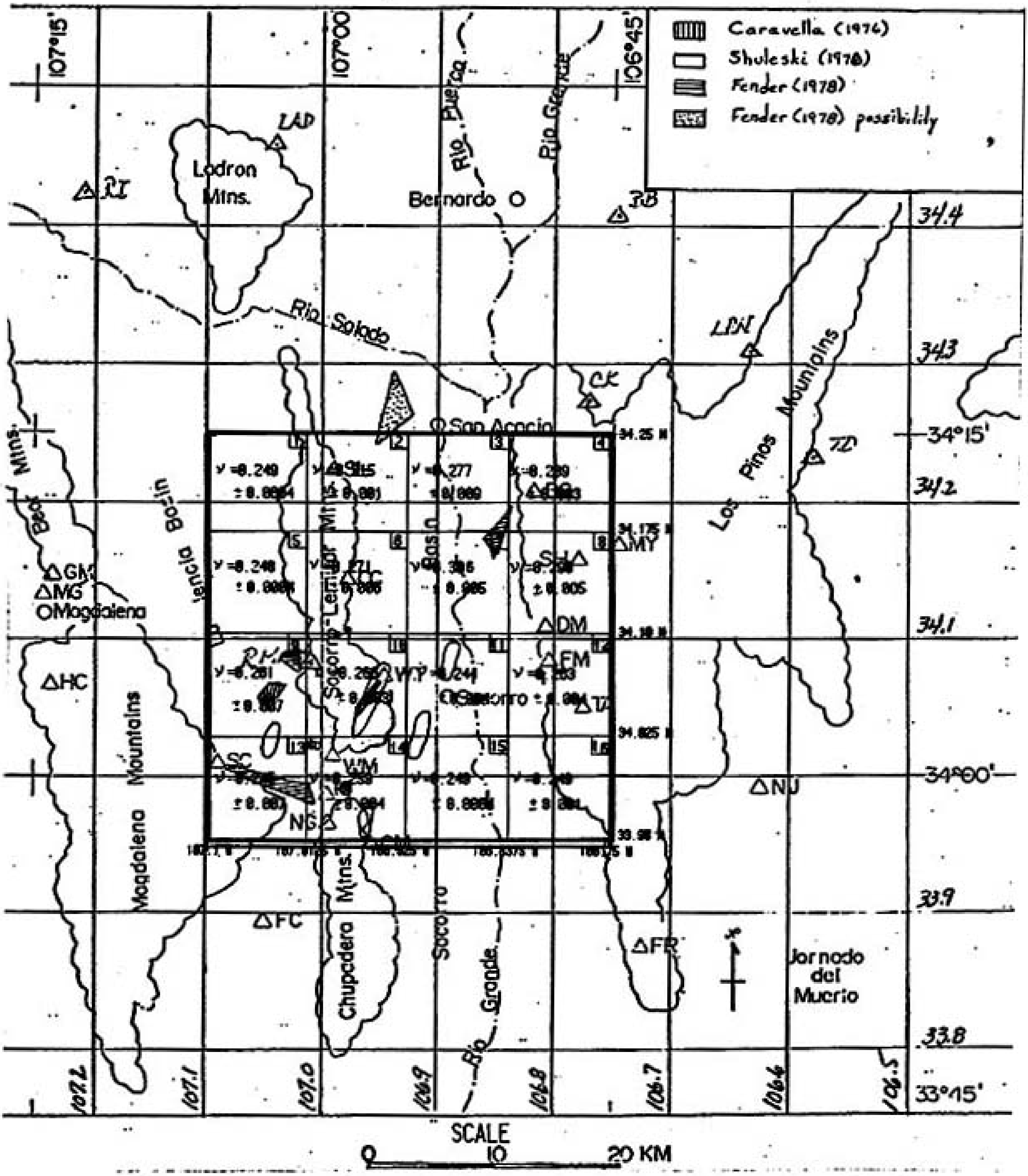

Figure 12. Locations of previously determined areas with high Poisson's ratios in relation to the Poisson's ratio distribution of Model 4' (overlay).

Model 5 was also rerun to obtain solutions based on an average of the standard deviations. The α solutions for each iteration for this new Model 5, herein designated as Model 5', are selected from the decomposition that retained 14 eigenvalues. This eliminated the eigenvalues associated with blocks 1, 2, 3, 4, 5, 6, 11, 15, 20, 24, and 25. The β solutions are selected from the decomposition that retained ten eigenvalues. This eliminates the eigenvalues associated with the same blocks as those eliminated in the α calculations, as well as blocks 7, 10, 21, and 23. Hence, the same argument may be applied here as was applied for Model 4', that is, blocks 1, 2, 3, 4, 5, 6, 11, 15, 20, 24, and 25 should have Poisson's ratios of approximately 0.25 which is the initial model assumption. The final Model 5' is selected from iteration 3 and the results summarized in Table 3. Appendix I shows the computer output for this model. The final R value is 1.061.

Model 5' has a slightly larger R value than does Model 5 for the same reasons described above for Models 4 and 4'.

Figure 13 shows the Poisson's ratios (ν) calculated for Model 5'. The lower than normal ν's associated with blocks 1 and 6 are eliminated because these blocks are more model dependent than data dependent for this model. However, the low Poisson's ratio associated with block 23, though higher than that obtained for Model 5, is still evident in Model 5'. High ν's are still associated with blocks 2, 3, 7, 8, 9, 12, 15, and 17. Anomalously high Poisson's ratios are associated with blocks 4, 10, 20 and 21 but are not evident in Model 5.

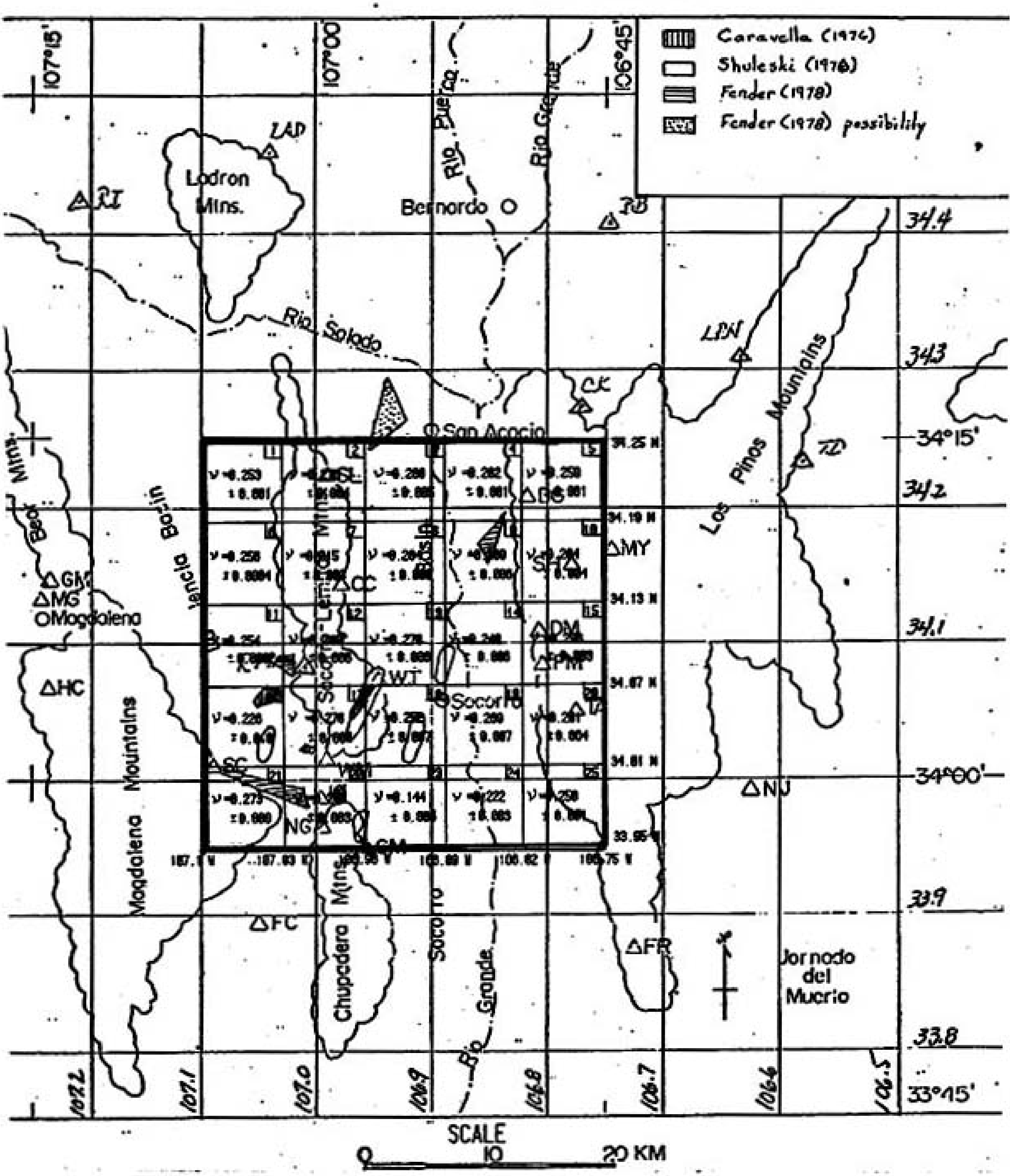

Figure 13. Locations of previously determined areas with high Poisson's ratios in relation to the Poisson's ratio distribution of Model 5' (overlay).

Comparing the two models in the 95% confidence level the low Poisson's ratio associated with block 23 would still be low with a maximum of 0.156 for Model 5'. Blocks 3, 4, 7, 9, 10, 15, and 20 would still have ν's greater than 0.27.

VII. INTERPRETATION

If the average Poisson's ratio for the entire study area is assumed to be that obtained from Model 1, i.e., 0.265 ± 0.001, then the average could conceivably be as high as 0.267 and as low as 0.263 at the 95% confidence level. This value for Poisson's ratio may be large when compared with the findings of Sakdejayont, (1974), and Fender (1978), however, this average Poisson's ratio correlates well with the Poisson's ratio of 0.262 obtained by Caravella (1976). The value of 0.265 is a good average for this total area, however, the standard deviation is misleading because the R value obtained for this model is greater than 1.0 (1.39). A better standard deviation is attained by finding the average Poisson's ratio of the model that has the R value closest to 1.0 for the final model. This is Model 4. Averaging the Poisson's ratios obtained for this model gives an average Poisson's ratio of 0.265 ± 0.034. This is the same value obtained for Model 1 and the same standard deviation obtained by Caravella (1976). This standard deviation is not as misleading as that obtained by Model 1. The average P-wave velocity of 5.895 ± 0.006 km/sec obtained for the study area corresponds well with an average P-wave velocity of 5.9 km/sec obtained by Ward (1979, personal communication), who has a similar study in progress using linear inverse techniques on nearly the same area. This average Poisson's ratio may provide a good basis for determining anomalous areas. From the determination of the a priori estimates by mineral percentages of the Precambrian basement near the study area, an average Poisson's ratio of 0.23 ± 0.0078 is determined (see table 2). At the 95% confidence level, this value may range from 0.214 to 0.246. Thus, let 0.214 be the lowest accepted value as an average. With these limits, let any Poisson's ratios which are below 0.21 be considered anomalously low at the 95% confidence level. Similarly, let any Poisson's ratios greater than 0.27 be considered anomalously high at the 95% confidence level. It should be noted that these limits, though supported by some evidence, are somewhat subjective.

Of the seven models studied, Model 5' will be chosen as the preferred model for further interpretation because 1) the R value is very reasonable (1.061); 2) the blocks are small enough to determine small anomalous areas; and 3) the relationship between model or data dependency of the blocks with the amount of data in each block has the best correspondence. Table 4 summarizes the anomalous areas found by Model 5'.

In any one block, the raypaths traversing the block sample the block where the raypaths passes through it. For example, block 22 of Model 5' (see Figure 6c) has raypaths passing primarily through the northern two-thirds of the block. Thus, the Poisson's ratio calculated for the entire block is actually representative of the northern two-thirds of the block.

TABLE 4
Results of Anomalies of Model 5'

Anomaly	Block Number	Number of Eigenvalues Retained α	β	P-wave Velocity (km/sec ± St. dev.)	S-wave Velocity (km/sec ± St. dev.)	Poisson's Ratio ± St. dev.)
A	23	14	10	5.338 ± 0.073	3.443 ± 0.029	0.144 ± 0.003
		14	14	5.338 ± 0.073	3.103 ± 0.011	0.244 ± 0.018
B	3	14	10	6.094 ± 0.073	3.367 ± 0.011	0.280 ± 0.005
B	4	14	10	5.952 ± 0.049	3.279 ± 0.022	0.282 ± 0.001
B	10	14	10	6.049 ± 0.055	3.322 ± 0.007	0.284 ± 0.004
		14	14	6.049 ± 0.055	3.323 ± 0.074	0.284 ± 0.008
B	20	14	10	5.792 ± 0.04	3.200 ± 0.046	0.281 ± 0.004
C	15	14	10	6.078 ± 0.072	3.274 ± 0.023	0.296 ± 0.003
D	9	14	10	5.991 ± 0.040	3.149 ± 0.058	0.309 ± 0.006
E	7	14	10	6.415 ± 0.021	3.332 ± 0.033	0.315 ± 0.003

With this in mind, and Model 1 as a control, Figure 14 shows the possible locations of the anomalies discerned by Model 5' on the basis of raypath coverage in each block. It is evident that the linear inversion method describes only one anomalous area (D) that corresponds to any of the anomalies found from previous studies. This is the anomaly found by Fender (1978) which is located in the east-central Socorro basin (block 9). Fender found that this anomalous area had a Poisson's ratio of 0.275. The linear inversion method obtained a Poisson's ratio of 0.309 for this same area. Block 9 from Model 5' shows a normal P-wave velocity and a lower than normal S-wave velocity (see Table 4). This indicates that the anomaly is due to crustal characteristics, such as partial melt, that decrease the S-wave velocity, but which have little or no effect on the P-wave velocity. Figure 15 shows the anomaly D.

Area A, which has a low Poisson's ratio, corresponds to an anomalous area found by Shuleski (1976) (see Figure 14). Shuleski defined this anomalous area on the basis of SV-wave screening, which would imply that a high Poisson's ratio would be required. However, area A, which corresponds to Shuleski's area, is a low anomaly, which would not screen or delay any seismic waves. This low anomaly would imply an increase in the seismic wave velocities. As previously discussed, in the decomposition and selection of α and β solutions for model 5', block 23 had α solutions that were data dependent, while the β solutions were model dependent.

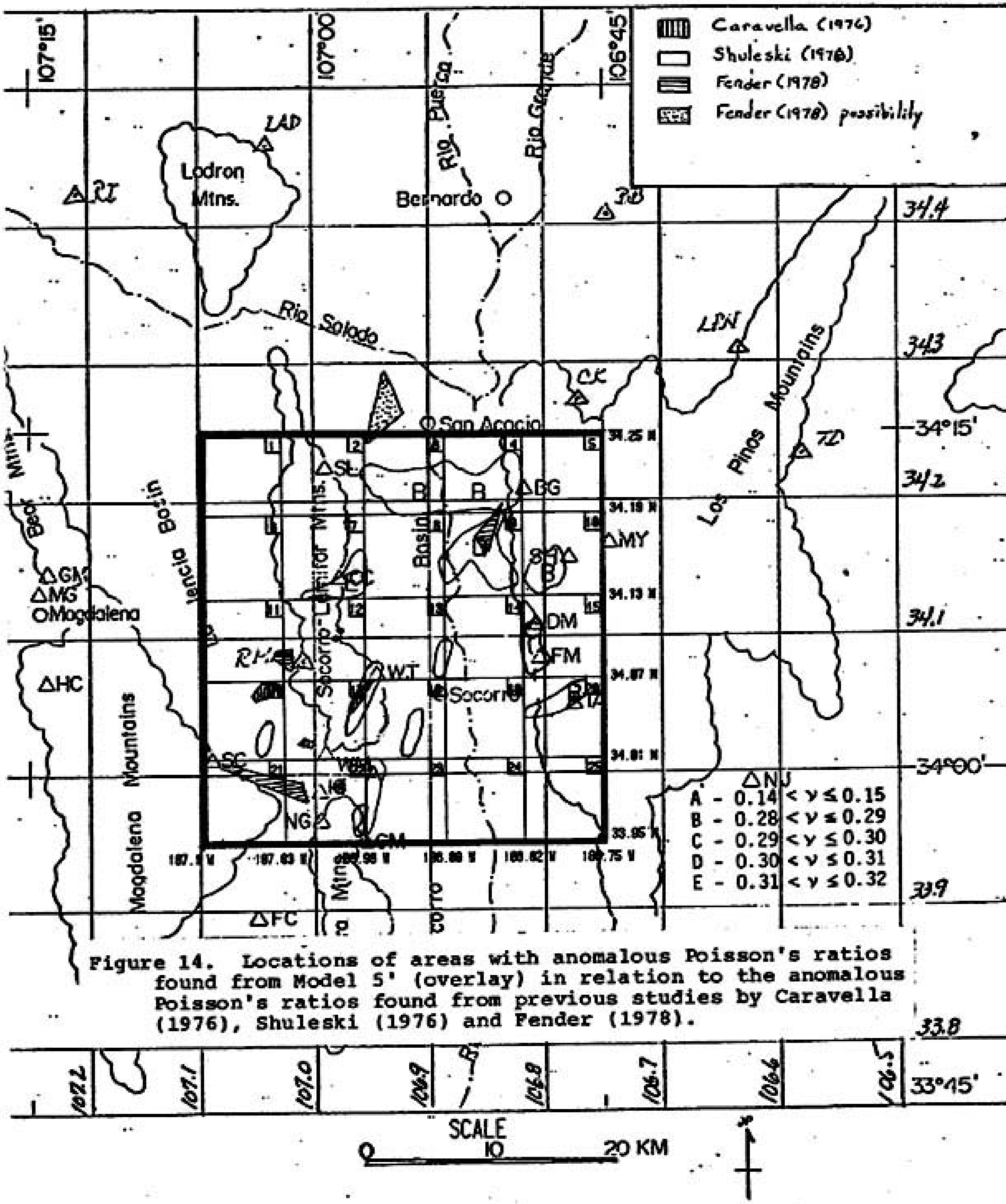

Figure 14. Locations of areas with anomalous Poisson's ratios found from Model 5' (overlay) in relation to the anomalous Poisson's ratios found from previous studies by Caravella (1976), Shuleski (1976) and Fender (1978).

This would produce a seemingly normal S-wave velocity for block 23 and a P-wave velocity that may or may not fall near the norm. In this case, the chosen P-wave velocity is below a norm of 5.8 km/sec (see Table 4), producing a low Poisson's ratio for block 23. If, however, the S-wave velocity for block 23 had been chosen from the decomposition that retained 14 eigenvalues, the same number as the chosen α solutions (see Table 4), then block 23 would be data dependent for both the α and β calculations, which would produce a Poisson's ratio of 0.244 ± 0.018. Even at the 95% confidence level this new value for block 23 could be only borderline between low and normal. If, on the other hand, the P-wave velocity for block 23 had been selected from the decomposition that retained the same number of eigenvalues for the selected β solutions, then block 23 would be nearly model dependent. This would produce a Poisson's ratio for block 23 that would be close to 0.25. Thus, because of the poor data distribution in block 23, anomaly A is eliminated as a definite anomaly.

Anomalies B and C of blocks 10, 15, and 20 may be associated with the Los Pinos Mountain range (see Figure 14). However, Table 2 implies that the gneiss-granites of the nearby Los Pinos Hills has a Poisson's ratio of 0.22, which is too low to allow Precambrian basement composition to be the sole cause for these anomalies. An inspection of the velocities obtained from Model 5' shows that the P-wave velocities for these blocks range between 5.8 km/sec and 6.0 km/sec which fall within a normal range for the study area;

while the S-wave velocities are somewhat lower than the normal 3.35 km/sec, ranging from 3.32 km/sec to 3.20 km/sec (see Table 4). This may imply that the anomaly is due to a structure or subsurface feature, such as partial melt material, which tends to reduce the S-wave velocity, but has little or no effect on the P-wave velocity. However, the decomposition of blocks 10, 15, and 20, as previously discussed, implies that the solutions for blocks 15 and 20 are more model dependent than data dependent for both the α and β solutions. Thus, blocks 15 and 20 would be expected to exhibit nearly normal Poisson's ratios while block 10 may or may not. Because blocks 15 and 20 exhibit anomalous Poisson's ratios and not normal ones as expected, the indication is that the elimination of the eigenvalues corresponding to these blocks does not necessarily cause the solutions of these blocks to be totally model dependent. For this reason, the anomalies associated with blocks 15 and 20 are not discarded as possible anomalies. If the β solutions for block 10 had been chosen from the decomposition that retained the same number of eigenvalues (14 eigenvalues retained) as the α decomposition, then the S-wave velocity associated with block 10 would be 3.323 ± 0.074 km/sec. This would produce a Poisson's ratio of 0.284 ± 0.008 for block 10. At the 95% confidence level, block 10 could not be considered anomalous. The azimuthal distribution of Poisson's ratios determined by Fender (1978) implied that the raypaths traveling through block 10 and arriving at station BG (see Figures 6e and 16) traveled through a medium that had a mean Poisson's ratio between 0.24 and 0.25. With this as supportive evidence, the anomaly associated with block 10 is disregarded as a definite anomaly until further data and information can be provided. Thus, the anomaly for block 10, in Figure 15, is dashed to indicate only a possible anomaly. For block 15, Fender indicated that the majority of raypaths arriving at station DM (see Figures 6e and 16) encountered a medium that had a mean Poisson's ratio greater than 0.28, while the raypaths arriving at station FM (see Figures 6e and 16) indicated a normal Poisson's ratio. Thus, an anomalous area (see Table 4) may be associated with block 15 near station DM as indicated by the refined anomaly in Figure 15. Fender also indicated that the raypaths from the two events in block 20 to the stations CC and BG (see Figures 6e and 16) implied that no anomalous Poisson's ratios were encountered by these raypaths, but the majority of raypaths arriving at station TA in block 20 encountered material with a mean Poisson's ratio between 0.27 and 0.28. This may imply that if an anomaly is associated with block 20 (see Table 4), it, in all likelyhood, is near station TA and is identified as anomaly B in block 20 of Figure 15.

Anomaly E in block 7 is somewhat difficult to explain. The anomaly has a P-wave velocity which is above normal, and a normal S-wave velocity (see Table 4). The exact cause for such a solution is unknown; however, it may be speculated that the azimuthal distribution of raypaths about Station CC

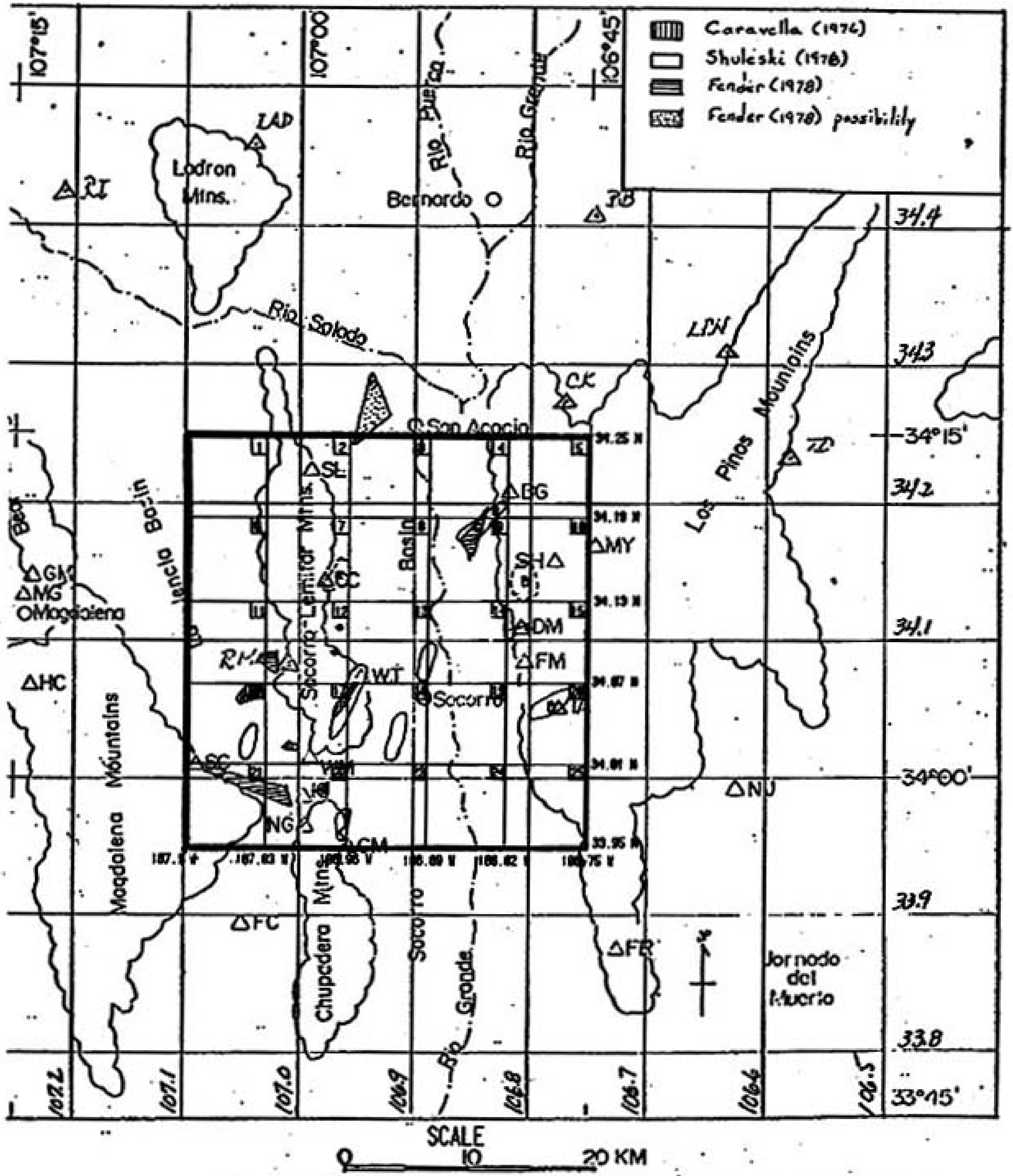

Figure 15. Modified locations of areas with anomalous Poisson's ratios determined from Model 5' (overlay).

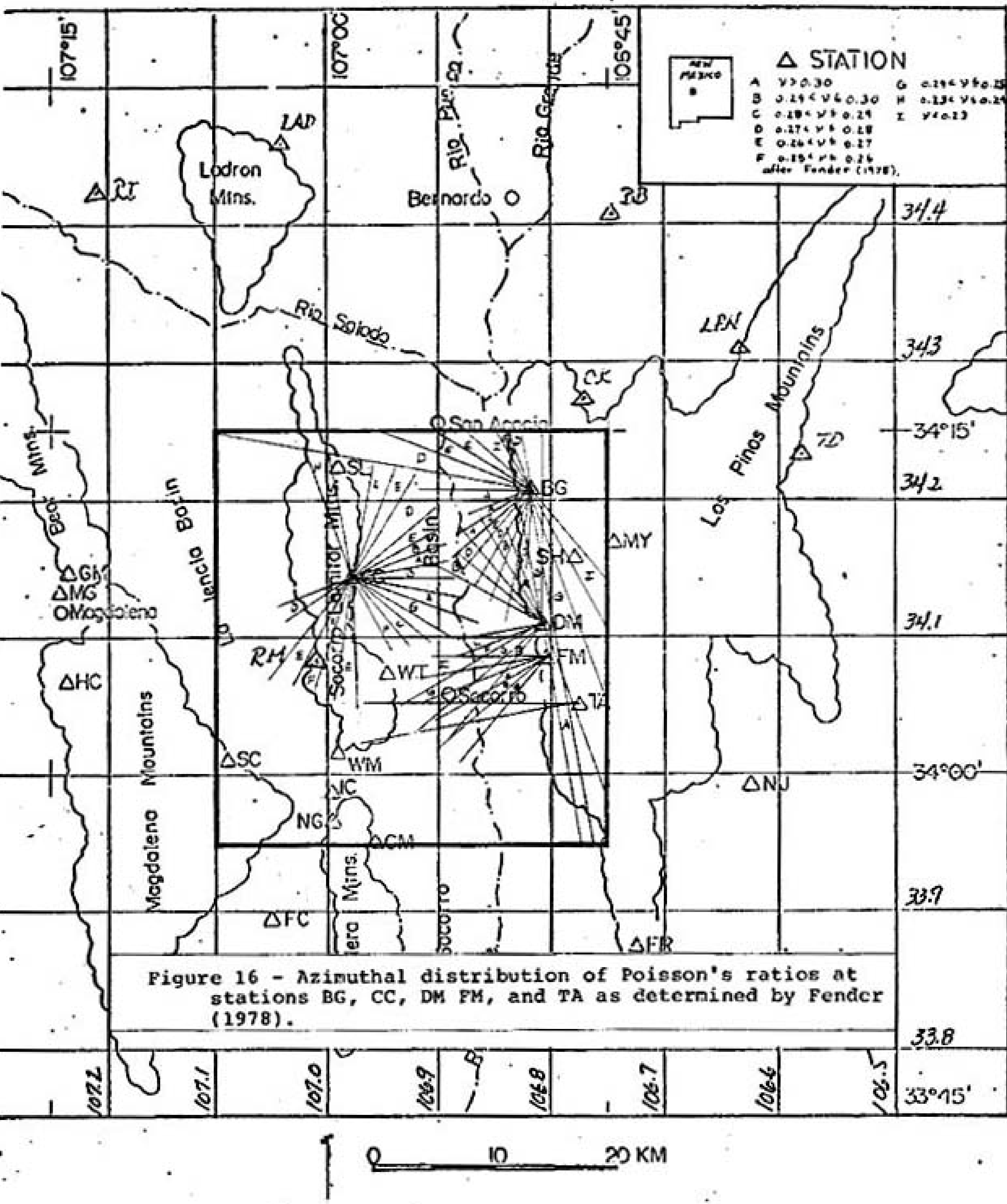

Figure 16 - Azimuthal distribution of Poisson's ratios at stations BG, CC, DM FM, and TA as determined by Fender (1978).

(see Figure 16) may play an important part in understanding the cause. As discussed previously, the α solutions for block 7 were more data dependent than the β solutions, which had the eigenvalue corresponding to block 7 eliminated in the decompostion. Had the S-wave velocity been selected from the decomposition that retained the same number of eigenvalues as those for the α solutions, i.e., 14 eigenvalues retained, (see Table 4), the S-wave velocity associated with block 7 would have been larger. This would have produced a lower Poisson's ratio for block 7 (see Table 4) which, with 95% confidence, would not be considered anomalous. Hence, anomaly E is disregarded as a definite anomaly , but is considered as a possible anomaly until further proof becomes available to definitely clarify it.

Anomaly B of blocks 3 and 4 (see Figure 14) are anomalous highs that are also somewhat difficult to explain. The P- and S-wave velocities of block 3 (see Table 4) are relatively normal velocities and should, therefore, produce a normal Poisson's ratio, not an anomalous one. A closer inspection of the Poisson's ratio of Model 5' (see Table 4) reveals that, at the 95% confidence level, the anomaly could very well be borderline between normal and anomalous at 0.270. Therefore, the Poisson's ratio of block 3 is eliminated from the model as an anomalous value and considered to be a high normal. Anomaly B of block 4 shows a normal P-wave velocity and a slightly lower than normal S-wave velocity (see Table 4). This anomaly may very well be associated with the same anomaly as that of block 9 (anomaly D). The anomaly isn't as large as that of block 9. The reason for this may be explained in the following manner: Suppose that a small portion of a certain block has an anomalous Poisson's ratio and that some, not all, of the raypaths traversing this block encounter this anomalous area. As a result, these raypaths will reflect a different velocity for the block than the remaining raypaths that do not encounter the anomalous area. Thus, when the block is considered as a whole, the resulting velocity will be an 'average' velocity for the block. Thus, this averaging effect would tend to obscure any small anomalous areas.

The averaging effect described above may be one of the reasons that none of the other previously determined areas scattered throughout the southwest quadrant of the study area (see Figure 2) was detected or confirmed by this method. The averaging effect of the large number of raypaths in the blocks in which the previously determined anomalies are located may be masking these small areas.

Figure 17 shows the graph of the final model R value versus the model number (and indirectly, the number of model parameters). A model with an R value of 1.0 is the best attainable model, as previously explained. It is evident that maintaining the same respective uncertainties for the α and β calculations and increasing the number of model parameters (blocks) consistently decreases the R value toward a value of 1.0 up through Model 4, and then increases

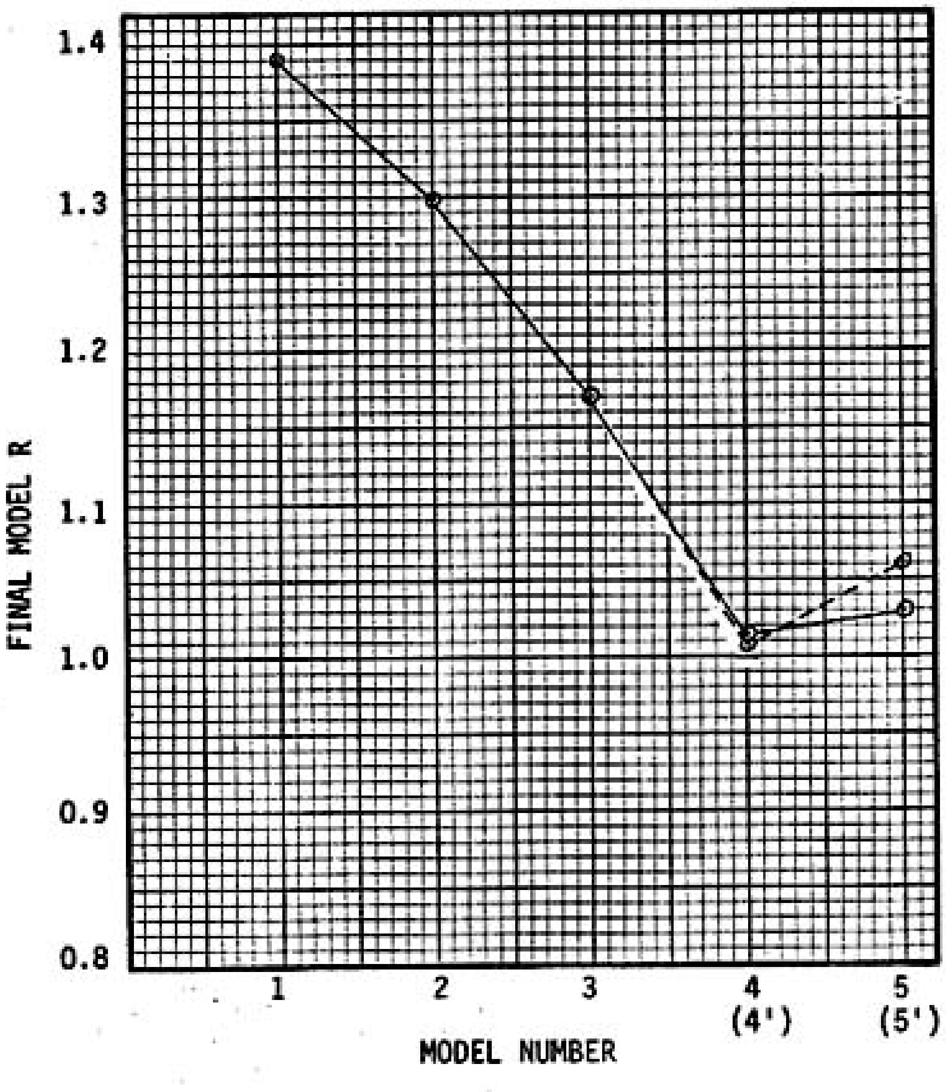

Figure 17 - Graph of the final model R value versus the model number (and indirectly, the number of model parameters). Dashed line is for Models 4' and 5'.

with Models 5 and 5'. indicating a movement towards a poorer solution as the number of model parameters increases beyond 16 blocks. The effects that varying uncertainties, more model parameters, and more data would have on R, and the degree of detail that could be attained, would constitute yet another study.

VIII. CONCLUSIONS

Many factors enter into the interpretation of the results, such as the degree of data and model dependency of the results, the data distribution, and the interpretations from past studies. It is a combination of these factors which discerned the final anomalies shown in Figure 15.

The average Poisson's ratio (ν) obtained from the single block Model 1 for the entire area is 0.265 ± 0.001. This value corresponds well with the value of 0.262 ± 0.034 obtained by Caravella (1976). The standard deviation is significantly lower than that obtained by Caravella, probably because the model is a poor fit to the data. Thus, a standard deviation of 0.034, obtained by averaging the Poisson's ratios of Model 4, is considered to be a more realistic standard deviation. The average P-wave velocity for the entire area of 5.895 ± 0.006 km/sec also corresponds well with the average P-wave velocity of 5.9 km/sec obtained by Ward (1979, personal communication).

In this study, the number of model parameters are altered to achieve better solutions with the R parameter used to indicate the quality of each final model. Model 4, which divides the study area into 16 equi-area blocks shows that it is a better model than the other models tested, i.e., the R value is closest to 1.0 for the data set used in this study. The R value for Model 5' indicates that Model 5' is not as good a model as Model 4, but the slight deviation from a better solution may have been a good sacrifice for more detail because the R value is only slightly higher than that of Model 4. Model 5', which has 25 model parameters, is used in the final interpretation because the block dimensions are smaller than those of Model 4, which allows smaller anomalous areas to be defined.

With the average Poisson's ratio of 0.265 defined to be normal, four anomalous areas are found using Model 5'. In addition, two other areas are defined as possible anomalies. These areas are shown in Figure 15. Only anomaly D of block 9 (ν =0.309) is correlated with any of the anomalous areas found by previous studies, namely, that located in the east-central Socorro basin by Fender (1978). Fender found that this anomalous area had a Poisson's ratio of 0.275 while the findings of this study imply a Poisson's ratio of 0.309.

Anomaly B of block 4 is correlated with anomaly D of block 9. Anomaly B is smaller than that of block 9 due, in part, to the averaging effects of the other raypaths in block 4.

Anomaly C of block 15 and anomaly B of block 20 are interpreted as anomalies associated with their respective blocks with the aid of the azimuthal distribution of Poisson's ratios about stations DM, FM, and TA (Fender, 1978).

The two possible anomalies B and E of blocks 10 and 7, respectively, are included only as possible anomalies because they lack any definite evidence to completely disregard them as non-anomalous.

The use of linear inverse techniques can be applied to microearthquake data to obtain seismic wave velocity distributions of an area and a map of Poisson's ratios. The size of areas with anomalous Poisson's ratios that can be defined depends largely on the distribution of the data. A better distributed data set than the one used could possibly allow models with smaller (more numerous) blocks to be used to examine the areas thought to contain the small anomalies found in previous studies and still maintain acceptable R values.

IX. RECOMMENDATIONS

This study was undertaken, in part, to determine the possibility of using linear inverse techniques to determine Poisson's ratio in the earth's crust around Socorro, New Mexico. It is hoped that this study will serve as a good base for future studies using these techniques. With this hope, I outline the following recommendations for future studies:

This study varied only the number of blocks or model parameters to achieve better models. However, further studies should be conducted to study the effects, if any, that varying the initial uncertainties, σ_i, may have on the quality of the solutions. This study also assumed a homogeneous half-space for Model 1. It would be interesting to see the effects that anisotropy, inhomogeneity, and/or layered models would have on the final solutions and interpretations of the other models.

It is recommended that any further studies of this kind use more data and a better distribution of data in the study area. This may include raypaths that lie partially outside the area. If such raypaths are included, it is recommended that a majority of the raypaths' total length lie within the study area.

More and better distributed data could allow models with smaller blocks to be used. If such a study produces acceptable models based on R, then smaller anomalous areas which have been found from past studies may possibly be confirmed or denied.

REFERENCES

Aki, K., A. Christoffersson and E. S. Husebye (1977). Determination of the three-dimensional seismic structure of the lithosphere, Jour. Geophy. Research 82, 277 - 296.

Bullen, K. E. (1963). An Introduction to the Theory of Seismology. Cambridge University Press, London, England pg. 213.

Caravella, F. J. (1976). A study of Poisson's Ratio in the Upper Crust in the Socorro, New Mexico Area, M.S. Independent Study, Geoscience Department, N.M.I.M.T.

Chapin, C. E. and W. R. Seager (1975). Evolution of the Rio Grande Rift in the Socorro and Las Cruces Area, in New Mexico Geol. Society Guidebook, 26th Field Conference, 297 - 321.

Chapin, C. E., R. M. Chamberlin, G. R. Osburn, D. White, and S. R. Sanford (1978). Exploration Framework of the Socorro Geothermal Area, New Mexico, Special Publication no. 7, 115 - 130.

Christiansen, N. E. and D. M. Fountain (1975). Constitution of the Lower Continental Crust Based on Experimental Studies of Seismic Velocities in Granulites, Geol. Soc. Amer. Bull. 86, 227 - 236.

Fender, J. J. (1978). A study of Poisson's Ratio in the Upper Crust in the Socorro, New Mexico Area, M.S. Independent Study, Geoscience Department, N.M.I.M.T.

Hughes, D. S. and C. Maurette (1956). Variaion of Elastic Wave Velocities on Granites with Pressure and Temperatures, Geophysics, 21, 277 - 284.

Jackson, D. D. (1972). Interpretation of Inaccurate, Insufficient and Inconsistent Data, G.J.R.A.S. 28, pg. 27 - 109.

Lanczos, C. (1961). Linear Differential Operators, D. Van Nostrand, Co., New York, NY, pg. 117.

Nettleton, L. L. (1940). Geophysical Prospecting for Oil, McGraw-Hill Book Company, N.Y., N.Y., pg. 236 - 237.

Rinehart, E. J. (1976). The Use of Microearthquakes to Map an Extensive Magma Body in the Socorro, New Mexico Area, M.S. Independent Study, Geoscience Department, N.M.I.M.T.

Sakdejayont, K. (1974). A study on Poisson's Ratio and V_p/V_s ratio in the Rio Grande rift, N. Mex. Inst. of Mining and Technol. Geosc. Dept., Geophysics Open-File Rpt. 5, Socorro.

Sanford, A. R. (1968). Gravity Survey in Central Socorro County, New Mexico, New Mexico Bureau of Mines and Mineral Resources, Circular 91, 14 p.

Shuleski, P. J. (1976). Seismic Fault Motion and SV-Wave Screening by Shallow Magma Bodies in the Vicinity of Socorro, New Mexico, M.S. Independent Study, Geoscience Department, N.M.I.M.T.

Tang, S. (1978). Three Dimensional Crustal Velocity Model Beneath the Socorro, New Mexico Area from Inversion of Relative Travel-time Residuals, M.S. Independent Study, Geoscience Department, N.M.I.M.T.

APPENDIX A

List of Events Used

Date, Origin Time, Location, and Stations

Uncertainties listed are the origin time standard deviations which were used as the uncertainties on the α calculations. The β uncertainties are obtained by adding 0.2 seconds to the listed uncertainties.

Date Mo/Day/Yr	Origin Time hr:min:sec	Location Longitude degrees	Location Latitude degrees	Location Depth km	Uncertainty seconds	Stations Recording Events
5 26 75	23:45:51.19	106.995	34.067	7.270	.26	CC,CM,FM
6 3 75	4: 3: 1.18	106.998	34.026	3.302	.05	SC
6 3 75	4:48:17.93	106.930	34.071	6.252	.05	CC,FM
6 3 75	15:10:15.61	107.042	34.017	6.876	.14	FM,CC
6 4 75	4:20:14.86	106.951	34.036	4.525	.17	FM,CC
6 16 75	23:43:20.95	107.037	34.018	7.294	.14	FM,CC,CT
6 26 75	2:56:45.09	107.045	34.053	4.908	.11	CT,CC,FM
7 1 75	13:35:59.09	107.037	34.023	2.155	.86	SC
7 9 75	2:12:24.57	106.931	34.051	7.972	.27	CM,CC
7 9 75	9:16:48.07	106.927	34.056	5.995	.21	FM,CM,CC
7 23 75	14:56:42.04	107.040	34.013	5.449	.79	FM,CC,CM
7 24 75	4:23:13.99	107.002	34.051	6.377	.07	CM
7 30 75	21:44:41.82	106.924	34.075	9.627	.08	WT,CC,FM
8 5 75	4:17:20.41	106.991	34.015	9.312	.10	CC,FM,WT
8 5 75	14:19:22.33	107.048	34.019	7.871	.16	WT,CC,CM,FM
8 6 75	20:12:33.12	106.981	34.020	6.856	.07	FM,CC,WT
8 8 75	10:53:57.80	106.923	34.062	6.762	.06	FM,WT,CC,SC
8 8 75	10:57:22.25	106.925	34.068	7.170	.06	CC,WT,FM
8 12 75	7: 9:10.72	106.802	34.020	1.987	.05	CC,WT
8 12 75	15:25:28.41	106.999	34.036	6.007	.06	FM,CM,WT,CC
8 13 75	5:29:49.05	107.086	34.219	8.038	.14	FM,WT,CC
8 13 75	7:39:18.27	106.930	34.069	8.231	.05	CC,WT
8 13 75	11:22:26.45	106.981	34.004	9.904	.09	FM,CM,WT
8 13 75	20:18:25.25	107.045	34.079	6.927	.15	CC,WT,FM,CM

Date Mo/Day/Yr	Origin Time hr:min:sec	Location: Longitude degrees	Location: Latitude degrees	Location: Depth km	Uncertainty seconds	Stations Recording Events
8 14 75	19: 3:28.12	106.926	34.079	8.988	.09	CC
8 15 75	6:36:45.93	106.877	34.113	3.181	.08	FM,CC,WT
8 19 75	8:11:46.62	106.969	34.045	8.946	.08	CM,FM,CC,WT
8 19 75	8:12:44.51	106.972	34.047	9.794	.09	CM,FM,CC,WT
8 19 75	10: 0: 6.71	107.014	33.971	11.405	.21	CM
8 19 75	20:10:22.78	106.921	34.070	7.818	.06	CC,WT,SC
8 20 75	5:22:19.65	106.923	34.074	9.347	.08	CC,WT,SC,FM
8 20 75	12:20:51.70	106.913	34.073	10.269	.09	SC,FM,CC
8 20 75	15:28:36.14	106.930	34.074	8.824	.07	WT,SC,FM,CC
8 20 75	21:59:44.38	106.918	34.069	7.754	.07	WT,CM,FM,CC
8 21 75	3:44:48.34	107.052	34.012	9.499	.19	CC,FM
8 21 75	19: 4: 5.94	106.970	34.040	9.912	.09	FM,WT,CM,CC
8 25 75	19:37:40.71	106.922	34.068	8.259	.07	WT,FM,CC
8 26 75	8:40:15.40	106.936	34.071	9.670	.08	CC,FM,SC
8 28 75	1:26: 1.81	106.942	34.169	3.301	.11	FM
9 16 75	13:30:52.68	106.936	34.068	5.255	.03	WT
9 19 75	8:42:57.25	106.860	34.011	5.243	.04	WT
9 24 75	2:17: 9.86	106.949	34.016	1.156	.04	WT
10 29 75	7:21:35.17	107.006	34.050	3.926	.05	WT
10 29 75	7:34:37.68	107.003	34.030	-1.774	.06	CC
10 29 75	20:50:49.51	107.014	33.997	1.768	.06	CM,WT,CC
10 30 75	7: 9:38.68	107.041	34.024	7.393	.16	CC,WT,CM
11 4 75	16:30:11.67	107.069	34.034	7.321	.14	CC,CM,WT
11 5 75	14:35: 4.61	107.084	34.017	11.144	.21	CM
11 5 75	22:28:26.30	107.046	34.035	5.580	.11	WT,CC,CM
11 6 75	11: 6:48.44	106.870	33.999	6.025	.06	CC,WT

Date Mo/Day/Yr	Origin Time hr:min:sec	Location Longitude degrees	Latitude degrees	Depth km	Uncertainty seconds	Stations Recording Events
11 7 75	8:27:35.83	107.055	34.037	6.405	.12	WT,CM,CC
1 21 76	5:34:40.55	106.988	34.064	6.690	.06	WT
1 21 76	14:18:28.09	106.955	33.957	7.425	.12	CM
1 22 76	15:58:47.71	107.026	34.018	4.403	.69	TA,DM
1 22 76	16: 0:52.28	107.046	34.025	7.727	.18	TA
1 23 76	2:53:33.13	107.032	34.021	6.003	.12	DM,WT,TA
1 23 76	7:22:14.75	107.042	34.053	2.577	.09	CM,DM,WT,TA
1 27 76	8:37:43.72	106.790	34.152	13.797	.28	WT,CC,TA
1 29 76	15: 6:40.22	106.982	33.983	4.484	.08	WT
1 29 76	18:24:27.42	106.988	33.979	6.040	.09	DM,TA,WT
1 30 76	13:56:23.70	106.993	34.054	5.518	.06	DM,CC,WT
2 17 76	6:17:49.22	107.065	34.027	6.528	.13	IC,WT,WM
2 17 76	17:34: 4.98	107.032	34.040	9.141	.13	WM,CC,CM,IC
2 17 76	23:19:38.71	107.044	34.105	5.705	.36	WT,CC,WM,IC
2 18 76	5:44:55.83	107.062	34.010	8.235	.13	CM,IC,WM,WT,CC
2 18 76	9:13:30.81	107.017	34.014	0.447	.04	IC,WM,CC,WT
2 18 76	23:25:35.31	107.076	34.028	6.769	.12	WT,CC,WM,IC
2 19 76	0: 8:36.61	107.071	34.012	8.470	.13	WM,IC,CC,WT
2 20 76	12:51:45.16	107.052	34.010	8.511	.16	WM,WT,IC
3 18 76	14:45:16.77	106.750	33.977	3.524	.09	DM,IC,TA,WT
3 18 76	18:34:50.54	107.096	34.028	6.951	.65	WT,TA,IC,CM,DM
3 23 76	12:50:26.74	106.766	33.969	0.220	.08	DM,TA
3 25 76	10:50:53.94	106.986	34.052	8.893	.29	TA,WT,CM,DM,IC
4 13 76	9:45:40.60	107.020	34.064	7.504	.10	CC,IC,CM,WM
4 13 76	11:41:25.35	107.060	34.028	8.111	.13	CC,IC,WM,WT
4 13 76	11:58:34.63	106.966	33.981	4.500	.07	WT,WM,CM,IC,CC

Date Mo/Day/Yr	Origin Time hr:min:sec	Location: Longitude degrees	Location: Latitude degrees	Location: Depth km	Uncertainty seconds	Stations Recording Events
4 13 76	13:31:59.84	107.038	33.993	2.898	.24	WT,CC
4 13 76	23:15:14.99	107.033	34.023	2.529	.05	WM,WT,CC,IC
4 14 76	1:50:28.80	107.014	33.975	8.000	.10	WM,IC,WT
4 14 76	13:12:20.94	107.032	34.060	6.430	.11	WT,IC,WM
4 15 76	8:45:52.42	107.016	34.062	7.021	.10	SC,IC,CC,WM,WT
4 15 76	18:28:37.20	106.963	34.042	6.563	.12	IC,WM,WT
4 16 76	5:34:39.45	106.988	34.020	0.355	.03	WT
4 16 76	9:33:42.83	107.019	34.057	5.661	.08	WM,WT,IC,CC,CM
4 16 76	14: 7:33.24	106.994	34.062	6.863	.09	IC,CC,WT,WM
4 20 76	8:32:19.35	106.842	34.105	1.885	.10	DM,WT,CU,BG,CC,SL
5 25 76	3: 8:16.68	107.041	34.040	-0.200	.32	WT,CM,TA
5 25 76	8:11:39.50	107.037	34.022	6.197	.69	TA,WT,DM
6 3 76	15:31:12.85	107.023	34.038	7.356	.48	CM,TA,DM,WT
6 8 76	5:24:54.36	106.997	34.052	7.848	.16	CC,NG
7 14 76	21:22:55.54	107.030	34.012	3.232	.27	WT
7 15 76	10:58:34.50	107.068	34.025	5.224	.05	WT
7 15 76	16:43: 7.97	107.066	34.026	5.880	.05	WT
8 10 76	12:18:42.29	107.009	34.044	5.152	.07	WT,NG
8 12 76	0:59: 8.18	107.008	34.042	8.372	.07	WT,NG
8 12 76	4:56: 5.43	107.010	34.040	6.875	.07	WT
8 12 76	23: 7:12.69	107.007	34.045	7.465	.17	NG,WT
8 24 76	1:31:13.91	107.028	34.037	3.507	.04	WT,NG
8 25 76	21: 4: 9.72	107.012	34.052	5.518	.06	WT
8 25 76	22:32:23.43	107.010	34.045	7.330	.11	WT,NG
8 27 76	1:44:39.98	107.013	34.040	5.793	.08	NG,WT
8 27 76	8:15:28.47	107.063	34.013	5.845	.06	WT

Date Mo/Day/Yr	Origin Time hr:min:sec	Location Longitude degrees	Location Latitude degrees	Location Depth km	Uncertainty seconds	Stations Recording Events
8 27 76	10:42:34.04	107.054	34.017	5.466	.06	WT
9 3 76	6:45:56.52	106.998	33.971	5.337	.06	WT
9 3 76	13:25:58.37	106.982	33.997	8.545	.09	WT,NG
10 5 76	19:26: 8.89	106.977	34.039	6.885	.05	IC,WT,DM
10 6 76	15:12:41.24	106.823	34.087	9.475	.16	WT,DM,IC
10 7 76	22:35:49.35	107.037	34.015	9.295	.11	DM,IC
10 7 76	22:37:37.71	107.039	34.025	7.583	.09	DM,WT,IC
10 7 76	23:21: 9.66	107.037	34.025	7.282	.09	WT,IC,DM
1 21 77	0: 6:15.69	107.083	33.962	12.631	.11	SC
1 21 77	16:38:11.26	107.061	34.005	7.758	.06	WT,CM
1 21 77	16:43:40.33	107.053	34.027	-0.679	.07	DM
1 22 77	4:24: 5.11	107.056	34.015	6.656	.06	CC,DM,CM
2 8 77	21:15:59.28	107.029	34.039	-2.000	.03	CC,DM
2 9 77	1:36:16.90	107.024	34.032	-2.000	.03	DM,CC
2 9 77	1:42:32.45	106.946	34.147	4.253	.12	DM,CC,CM
2 9 77	8:38:47.18	106.980	33.984	6.886	.17	DM,CC,CM
2 9 77	10:59:58.90	106.998	34.018	4.156	.16	CC,NG,DM
2 9 77	11: 7:13.58	107.007	34.006	8.405	.23	NG,DM,CC,CM
2 9 77	11:33:43.82	107.007	33.970	7.602	.31	CC
2 9 77	11:38:53.24	106.997	34.024	1.485	.12	DM,CC
2 9 77	12:26:35.93	107.034	34.039	0.118	.23	DM,CC
2 10 77	5:24:51.65	107.010	33.967	8.835	.35	NG
2 10 77	7:33:28.04	106.927	34.138	6.355	.17	NG,DM,CM,CC
2 11 77	8:31:46.30	106.970	34.007	3.448	.45	CC
2 16 77	8:51:16.43	107.067	34.014	9.396	.16	WT,DM,IC,CC,CM
2 16 77	14:44:49.38	107.061	34.005	7.807	.14	DM,IC,WT

Date Mo/Day/Yr	Origin Time hr:min:sec	Location Longitude degrees	Latitude degrees	Depth km	Uncertainty seconds	Stations Recording Events
2 17 77	14:27:44.71	106.825	34.222	9.442	.53	WT,DM,CC
2 25 77	0: 7: 8.32	107.049	34.015	5.873	.13	WT,CC
3 8 77	4:30:41.01	107.061	34.002	6.478	.06	WT,DM
3 8 77	4:55: 6.16	107.058	34.012	6.287	.05	CM,DM,WT
3 9 77	11:25:44.42	107.062	34.003	6.781	.06	WT,DM,CM
3 9 77	11:49: 2.52	107.061	34.010	6.302	.05	WT,DM,CM
3 9 77	11:50:16.12	107.051	33.996	4.737	.05	DM,WT
3 9 77	12:27:56.05	107.055	34.009	6.761	.06	DM,CM
3 9 77	12:33:19.21	107.059	34.009	6.204	.05	WT,DM
3 9 77	12:39: 0.29	107.061	34.008	6.350	.06	WT,DM
3 10 77	1:29:50.13	107.063	34.016	7.535	.06	DM
3 10 77	2: 3:42.72	107.061	34.002	6.507	.06	WT,CM,DM
3 10 77	13:27:33.54	107.062	33.999	7.043	.06	WT,CM,DM
4 5 77	19:34:31.44	107.031	34.010	4.240	.05	DM,CC
4 12 77	3:25: 3.22	107.037	34.061	3.034	.06	CC,DM
4 13 77	4:22:53.77	107.062	34.085	-2.000	.13	SC
4 13 77	19:15:23.90	107.037	34.066	0.714	.03	CM,CC,DM
4 13 77	19:39:36.58	107.040	34.068	1.679	.05	CC,DM
4 13 77	20:15:32.01	106.860	34.176	3.969	.04	DM,CC
4 15 77	6:35:36.71	107.068	34.035	8.889	.08	DM
4 15 77	6:40:24.87	107.067	34.035	8.020	.07	SC,DM
4 19 77	16:40:20.04	106.957	33.992	3.399	.06	CM,WT,CC,DM
4 26 77	2: 8:20.56	107.028	34.059	6.145	.05	WT,CC,DM
4 26 77	16:56: 8.11	107.052	34.047	4.336	.04	WT,CC
4 27 77	8: 4:40.37	107.030	34.028	1.578	.04	WT,CM,CC,DM
4 27 77	11:52:50.40	107.034	34.065	5.502	.06	WT,CC,DM

Date Mo/Day/Yr	Origin Time hr:min:sec	Location: Longitude degrees	Location: Latitude degrees	Location: Depth km	Uncertainty seconds	Stations Recording Events
4 27 77	12:15:56.26	107.060	34.011	7.172	.06	DM,CM,WT
4 27 77	12:23:27.39	107.058	34.022	6.072	.05	WT,DM,CM,CC
4 27 77	13:49: 4.34	107.034	34.060	6.608	.05	WT,CC,DM
4 27 77	15:34:28.88	107.088	34.132	2.352	.14	CC,WT
4 28 77	10:59:10.71	107.054	34.048	5.217	.05	CM,CC,WT
4 28 77	11: 3:31.17	107.050	34.041	5.290	.07	WT,CC,DM
5 6 77	10:43:18.38	106.923	34.194	2.668	.05	CC,DM
5 11 77	17:45: 0.03	107.024	34.020	5.746	.62	WT,FM
5 12 77	6:19:14.20	107.040	34.046	8.572	4.95	WV,WT,FM
6 1 77	6:40:44.84	107.056	34.020	7.129	.06	WT,CM,SC
6 2 77	6:45:50.86	107.064	34.007	4.342	.05	WT,DM
6 2 77	6:48:16.11	107.055	34.031	8.079	.05	SC,CM,DM
6 2 77	6:50:24.32	107.067	34.013	6.643	.05	WT,CM,DM
6 2 77	6:51:56.55	107.062	33.993	2.829	.08	WT,DM
6 2 77	6:55:21.48	107.061	34.012	4.888	.05	WT,DM
6 2 77	8:11:47.69	107.068	34.008	2.794	.04	WT,DM
6 2 77	11:42: 0.51	107.064	34.010	4.494	.05	WT,DM
6 2 77	12: 7: 4.07	107.064	34.009	4.565	.05	WT,DM
6 2 77	14:29: 6.75	107.061	34.013	4.551	.05	DM
6 2 77	17:30: 8.12	107.065	34.004	6.034	.05	WT,DM
6 3 77	0:10: 4.30	107.061	34.009	7.266	.09	CM,WT,DM
6 3 77	3:49: 1.58	107.060	34.013	6.118	.05	WT,DM,CM
6 3 77	4:50:19.82	107.064	34.006	8.003	.10	CM,WT,DM
6 3 77	6: 2:45.96	107.061	34.004	6.032	.09	CM,WT,DM
6 3 77	19:38:30.01	106.894	34.227	8.723	.09	DM,CM
6 3 77	20:45: 3.12	106.901	34.228	7.260	.09	CM,DM

Date Mo/Day/Yr	Origin Time hr:min:sec	Location: Longitude degrees	Location: Latitude degrees	Depth km	Uncertainty seconds	Stations Recording Events
6 3 77	23: 1:19.19	107.010	33.984	6.085	.08	CM,WT
6 4 77	1: 7:54.31	107.016	34.058	5.706	.05	WT,DM
6 4 77	6:18:51.58	106.900	34.227	5.463	.06	DM,CM
6 4 77	7: 6:23.18	107.066	33.975	7.633	.09	WT,DM
6 7 77	12:25:27.89	107.063	33.972	9.437	.23	DM
6 8 77	3:32:23.27	106.930	34.204	10.340	.16	WT,DM
6 8 77	5:30:29.53	107.052	34.012	9.707	.14	WT,DM
6 10 77	4: 4:44.93	107.062	34.018	6.712	.05	CM,DM,WT
7 11 77	22:24:55.82	107.039	34.120	4.529	.04	CC
7 11 77	23:52:34.82	107.038	34.120	5.054	.04	BG,CC
7 12 77	7:28:59.56	106.810	34.116	8.436	.14	BG,CC,SC
7 14 77	1:28:56.59	106.884	34.158	2.503	.05	BG,CC
7 14 77	2:34: 1.99	106.880	34.160	4.494	.06	CC,BG,DM
7 14 77	10: 0:32.65	106.870	34.158	6.034	.03	CC,BG,DM
7 14 77	11:31:51.38	106.893	34.157	0.971	.02	BG,CC,DM
7 14 77	20:24:16.69	107.054	34.036	7.661	.05	WT,CC,CM,BG
7 15 77	11: 3: 1.39	107.000	34.016	1.391	.06	CC
7 15 77	12:26:25.62	107.068	34.003	8.116	.06	BG,CM,WT
7 19 77	6:16:54.90	106.876	34.159	2.435	.06	CC,BG
7 21 77	3:12:27.81	107.066	34.034	4.119	.04	CM
7 22 77	7:19: 0.78	106.880	34.163	2.017	.06	BG
7 27 77	12: 7:30.35	106.950	33.960	4.768	.14	CC,BG
7 27 77	15:53:15.04	107.057	34.003	8.349	.07	CC
7 27 77	17:17:29.43	106.907	34.157	4.429	.04	CC
7 29 77	12: 7:22.64	106.905	34.149	5.423	.04	CC,BG
8 17 77	6: 3:19.95	106.871	34.165	4.930	.04	DM,BG,CC,WT

Date Mo/Day/Yr	Origin Time hr:min:sec	Location Longitude degrees	Latitude degrees	Depth km	Uncertainty seconds	Stations Recording Events
8 19 77	9:28:22.69	107.070	34.009	8.629	.08	DM,CM,BG
8 24 77	11:22:35.29	107.062	34.002	11.105	.08	NG,BG
8 26 77	10:32:57.90	107.063	34.011	7.890	.05	CM,BG,NG,CC,WT
8 30 77	18:37:28.93	107.004	34.039	2.307	.05	CC,CM
9 1 77	18:20: 2.21	106.758	34.056	7.116	.09	CC,NG,BG,WT
9 1 77	21:58:48.64	107.049	34.012	6.814	.05	CC
9 13 77	0:13:45.56	107.046	34.185	16.830	.09	CC
9 14 77	4: 1:27.84	107.027	34.043	1.527	.07	CC
9 15 77	0:53:35.32	107.061	34.034	6.995	.07	BG,CC
9 16 77	8: 4: 8.16	107.001	34.071	4.934	.03	SC,CC
9 20 77	1:20: 8.84	107.052	34.035	8.193	.06	FM,CC
9 20 77	8:19:23.31	106.879	34.164	3.150	.03	BG,CC,FM
10 18 77	8:16:32.74	107.062	34.030	7.084	.07	BG,CC,SC
10 28 77	13: 0:13.29	106.910	34.141	6.950	.07	BG
10 28 77	13:26:51.34	106.911	34.133	-1.589	.05	CC,BG
11 15 77	0:42:39.21	106.804	34.002	-1.787	.05	CC,SC,IC,WT
11 15 77	19: 2:41.77	106.885	34.139	3.452	.03	WT,FM,CC,IC,BG
11 18 77	9: 9:38.45	107.015	34.035	4.327	.07	CC,IC
11 18 77	14:22:18.21	106.762	34.054	-2.000	.04	CC,BG,WT,SC
12 6 77	8:43:45.38	106.873	34.193	3.148	.07	SL,BG,CC
12 8 77	3:42:42.13	106.910	34.195	-1.433	.31	SL,BG,CC
12 22 77	10: 5:16.26	106.866	34.081	4.998	.12	CC,SL
12 23 77	1:37:40.15	107.029	34.126	5.021	.17	CC,BG,SL
1 5 78	13:27:47.81	106.912	34.218	-2.000	.03	CC,SL
1 6 78	1:49: 2.89	106.998	34.213	2.879	.04	CC,SL,BG
1 11 78	7:22:47.19	107.073	34.014	6.031	.73	CC,SL,BG

Date Mo/Day/Yr	Origin Time hr:min:sec	Longitude degrees	Latitude degrees	Depth km	Uncertainty seconds	Stations Recording Events
1 17 78	13:18:14.89	106.888	34.124	-0.979	.23	CC
1 18 78	12:24:32.88	106.859	34.167	1.933	.04	CC,BG,SL
1 18 78	12:49:42.97	106.865	34.171	3.405	.04	CC,BG,SL
1 18 78	14:55:58.05	106.858	34.166	1.788	.04	CC,BG,SL

APPENDIX B

List of Program IS.FOR

Used for linear inversion method

```
      INTEGER STA,STEST,XFILE
      DIMENSION A(600,25),
     1HT(25,600),ATA(400),
     1B(600,25),BIGR(25),DBIGR(25,2),DELY(600),D1(2),
     1D2(2),D3(2),D4(2),DUMMY(600),
     1DTT(600,1),DX(25,1),DXCAP(25,1),DYCAP(600,1),
     1EIGVAL(25,25),EIGVEC(25,25),EIGVLL(25),EV(25,25),
     1GNOL(10),H(25,600),INT(2),IVAR(25),R(25,25),
     1S(25,1),STA(20),SX(20),SY(20),SZ(20),
     1TAL(10),TAU(25,2),TD(5,5,2),TDZ(5,5,2),
     1TTB(5,5,2),TTD(600,1),TTOBS(600,2),
     1TTT(600,2),U(600,25),UNC(600,2),UTEMP(25,25),
     1UTRP(25,600),V(5,5,2),VAR(5,5,2),VARMTX(25,25,2),
     1VART(25,25,2),WP(20),
     1WS(20),WK(1000),ZT(25)
C
      EQUIVALENCE(HT(1,1),UTRP(1,1))
C
      DATA INT/'ALPH','BETA'/
      TYPE 1
      READ(5,2) VFN
      TYPE 3
      READ(5,*) GNLMAX,GNLMIN,TALMAX,TALMIN
      TYPE 4
      READ(5,*) GNLINC,TALINC
      TYPE 5
      READ(5,6) NBLK
      N1=NBLK*NBLK
      N2=NBLK
      N3=NBLK+1
      PRINT 7,VFN
      PRINT 8,GNLMAX,GNLMIN,TALMAX,TALMIN
      PRINT 9,GNLINC,TALINC
      PRINT 10,N2,N2
      MAXDIM=600
      NRA=MAXDIM
      NCA=N1
      NRDY=MAXDIM
      NCDY=1
      NRDX=N1
      NCDX=1
      IDGT=2
      KDUM=N1
      IJOB=1
      IA=MAXDIM
      IB=25
C
C     **************************************************************
C     N IS THE NUMBER OF RAYPATHS
C     N1 IS THE TOTAL NUMBER OF BLOCKS
```

```
C       N2 IS THE NUMBER N WHEN AREA IS DIVIDED INTO N BY N
C       BLOCKS
C       MAXDIM IS THE MAXIMUM DIMENSION USED IN THE IMSL SUBRO
C       UTINES; MAXDIM EQUALS THE NUMBER OF RAYPATHS
C       NRA IS THE NUMBER OF ROWS OF MATRIX A; NRA=N
C       NCA IS THE NUMBER OF COLUMNS OF MATRIX A; NCA=N1
C       NRDY IS THE NUMBER OF ROWS OF MATRIX DELTA Y; =N
C       NCDY IS THE NUMBER OF COLUMNS OF MATRIX DELTA Y; =1
C       NRDX IS THE NUMBER OF ROWS OF MATRIX DELTA X; =N1
C       NCDY IS THE NUMBER OF COLUMNS OF MATRIX DELTA X; =1
C       IDGT IS A PARAMETER SET FOR THE IMSL SUBROUTINES
C       KDUM IS A DUMMY VARIABLE THAT REMAINS FIXED AS
C       NCA VARIES THROUGH THE DECOMPOSITION PROCEDURE
C       IJOB IS SET TO 1 TO BE USED IN IMSL SUBROUTINE EIGRS
C       IA AND IB ARE PARAMETERS SET FOR IMSL SUBROUTINES
C       ***********************************************************
C
C
C       ***********************************************************
C       READ IN TAU, A PRIORI ESTIMATES ON THE MODEL
C       PARAMETERS FROM TAU1.DAT AND TAU2.DAT
C       ***********************************************************
C
        DO 100 I=1,N1
        DBIGR(I,1)=0.0
        DBIGR(I,2)=0.0
100     IVAR(I)=I
        DO 101 I=1,2
        IF(I.EQ.1) OPEN(UNIT=1,FILE='TAU1')
        IF(I.EQ.2) OPEN(UNIT=1,FILE='TAU2')
        DO 102 J=1,N1
        READ(1,12) TAU(J,I)
102     CONTINUE
        CLOSE(UNIT=1)
101     CONTINUE
        DO 103 II=1,N2
        DO 103 JJ=1,N2
        V(II,JJ,1)=5.8
        V(II,JJ,2)=3.35
103     CONTINUE
        NT=1
C
C       ***********************************************************
C       READ IN EVENT LOCATIONS & STATION LOCATIONS FROM
C       DATA SET
C       ***********************************************************
C
        OPEN(UNIT=1,DEVICE='DSK',MODE='ASCII',ACCESS='SEQIN',
        1FILE=VFN)
        OPEN(UNIT=20,DEVICE='DSK',MODE='ASCII',ACCESS='SEQIN',
        1FILE='STA')
```

```
104   READ(1,*,END=105) NSTA,IMO,IDA,IYR
      READ(1,*) XE,WP1,YE,WP2,ZE,WP3
      READ(1,*) IHR,IMIN,SEC,WP4
      DO 110 I=1,NSTA
      READ(1,13) STA(I),ISPMIN,STPSEC,WP(I),ISSMIN,STSSEC,WS(I)
      REWIND 20
106   CONTINUE
      READ(20,14,END=107) STEST,SY(I),SX(I),SZ(I)
      IF(STEST.EQ.STA(I)) GO TO 108
      GO TO 106
107   PRINT 15,STA(I),IMO,IDA,IYR,IHR,IMIN
      GO TO 110
108   CONTINUE
      N=N+1
C
C     ***********************************************************
C     CALCULATE OBSERVED TRAVEL TIMES
C     ***********************************************************
C
      TTOBS(N,1)=(STPSEC+((ISPMIN-IMIN)*60.0))-SEC
      TTOBS(N,2)=(STSSEC+((ISSMIN-IMIN)*60.0))-SEC
C
C     ***********************************************************
C     CREATE UNCERTAINTIES UNC
C     ***********************************************************
C
      UNC(N,1)=WP4
      UNC(N,2)=WP4+0.2
C
C     ***********************************************************
C     CALCULATE RAY PATH DISTANCES FROM TTYM
C     ***********************************************************
C
      XP=XE
      YP=YE
      ZP=ZE
      OPEN (UNIT=25,DEVICE='DSK')
      CALL TTYM(XP,YP,ZP,SX(I),SY(I),SZ(I),TTB,V,TD,TALMIN,
      1GNLMAX,GNLINC,TALINC,NBLK)
      CLOSE (UNIT=25)
C
C     ***********************************************************
C     WEED OUT GRID FOR SELECTED BLOCKS & PUT IN MATRIX
C     ***********************************************************
C
      KL=0
      DO 109 IL=1,N2
      DO 109 JL=1,N2
      KL=KL+1
109   B(N,KL)=TD(IL,JL,1)
110   CONTINUE
```

```
C
C     ******************************************************
C     CREATE MATRIX A FOR INVERSION
C     ******************************************************
C
      GO TO 104
  105 CONTINUE
      CLOSE(UNIT=1)
      CLOSE(UNIT=20)
      PRINT 16,N
C     DO 111 I=1,N
C     PRINT 17,(B(I,J),J=1,N1)
C     111    CONTINUE
      DO 112 I=1,N
      DO 112 J=1,N1
      TTD(I,1)=TTD(I,1)+B(I,J)
  112 CONTINUE
      NITER=0
  113 CONTINUE
      EBIGR=0.0
      PRINT 18,NITER
      PRINT 19,INT(NT)
      GO TO 115
  114 NT=2
      PRINT 19,INT(NT)
C
C     ******************************************************
C     DIVIDE ROWS OF MATRIX A BY ALPHA OR BETA SQUARED AND
C     NEGATE ELEMENTS
C     ******************************************************
C
  115 CONTINUE
      NCA=N1
      DO 116 I=1,N
      D1(NT)=0.0
      D2(NT)=0.0
      D3(NT)=0.0
      D4(NT)=0.0
      T1=0.0
      K=0
      L=1
      DO 116 J=1,N1
      BIGR(J)=0.0
      K=K+1
      IF(K.LT.N3) GO TO 117
      K=1
      L=L+1
  117 T1=T1+(B(I,J)/V(L,K,NT))
      TTT(I,NT)=T1
  116 A(I,J)=-(B(I,J)/(V(L,K,NT)**2))
C     PRINT 20
```

```
C         DO 118 I=1,N
C         118     PRINT 21,TTD(I,1)
C         PRINT 22
C         DO 119 I=1,N
C         119     PRINT 21,TTT(I,NT)
C
C         ***********************************************************
C         CALCULATE DELTA TRAVEL TIMES, IE OBS. TT MINUS THEO.
C         ***********************************************************
C
          DO 120 I=1,N
          DTT(I,1)=(TTOBS(I,NT)-TTT(I,NT))/UNC(I,NT)
          DUMMY(I)=TTOBS(I,NT)-TTT(I,NT)
          D1(NT)=D1(NT)+DUMMY(I)
          D2(NT)=D2(NT)+(DUMMY(I)**2.0)
C         PRINT 21,DTT(I,1)
120       CONTINUE
C         PRINT 23
C         DO 121 I=1,N
C         121     PRINT 21,(B(I,J),J=1,N1)
C
C         ***********************************************************
C         MAXDIM,DIMENSIONS,NRA,AND NCA ARE DEPENDENT ON
C         MATRIX DIMENSIONS
C         ***********************************************************
C
C         ***********************************************************
C         DESIGNATE MATRIX PARAMETERS
C         ***********************************************************
C
C
C         ***********************************************************
C         PRINT MATRIX A
C         ***********************************************************
C
C         PRINT 24
C         DO 122 I=1,NRA
C         122     PRINT 21,(A(I,J),J=1,NCA)
C         DO 123 I=1,NRA
C         IF (UNC(I,NT).EQ.1.) GO TO 123
C         GO TO 124
C         123     CONTINUE
C         GO TO 125
C         124     CONTINUE
C         124     PRINT 25
C         PRINT 26
C         DO 126 I=1,NRA
C         126     PRINT 21,UNC(I,NT)
C         GO TO 127
C         125     CONTINUE
C         125     PRINT 27
```

```
C
C         *******************************************************
C         APPLY UNCERTAINTIES, SIGMA, TO MATRIX A
C         *******************************************************
C
127       DO 128 I=1,NRA
          DO 128 J=1,NCA
128       A(I,J)=A(I,J)/UNC(I,NT)
C         DO 129 I=1,NCA
C         IF (TAU(I,NT).EQ.1.) GO TO 129
C         GO TO 130
C         129     CONTINUE
C         GO TO 131
C         130     CONTINUE
C         130     PRINT 28
C         PRINT 29
C         DO 132 I=1,NCA
C         132     PRINT 30,IVAR(I),TAU(I,NT)
C         GO TO 133
C         131     CONTINUE
C         131     PRINT 31
C
C         *******************************************************
C         APPLY TAU ESTIMATES TO MATRIX A
C         *******************************************************
C
133       DO 134 I=1,NCA
          DO 134 J=1,NRA
134       A(J,I)=A(J,I)*TAU(I,NT)
C
C         *******************************************************
C         OBTAIN INITIAL MODEL BIG R
C         *******************************************************
C
          XBIGR=0.0
          DO 135 I=1,N
135       XBIGR=XBIGR+(DTT(I,1)**2)
          YBIGR=XBIGR/N
          ZBIGR=SQRT(YBIGR)
          PRINT 32,INT(NT),ZBIGR
C         PRINT 33
C         DO 136 I=1,NRA
C         136     PRINT 21,(A(I,J),J=1,NCA)
C
C         *******************************************************
C         OBTAIN ATA VIA SUBROUTINE VTPROF
C         *******************************************************
C
          OPEN(UNIT=6,DEVICE='DSK')
          CALL VTPROF (A,N,N1,MAXDIM,ATA)
C
```

```
C         ************************************************************
C         OBTAIN EIGENVALUES AND EIGENVECTORS
C         ************************************************************
C
          CALL EIGRS (ATA,N1,IJOB,EIGVLL,EIGVEC,IB,WK,IER)
C
C         ************************************************************
C         CONVERT EIGENVALUES TO MATRIX FORM, TAKE THE
C         SQUARE ROOTS, AND PRINT EIGENVALUES
C         ************************************************************
C
C         ************************************************************
C         CONVERT EIGENVECTORS TO MATRIX FORM AND PRINT
C         ************************************************************
C
          DO 138 I=1,NCA
          DO 138 J=1,NCA
          K=NCA+1-I
          EV(J,I)=(EIGVEC(J,K))
    138   CONTINUE
          NP=N1
          DO 167 L=1,NP
C         PRINT 34
C         DO 139 I=1,N
C         139     PRINT 21,(A(I,J),J=1,N1)
          K=NP-L+1
          DO 140 I=1,NP
          KK=NP-I+1
          IF(EIGVLL(KK).LE.0.0) GO TO 141
          EIGVAL(I,I)=SQRT(EIGVLL(KK))
          GO TO 142
    141   EIGVAL(I,I)=0.0
    142   DO 140 J=1,NP
          EIGVEC(I,J)=EV(I,J)
    140   CONTINUE
          IF(EIGVAL(K,K).EQ.0.0) GO TO 167
          NCA=K
          IF(NCA.LT.NP) GO TO 143
          PRINT 35,NP
          GO TO 144
C         143     CONTINUE
    143   PRINT 36,NCA
C         PRINT 37
    144   CONTINUE
          IF(NCA.LT.NP) GO TO 145
          PRINT 38
          DO 146 I=1,NCA
    146   PRINT 21,EIGVAL(I,I)
          PRINT 60,INT(NT)
          DO 185 I=1,N2
          PRINT 61,(V(I,J,NT),J=1,N2)
```

```
185   PRINT 61,(VAR(I,J,NT),J=1,N2)
145   CONTINUE
C     PRINT 39
C     DO 147 I=1,KDUM
C     147    PRINT 21,(EIGVEC(I,J),J=1,NCA)
C     PRINT 40,IER
      DO 148 I=1,NCA
C
C     ***********************************************************
C     OBTAIN LAMBDA INVERSE
C     ***********************************************************
C
148   EIGVAL(I,I)=1./EIGVAL(I,I)
C
C     ***********************************************************
C     OBTAIN MATRIX U
C     ***********************************************************
C
      CALL VMULFF(EIGVEC,EIGVAL,KDUM,NCA,NCA,IB,IB,UTEMP,IB,IER)
      CALL VMULFF(A,UTEMP,NRA,KDUM,NCA,IA,IB,U,IA,IER)
C
C     ***********************************************************
C     OBTAIN MATRIX H
C     ***********************************************************
C
      DO 149 I=1,NCA
      DO 149 J=1,NRA
149   UTRP(I,J)=U(J,I)
      CALL VMULFF(UTEMP,UTRP,KDUM,NCA,NRA,IB,IB,H,IB,IER)
C
C     ***********************************************************
C     OBTAIN MATRIX R=(H)(A), WHERE ASAVE=A, VIA
C     SUBROUTINE VMULFF
C     ***********************************************************
C
C     CALL VMULFF (H,A,KDUM,NRA,KDUM,IB,IA,R,IB,IER)
C     PRINT 42
C     DO 150 I=1,KDUM
C     150    PRINT 21,(R(I,J),J=1,KDUM)
C     PRINT 40,IER
      DO 151 I=1,NRA
      DELY(I)=0.0
151   CONTINUE
C
C     ***********************************************************
C     PRINT DELTA Y (DTT)
C     ***********************************************************
C
C     PRINT 41
C     DO 152 I=1,NRDY
C     152    PRINT 43, DTT(I,1)
```

```
      CALL VMULFF(H,DTT,KDUM,NRA,IJOB,IB,IA,S,IB,IER)
      DO 153 I=1,KDUM
153   DXCAP(I,1)=S(I,1)*TAU(I,NT)
C
C     ***************************************************************
C     READ IN MATRIX DELTA X OMITTING VARIABLES
C     ***************************************************************
C
      KKK=0
      DO 154 I=1,N2
      DO 154 MM=1,N2
      KKK=KKK+1
      DX(KKK,1)=V(I,MM,NT)
154   CONTINUE
C     PRINT 44
C
C     ***************************************************************
C      PRINT MATRIX DELTA X
C     ***************************************************************
C     PRINT 21,(S(I,1),I=1,N1)
C     DO 155 I=1,N1
C     155    PRINT 43, DX(I,1)
C
C     ***************************************************************
C     FIND VARIABLES A & B, IE, BY DXCAP (DELTA X CAP)=
C     H * DELTA Y AND SUBTRACTING DX FROM DXCAP
C     ***************************************************************
C
C     ***************************************************************
C     OBTAIN DXCAP
C     ***************************************************************
C
C     PRINT 45
      DO 156 I=1,NRDX
C     PRINT 43, DXCAP(I,1)
C
C     ***************************************************************
C     OBTAIN VARIABLES A AND B
C     ***************************************************************
C
156   VARMTX(I,L,NT)=DXCAP(I,1)+DX(I,1)
C     DO 157 I=1,NRDX
C     PRINT 46,IVAR(I),INT(NT),VARMTX(I,L,NT)
C     157    CONTINUE
C
C     ***************************************************************
C     OBTAIN VARIANCES ON A CAP AND B CAP
C     ***************************************************************
C
      DO 158 I=1,N
      DO 158 J=1,N1
```

```
158    HT(J,I)=H(J,I)
       CALL VMULFP(H,HT,N1,N,N1,IB,IB,R,IB,IER)
       DO 159 I=1,N1
159    VART(I,L,NT)=R(I,I)*(TAU(I,NT)**2)
       DO 160 I=1,KDUM
       VART(I,L,NT)=SQRT(VART(I,L,NT))
C      PRINT 47,INT(NT),IVART(I),VART(I,L,NT)
160    CONTINUE
C
C      ******************************************************
C      OBTAIN NEW DELTA YS
C      ******************************************************
C
       TX=0.0
       DO 161 I=1,NRDY
       DO 162 J=1,N1
162    TX=TX+(B(I,J)/VARMTX(J,L,NT))
       DELY(I)=TX
161    TX=0.0
C
C      *********************************************************
C      CALCULATE BIG R FOR EACH DECOMPOSITION
C      *********************************************************
C
       ABIGR=0.0
       CBIGR=0.0
       DO 163 I=1,NRDY
163    ABIGR=ABIGR+(((TTOBS(I,NT)-DELY(I))/UNC(I,NT))**2)
       DBIGR(L,NT)=ABIGR
       CBIGR=ABIGR/NRDY
       BIGR(L)=SQRT(CBIGR)
       PRINT 48,BIGR(L)
C
C      *********************************************************
C      CALCULATION OF SMALL R
C      *********************************************************
C
C      DO 164 I=1,KDUM
C      SMLLR=0.0
C      DO 165 J=1,KDUM
C      RIJ=R(I,J)
C      IF(I.EQ.J) RIJ=R(I,J)-1.0
C      165     SMLLR=SMLLR+(RIJ**2)
C      PRINT 49,IVAR(I),SMLLR
C      164     CONTINUE
       PRINT 50
       PRINT 21, (VARMTX(I,L,NT),I=1,N1)
       PRINT 51
       PRINT 21,(VART(I,L,NT),I=1,N1)
167    CONTINUE
168    CLOSE(UNIT=6)
```

```
C
C          ************************************************************
C          SORT TEST FOR BIG R OR AVE STANDARD DEVIATION
C          ************************************************************
C
           DO 169 I=1,N1
      169  IF(BIGR(I).GE.1.0) GO TO 179
           PRINT 59,INT(NT),TAU(1,NT)
           IF(NBLK.EQ.1) GO TO 166
           DO 170 I=1,N1
           E1=0.0
           DO 171 J=1,N1
      171  E1=E1+VART(J,I,NT)
           E2=E1/N1
      170  IF(E2.LE.TAU(1,NT)) GO TO 172
      166  I=1
      172  K1=I
           LL=N1-I+1
           GO TO 183
      179  PRINT 57,INT(NT)
           DO 180 I=1,N1
           ZT(I)=1.-BIGR(I)
      180  ZT(I)=ABS(ZT(I))
           IF(NBLK.EQ.1) GO TO 184
           DO 181 I=1,N1
           K2=I+1
      181  IF(ZT(K2).GE.ZT(I)) GO TO 182
      184  I=1
      182  K1=I
           LL=N1-I+1
      183  DBIGR(1,NT)=DBIGR(K1,NT)
           KI=0
           PRINT 58,INT(NT),LL
           DO 174 I=1,N2
           DO 174 J=1,N2
           KI=KI+1
           V(I,J,NT)=VARMTX(KI,K1,NT)
      174  VAR(I,J,NT)=VART(KI,K1,NT)
           PRINT 53
           DO 175 I=1,N2
           PRINT 54,(V(I,J,NT),J=1,N2)
           PRINT 54,(VAR(I,J,NT),J=1,N2)
      175  CONTINUE
           EBIGR=EBIGR+DBIGR(1,NT)
           IF (NT.EQ.1) GO TO 114
           DO 186 M=1,2
           PRINT 62,INT(M)
           DO 186 I=1,N2
           PRINT 61,(V(I,J,M),J=1,N2)
      186  PRINT 61,(VAR(I,J,M),J=1,N2)
C
```

```
C          ************************************************************
C          CALCULATIONS OF POISSON'S RATIOS AND STANDARD DEVIAT'N
C          ************************************************************
C
           K=0
           DO 176 I=1,N2
           DO 176 J=1,N2
           K=K+1
           A1=(V(I,J,1)/V(I,J,2))**2.
           B1=A1-1.
           A1=A1-2.
           POI=A1/(B1*2.)
           PSTD1=V(I,J,1)*V(I,J,2)
           PSTD2=((V(I,J,1)**2.0)-(V(I,J,2)**2.0))**2.0
           PSTD3=(V(I,J,2)*VAR(I,J,1))-(V(I,J,1)*VAR(I,J,2))
           PSTD4=(PSTD1*PSTD3)/PSTD2
           PSTD=ABS(PSTD4)
           PRINT 55,IVAR(K),POI,PSTD
176        CONTINUE
           DO 177 I=1,2
           D3(I)=((N*D2(I))-(D1(I)**2.0))/(N*(N-1))
           D4(I)=SQRT(D3(I))
177        PRINT 56,INT(I),D4(I)
           FBIGR=EBIGR/(N*2)
           BIGR1=SQRT(FBIGR)
           PRINT 48,BIGR1
           NITER=NITER+1
           IF(NITER.GT.5) GO TO 178
           NT=1
           GO TO 113
178        CONTINUE
1          FORMAT(1X,'IN WHAT DATA FILE ARE THE EVENTS?')
2          FORMAT(A5)
3          FORMAT(1X,'WHAT ARE THE MAX & MIN LONG & LAT OF AREA?')
4          FORMAT(1X,'AT WHAT INCREMENTS ARE THE BLOCKS TO BE
           1 DIVIDED ALONG LONG & LAT?')
5          FORMAT(1X,'THIS WILL CREATE A SQUARE AREA OF X BLOCKS
           1 ACROSS AND X BLOCKS HIGH. INPUT X.')
6          FORMAT(I3)
7          FORMAT('1',///,5X,'THE DATA IS FROM DATA SET ',A5,'.DAT')
8          FORMAT(///,5X,'THE MAXIMUM LONGITUDE OF THE STUDY AREA
           1IS ',F8.4,/,1X,'THE MINIMUM LONGITUDE OF THE STUDY AREA I
S '
           1,F8.4,/,1X,'THE MAXIMUM LATITUDE OF THE STUDY AREA IS '
           1,F7.4,/,1X,'THE MINIMUM LATITUDE OF THE STUDY AREA IS '
           1,F7.4)
9          FORMAT(///,5X,'THE BLOCK INCREMENTS ARE ',F4.3,' DEGREES
           1 ALONG THE LONGITUDE AND ',F4.3,' DEGREES ALONG THE LATIT
UDE.')
10         FORMAT(///,5X,'THIS DIVIDES THE STUDY AREA INTO ',I2,'
           1BLOCKS BY ',I2,' BLOCKS.')
12         FORMAT(1F15.5)
13         FORMAT(A3,2(1X,I2,1X,F5.2,1X,F3.2))
```

```
14     FORMAT(A3,1X,F7.4,1X,F8.4,2X,F5.3)
15     FORMAT(1X,'STATION ',A3,' NOT FOUND ON DATE ',5I3)
16     FORMAT(//,1X,'THE TOTAL NUMBER OF RAYPATHS IS ',I4)
17     FORMAT(1X,9F9.4)
18     FORMAT('1',20X,'ITERATION NUMBER ',I2)
19     FORMAT(/,20X,'THE FOLLOWING OUTPUT IS FOR ',A4,'.')
20     FORMAT(//,2X,'THE TOTAL TRAVEL DISTANCES ARE')
21     FORMAT (' ',10F10.4)
22     FORMAT(//,2X,'THE TOTAL TRAVEL TIME IS')
23     FORMAT(//,30X,'MATRIX A PRIOR TO NEGATION & VEL. DIV.')
24     FORMAT (//,30X,'MATRIX A IS')
25     FORMAT(//,3X,'THE UNCERTAINTIES, SIGMA, ARE NOT UNITY')
26     FORMAT(/,3X,'THE UNCERTAINTIES ARE')
27     FORMAT(//,3X,'THE UNCERTAINTIES, SIGMA, ARE UNITY')
28     FORMAT(//,3X,'THE TAU ESTIMATES ARE NOT UNITY')
29     FORMAT(/,3X,'THE TAU VALUES ARE')
30     FORMAT(/,3X,'TAU(',A1,') = ',1F10.4)
31     FORMAT(//,3X,'THE TAU ESTIMATES ARE UNITY')
32     FORMAT(/,1X,'THE BIG R ON THE INITIAL ',A4,' MODEL IS '
       1,F8.5)
33     FORMAT('-',18X,'MATRIX A WITH TAU AND SIGMA APPLIED IS')
34     FORMAT(//,30X,'MATRIX A AFTER NEG. & VEL. DIV.')
35     FORMAT(///,20X,'ALL EIGENVALUES AND EIGENVECTORS ARE RETAI
N
       1ED, IE, P=',1I3,/)
36     FORMAT(///,20X,'ONLY LARGEST EIGEN NUMBERS ARE RETAINED, I
       1E, P=',1I3,/)
37     FORMAT('-',18X,'THE EIGENVALUE MATRIX, LAMBDA CAP, IS')
38     FORMAT(/,5X,'THE EIGENVALUES ARE')
39     FORMAT('-',22X,'THE EIGENVECTOR MATRIX, V, IS')
40     FORMAT (' ',3X,'IER=',1X,1F10.2)
41     FORMAT ('-',3X,'DELTA Y IS')
42     FORMAT ('-',31X,'MATRIX R IS')
43     FORMAT (' ',3X,1F10.2)
44     FORMAT ('-',3X,'MATRIX X IS')
45     FORMAT ('-',3X,'MATRIX DELTA X CAP IS')
46     FORMAT ('-',3X,'FOR BLOCK ',A1,',',1X,A4,' IS',1F10.4)
47     FORMAT('-',3X,'THE STANDARD DEVIATION OF ',A4,'(',A1,') HA
T
       1 IS + OR - ',1F10.4)
48     FORMAT('-',3X,'THE SCALAR BIG R IS',1F10.6)
49     FORMAT('-',3X,'SMALL R(',A1,') IS ',1F10.4)
50     FORMAT(/,25X,'THE VELOCITIES ARE')
51     FORMAT(/,20X,'THE STANDARD DEVIATIONS ARE')
53     FORMAT (//,9X,'SORT TEST',//)
54     FORMAT (1X,5F10.4)
55     FORMAT(1X,'POISSONS RATIO FOR BLOCK ',I2,' IS ',1F8.5,
       1' + OR - ',1F8.5)
56     FORMAT(/,1X,'THE STANDARD DEVIATION ON THE ',A4,' RESI
       1DUALS IS ',F6.4)
57     FORMAT(/,1X,'THE ',A4,' SOLUTION IS BASED ON BIG R.',/)
58     FORMAT(/,1X,'SORTED CALCULATIONS FOR ',A4,' KEEPING ',
       1I2,' EIGENVALUES.',/)
```

```
 59   FORMAT(/,1X,'THE ',A4,' SOLUTION IS BASED ON AN AVERAGE
     1 STANDARD DEVIATION THAT IS CLOSEST YET LESS THAN
     1 ',F6.4,/)
 60   FORMAT(/,95X,A4,' MODEL')
 61   FORMAT(80X,5F10.4)
 62   FORMAT(/,85X,A4,' SOLUTIONS FOR NEXT MODEL')
      STOP
      END
      SUBROUTINE TTYM(XP,YP,HPZ,SX,SY,SZ,TTB,V,TD,TALMIN,GNLMAX,
     1GNLINC,TALINC,NBLK)
      DIMENSION TAL(10),GNOL(10),TD(5,5,2),V(5,5,2),
     1TDZ(5,5,2)
     $ ,TTB(5,5,2)
      TAN(A)=SIN(A)/COS(A)
      NB=NBLK+1
      N5=NBLK
      N6=NBLK-1
      DO 700 MM=1,2
      DO 700 I=1,N5
      DO 700 J=1,N5
      TDZ(I,J,MM)=0.
 700  TD(I,J,MM)=0.
      STO=0.
      Z=HPZ
      M=2
      IF(Z.LE.100.)M=1
      DPP=HPZ+SZ
      DTI=100.0
      DGU=Z-DTI
      II=0
      JJ=0
      NTAL=NB
      NGNOL=NB
      TAL(1)=TALMIN
      GNOL(1)=GNLMAX
      DO 1 I=2,NB
      IM1=I-1
      TAL(I)=TAL(IM1)+TALINC
    1 GNOL(I)=GNOL(IM1)-GNLINC
      IF(SY.LT.TAL(1).OR.SY.GT.TAL(NTAL))GO TO 500
      IF(YP.LT.TAL(1).OR.YP.GT.TAL(NTAL))GO TO 500
      IF(SX.GT.GNOL(1).OR.SX.LT.GNOL(NGNOL))GO TO 500
      IF(XP.GT.GNOL(1).OR.XP.LT.GNOL(NGNOL))GO TO 500
      GO TO 520
 500  CONTINUE
      PRINT 511,TAL(1),TAL(NTAL),GNOL(1),GNOL(NGNOL)
 511  FORMAT(10X,4F10.4)
      PRINT 511,SX,SY,XP,YP
      PRINT 510
 510  FORMAT(10X,'INCORRECT ENTRY',/)
      GO TO 90
```

```
  520 PI=3.1415927
      CF=PI/180.
      XKDEG=((SY+YP)/2.-34.1)*.018+110.922
      XKC=COS(CF*(SY+YP)/2.)*111.4399
      YTN=90.*CF
      OETY=180.*CF
      TSV=270.*CF
      TSX=360.*CF
      XX=ABS(SX-XP)*XKC
      YY=ABS(SY-YP)*XKDEG
      IF(YY.LE..001)YY=.001
      TH=XX/YY
      AZI=ATAN(TH)
      IF(SY.LT.YP.AND.SX.LT.XP)AZI=OETY-AZI
      IF(SY.LT.YP.AND.SX.GT.XP)AZI=OETY+AZI
      IF(SY.GT.YP.AND.SX.GT.XP)AZI=TSX-AZI
      IF(SY.EQ.YP.AND.SX.GT.XP)AZI=TSV
      IF(SX.EQ.XP.AND.SY.GT.YP)AZI=TSX
      IF(SX.EQ.XP.AND.SY.LT.YP)AZI=OETY
      ANG=ABS(DPP)/SQRT(XX*XX+YY*YY)
      ANG=ATAN(ANG)
      IF(AZI.GT.YTN)GO TO 60
      IF(AZI.LE..0001)AZI=.0001
      DIF=YTN-AZI
      IF(DIF.LE..0001)AZI=AZI-.0001
   10 J=0
      I=0
   30 I=I+1
      K=I-1
      IF(XP.LT.GNOL(I))GO TO 30
      IF(SX.GE.GNOL(I)) II=1
      XE=ABS(GNOL(I)-XP)
      XD=XE*XKC/SIN(AZI)
   40 J=J+1
      L=NTAL+1-J
      IF(YP.GT.TAL(J))GO TO 40
      IF(SY.LT.TAL(J))JJ=1
      YE=ABS(TAL(J)-YP)
      YD=YE*XKDEG/COS(AZI)
      IPJ=II+JJ
      IF(IPJ.EQ.2)GO TO 70
      IF(YD.GT.XD)GO TO 50
      YP=TAL(J)
      XP=XP-YE*TAN(AZI)*XKDEG/XKC
      TD(L,K,M)=YD/COS(ANG)
      TDZ(L,K,M)=TD(L,K,M)*SIN(ANG)
      CALL BLCHG(TDZ,DGU,TD,L,K,M,ANG,N5)
      I=I-1
      GO TO 30
   50 CONTINUE
      XP=GNOL(I)
```

```
      YP=YP+(XE/TAN(AZI))*XKC/XKDEG
      TD(L,K,M)=XD/COS(ANG)
      TDZ(L,K,M)=TD(L,K,M)*SIN(ANG)
      CALL BLCHG(TDZ,DGU,TD,L,K,M,ANG,N5)
      J=J-1
      GO TO 30
 70   CONTINUE
      TD(L,K,M)=ABS((SY-YP)*XKDEG/(COS(AZI)*COS(ANG)))
      IF(YY.LT..01)TD(L,K,M)=ABS(SX-XP)*XKC/COS(ANG)
      TDZ(L,K,M)=TD(L,K,M)*SIN(ANG)
      CALL BLCHG(TDZ,DGU,TD,L,K,M,ANG,N5)
      GO TO 90
 60   CONTINUE
      IF(AZI.GT.OETY)GO TO 160
      DIF=AZI-YTN
      IF(DIF.LE..0001)AZI=AZI+.0001
      DIF=OETY-AZI
      IF(DIF.LE..0001)AZI=AZI-.0001
      J=NTAL+1
      I=0
130   I=I+1
      K=I-1
      IF(XP.LT.GNOL(I))GO TO 130
      IF(SX.GE.GNOL(I))II=1
      XE=ABS(GNOL(I)-XP)
      XD=XE*XKC/COS(AZI-YTN)
140   J=J-1
      L=NTAL-J
      IF(YP.LT.TAL(J))GO TO 140
      IF(SY.GE.TAL(J))JJ=1
      YE=ABS(TAL(J)-YP)
      YD=YE*XKDEG/SIN(AZI-YTN)
      IPJ=II+JJ
      IF(IPJ.EQ.2)GO TO 170
      IF(YD.GT.XD)GO TO 150
      YP=TAL(J)
      XP=XP-YE*TAN(OETY-AZI)*XKDEG/XKC
      TD(L,K,M)=YD/COS(ANG)
      TDZ(L,K,M)=TD(L,K,M)*SIN(ANG)
      CALL BLCHG(TDZ,DGU,TD,L,K,M,ANG,N5)
      I=I-1
      GO TO 130
150   CONTINUE
      XP=GNOL(I)
      YP=YP-XE*TAN(AZI-YTN)*XKC/XKDEG
      TD(L,K,M)=XD/COS(ANG)
      TDZ(L,K,M)=TD(L,K,M)*SIN(ANG)
      CALL BLCHG(TDZ,DGU,TD,L,K,M,ANG,N5)
      J=J+1
      GO TO 130
170   CONTINUE
```

```
      TD(L,K,M)=ABS(SY-YP)*XKDEG/(COS(OETY-AZI)*COS(ANG))
      TDZ(L,K,M)=TD(L,K,M)*SIN(ANG)
      CALL BLCHG(TDZ,DGU,TD,L,K,M,ANG,N5)
      GO TO 90
160   CONTINUE
      IF(AZI.GT.TSV)GO TO 260
      DIF=AZI-OETY
      IF(DIF.LE..0001)AZI=AZI+.0001
      DIF=TSV-AZI
      IF(DIF.LE..0001)AZI=AZI-.0001
      J=NTAL+1
      I=NGNOL+1
230   I=I-1
      K=I
      IF(XP.GT.GNOL(I))GO TO 230
      IF(SX.LE.GNOL(I))II=1
      XE=ABS(GNOL(I)-XP)
      XD=XE*XKC/SIN(AZI-OETY)
240   J=J-1
      L=NTAL-J
      IF(YP.LT.TAL(J))GO TO 240
      IF(SY.GE.TAL(J))JJ=1
      YE=ABS(TAL(J)-YP)
      YD=YE*XKDEG/COS(AZI-OETY)
      IPJ=II+JJ
      IF(IPJ.EQ.2)GO TO 270
      IF(YD.GT.XD)GO TO 250
      YP=TAL(J)
      XP=XP+YE*TAN(AZI-OETY)*XKDEG/XKC
      TD(L,K,M)=YD/COS(ANG)
      IF(YY.LT..01)TD(L,K,M)=ABS(SX-XP)*XKC/COS(ANG)
      TDZ(L,K,M)=TD(L,K,M)*SIN(ANG)
      CALL BLCHG(TDZ,DGU,TD,L,K,M,ANG,N5)
      IF(XD.NE.GNOL(I))I=I+1
      GO TO 230
250   CONTINUE
      XP=GNOL(I)
      YP=YP-XE*TAN(TSV-AZI)*XKC/XKDEG
      TD(L,K,M)=XD/COS(ANG)
      TDZ(L,K,M)=TD(L,K,M)*SIN(ANG)
      CALL BLCHG(TDZ,DGU,TD,L,K,M,ANG,N5)
      IF(YD.NE.TAL(J))J=J+1
      GO TO 230
270   CONTINUE
      TD(L,K,M)=ABS(SY-YP)*XKDEG/(SIN(TSV-AZI)*COS(ANG))
      IF(YY.LT..01)TD(L,K,M)=ABS(SX-XP)*XKC/COS(ANG)
      TDZ(L,K,M)=TD(L,K,M)*SIN(ANG)
      CALL BLCHG(TDZ,DGU,TD,L,K,M,ANG,N5)
      GO TO 90
260   CONTINUE
      J=0
```

```
      DIF=AZI-TSV
      IF(DIF.LE..0001)AZI=AZI+.0001
      DIF=TSX-AZI
      IF(DIF.LE..0001)AZI=AZI-.0001
      I=NGNOL+1
330   I=I-1
      K=I
      IF(XP.GT.GNOL(I))GO TO 330
      IF(SX.LE.GNOL(I))II=1
      XE=ABS(GNOL(I)-XP)
      XD=XE*XKC/COS(AZI-TSV)
340   J=J+1
      L=NTAL+1-J
      IF(YP.GT.TAL(J))GO TO 340
      IF(SY.LE.TAL(J))JJ=1
      YE=ABS(TAL(J)-YP)
      YD=YE*XKDEG/SIN(AZI-TSV)
      IPJ=II+JJ
      IF(IPJ.EQ.2)GO TO 370
      IF(YD.GT.XD)GO TO 350
      YP=TAL(J)
      XP=XP+YE*TAN(TSX-AZI)*XKDEG/XKC
      TD(L,K,M)=YD/COS(ANG)
      TDZ(L,K,M)=TD(L,K,M)*SIN(ANG)
      CALL BLCHG(TDZ,DGU,TD,L,K,M,ANG,N5)
      I=I+1
      GO TO 330
350   CONTINUE
      XP=GNOL(I)
      YP=YP+XE*TAN(AZI-TSV)*XKC/XKDEG
      TD(L,K,M)=XD/COS(ANG)
      TDZ(L,K,M)=TD(L,K,M)*SIN(ANG)
      CALL BLCHG(TDZ,DGU,TD,L,K,M,ANG,N5)
      J=J-1
      GO TO 330
370   CONTINUE
      TD(L,K,M)=ABS(SY-YP)*XKDEG/(COS(TSX-AZI)*COS(ANG))
      IF(YY.LT..01)TD(L,K,M)=ABS(SX-XP)*XKC/COS(ANG)
      TDZ(L,K,M)=TD(L,K,M)*SIN(ANG)
      CALL BLCHG(TDZ,DGU,TD,L,K,M,ANG,N5)
 90   CONTINUE
      TTT=0.
      TTD=0.
C     DO 89 MM=1,2
C     DO 89 LL=1,N6
C     DO 89 KK=1,NB
C     TTD=TTD+TD(LL,KK,MM)
C     TTB(LL,KK,MM)=TD(LL,KK,MM)/V(LL,KK,MM)
C     89     TTT=TTT+TTB(LL,KK,MM)
      RETURN
      END
```

```
      SUBROUTINE BLCHG(TDZ,DGU,TD,L,K,M,ANG,N5)
      DIMENSION TDZ(5,5,2),TD(5,5,2)
      IF(M.EQ.1) RETURN
      STDZ = 0.
      DO 1 LL=1,N5
      DO 1 KK=1,N5
    1 STDZ=STDZ+TDZ(LL,KK,2)
      IF(STDZ.LT.DGU) RETURN
      TZ=TDZ(L,K,2)
      TDZ(L,K,2)=DGU-STDZ+TDZ(L,K,2)
      TD(L,K,2)=TDZ(L,K,2)/SIN(ANG)
      TDZ(L,K,1)=TZ-TDZ(L,K,2)
      TD(L,K,1)=TDZ(L,K,1)/SIN(ANG)
      M=1
      RETURN
      END
```

APPENDIX C

Computer Output for Model 1

(Under Separate Cover)

APPENDIX D

Computer Output for Model 2

(Under Separate Cover)

APPENDIX E

Computer Output for Model 3

(Under Separate Cover)

APPENDIX F

Computer Output for Model 4

(Under Separate Cover)

APPENDIX G

Computer Output for Model 5

(Under Separate Cover)

APPENDIX H

Computer Output for Model 4'

(Under Separate Cover)

APPENDIX I

Computer Output for Model 5'

(Under Separate Cover)

APPENDIX J

Listing of Data Set Including P- and S-wave Arrival Times

(Under Separate Cover)